EFFECTIVE INTERACTIONS

HIGHER ORDER CORE POLARIZATION CORRECTIONS TO THE EFFECTIVE NUCLEAR INTERACTION

By

ANTON MICHAEL JOPKO, B.Sc., M.Sc.

A Thesis

Submitted to the School of Graduate Studies

in Partial Fulfilment of the Requirements

for the Degree

Doctor of Philosophy

McMaster University

November 1974

DOCTOR OF PHILOSOPHY (1974) McMASTER UNIVERSITY
(Physics) Hamilton, Ontario

TITLE: Higher Order Core Polarization Corrections to the Effective Nuclear Interaction

AUTHOR: Anton Michael Jopko, B.Sc. (McMaster University)
M.Sc. (McMaster University)

SUPERVISOR: Professor Donald W. L. Sprung

NUMBER OF PAGES: (xiv), 187

SCOPE AND CONTENTS

Various higher order core polarization corrections to the effective nuclear interaction, suggested by Kuo and Brown have been calculated for mass 18 and mass 42 nuclei. The corresponding spectra resulting from these corrections were compared with each other and with experiment.

The bare nucleon-nucleon interactions used in the calculation were of two different forms. For the one interaction, the G-matrix elements of Kahana, Lee and Scott derived from their separable nucleon-nucleon potential, were used. For the other, matrix elements of the interaction were derived in a phase-shift approximation at McMaster. In a certain approximation these are the free reaction matrix elements. The effects of the 2 forces were compared.

The schematic model of Brown and Bolsterli was extended to these higher order core polarization corrections and it was found to corroborate the results of the detailed, more realistic calculation.

ACKNOWLEDGEMENTS

It is with great pleasure that I express my gratitude to Professor Donald Sprung for his contributions to and supervision of this work. I would also like to thank him for arranging and providing financial support for my visit to Paris in the summer of 1970.

While in Paris, I greatly appreciated the hospitality of M. Veneroni and the Institute of Nuclear Physics at Orsay.

I wish to thank Dr. C. K. Scott, Dr. M. K. Srivastava, and Dr. M. W. Kermode for their patience in answering so skillfully my many questions.

Valuable correspondence was gratefully received from N. Vinh Mau, P. J. Ellis, C. S. Warke, S. Siegel, M. W. Kirson, B. R. Barrett, and F. C. Khanna.

Special thanks are due to C. S. Warke and S. Siegel who helped initiate me to the concepts of core polarization and to their calculations.

I thank my fellow graduate students Dr. K. R. Lassey Dr. P. Grangé, Dr. C. K. Ross, Mr. P. Dunmore and Dr. T. Taylor for discussions that have contributed to this thesis. Special thanks to Dr. J. Stephens, Mr. P. Dunmore

and Mr. R. Griffin who provided me with valuable aid and computing advice.

I am also indebted to the director and staff of the computer centre for their courteous assistance and cooperation.

The financial assistance I have received from the National Research Council of Canada, and McMaster University is gratefully acknowledged.

Finally I thank Miss E. Long for the patient, skillful and cheerful manner in which this thesis was typed and Miss A. Gillespie for aid in preparation of diagrams.

Perturbative Approach to Physical Understanding

TRUTH = REASON PLUS THE REASON FOR THE TRUTH

To STEPHANIE AND MICHELLE

TABLE OF CONTENTS

TABLE OF CONTENTS - continued

LIST OF TABLES

LIST OF TABLES - continued

LIST OF FIGURES

LIST OF FIGURES - continued

LIST OF FIGURES - continued

CHAPTER I

INTRODUCTION

Physics is concerned with the study of matter and its motion. In particular, nuclear physics deals with the particles of matter (and their motion) in the atomic nucleus. These particles (called nucleons) and their interactions with each other determine the properties of the nucleus. The properties include the size, shape and density of the nucleus, the binding energies, energy levels and their spins and parities and transition properties between these levels. In addition, the nucleon-nucleon interaction determines if a nucleus is stable or will undergo radioactive decay.

The aim of a large group of researchers is to experimentally measure these nuclear properties. Another equally large group of researchers attempt to calculate these properties from a fundamental point of view. In this way, one may try to understand the processes that take place in a nucleus. This thesis is concerned with the latter point of view.

For the remainder of Chapter I, the nature of the two nucleon interaction and how it lends itself to certain

models of the nucleus will be briefly described. One of these models, the shell model, forms an important theoretical method in this thesis and is described in greater detail. The use of a model leads naturally to the concept of effective or residual interactions. These are of two kinds. The first is a phenomenological approach in which parameters are adjusted to obtain the best fit to experimental properties. The second approach is more fundamental and attempts to calculate the effective interaction in a microscopic way through the use of perturbation theory (or other suitable methods).

In Chapter II, the theoretical methods employed in this thesis are described in more detail. The use of many body perturbation theory and the associated angular momentum algebra as well as the nature of the free interaction are discussed and their application illustrated in Chapter III. In this chapter, the schematic model of Brown and Bolsterli (1959) is used to apply the theoretical methods of Chapter II in a simple way and then in a more detailed fashion to the core polarization processes. The results of the calculation are presented in Chapter IV for mass 18 and 42 nuclei using two types of bare interactions. Finally in Chapter V, we discuss other approaches to this problem and compare with ours if possible. Conclusions are then presented.

The main objectives of this thesis are to:

1) apply higher order core polarization processes to the schematic model as a means of understanding the more detailed calculations,
2) correct the treatment of energy denominators required in the screening calculation,
3) recalculate the core polarization of mass 18 nuclei,
4) extend core polarization calculations to mass 42 nuclei,
5) identify the source of the large and repulsive effect of the renormalized vertices on the calculated spectra, and
6) demonstrate the transformation properties of higher order diagrams, for example, in terms of the same transformation between two body vertices.

1.1 Nuclear Forces and Models

Accepting that the nucleus consists only of neutrons and protons, the basic information that is required to explain the nuclear properties is the nature of the nucleon-nucleon interaction. The force between nucleons in a nucleus may be different than the force between two isolated or "free" nucleons. However, it is experimentally much easier to investigate the forces

between isolated nucleons. As difficult as this problem is, it may still be necessary to investigate many body forces in the nucleus for a complete understanding.

The most important and accurate way to obtain information on the two body force is to accelerate positively charged protons electrically and to scatter them off a target of hydrogen gas. Measuring the resulting cross section for different energies of the accelerated protons yields information about the strength and range of the proton-proton (pp) force. By using a deuterium target, n-p scattering can be studied as well. Relatively little has been done to date regarding the neutron-neutron (nn) force but assuming charge symmetry, it should be identical to the p-p nuclear force.

Another way to obtain information about the nuclear force is to study the properties of simple, bound nuclear systems. The best example is the deuteron which consists of one proton and one neutron. Since the ground state of the deuteron is mainly $^3S_1$ and not $^1S_0$, the n-p force must be spin dependent, that is, depending on the relative spin directions of the two nucleons. Because the deuteron is bound, the n-p force must be attractive at least at large separations. For various reasons, among them to prevent collapse of the nucleus, the force is believed to be repulsive at very short distances. As a result of twenty years of intensive investigation of two body scattering, a

good deal of quite accurate information is available regarding the pp and np forces. This has been summarized in the form of phenomenological potential models, adjusted to reproduce the observed scattering data. A number of competing, but more or less equivalent potentials are available. The best known of them are due to Hamada and Johnston (1962), Reid (1968), and de Tourreil and Sprung (1973, 1974). It is not our purpose here to describe these in any detail.

The properties of the nuclear force should be manifest in the structure of the nucleus. Because of the great strength of the nuclear force, many people felt that the nucleons in the nucleus were not free to move so that the nucleus may be a rigid body. The rotational spectrum of a rigid body has level excitations proportional to $J(J+1)$ where J is the total angular momentum of the nucleus. Indeed, certain nuclei do exhibit this kind of spectrum. However, many nuclei do not possess such a spectrum and the rigid body moment of inertia tends to be too large compared to the observed one.

If the nuclei were not rigid, then perhaps the nucleons are free to move but are strongly coupled. Experimental cross sections for nuclear scattering exhibited many narrow resonances implying that very long lived states ($\tau \approx \frac{\hbar}{\Delta E}$) are involved. Bohr developed the compound nucleus

model to explain this observation. According to Bohr, an incident nucleon would share its energy among many nucleons. Only after a long time would the energy be collected together again to re-emit the scattered particle.

Another aspect of nuclear binding is the roughly constant binding energy per particle. This can be understood from the liquid drop model. The energy of the nucleus is viewed as a sum of a volume energy ($\sim A$) less a surface energy ($\sim A^{2/3}$) plus coulomb, symmetry energy and other corrections.

The liquid drop model is not unrelated to the problem of nuclear rotation. One way for the nucleus to rotate is by hydrodynamic, irrotational flow. Essentially a wave propagates around the surface, causing the shape to rotate. The moment of inertia calculated on this model is much less than the rigid body moment, and in fact is too low compared to experiment. Large amplitude vibrations of the liquid drop lead to a semi classical view of the fission process, developed by Bohr and Wheeler (1939).

Evidence from the pattern of nuclear binding energies, excitation energies of first excited states, trends in the shape of nuclei and direct reaction processes indicates that the nucleons may move independently from one another in the nucleus. The independent particle model was proposed by Mayer and Jensen (1955). Even though the nuclear force is strong, the overall effect is to produce an average field in

which the nucleons move more or less independently. The process by which this occurs is similar to the Hartree Fock approximation for atoms. This model in all its sophistication is called the shell model and will be described in greater detail in Section 1.2. The success of the shell model has been great for the prediction of ground state spins and parities as well as some features of the low lying spectrums. The main limitation of this model is in the rapid increase in complexity of calculations as more valence particles are added.

All the models listed above have some virtues, as aids to understanding nuclear behaviour. However, of them all, it is the shell model which offers the greatest possibility of microscopic justification. For this reason, we turn to describe it in more detail.

1.2 The Shell Model

In surveying the properties of nuclei throughout the periodic table, it was found that in certain regions the binding energies per nucleon were greater than the average. In addition, the excitation energy of the first excited state was high and the magnetic and electric quadrupole moments varied systematically. These striking regularities

are explained by the shell model of the nucleus. It is clearly impossible to reproduce all the nuclear properties through model calculations unless the model consists of the real life nucleus. However, it has been possible to explain a large amount of data within the shell model.

In the simplest version of the shell model, we assume that the nucleons move independently of one another in a central potential well of usually Woods-Saxon (WS) shape. The WS shape is fairly constant and attractive in the interior of the nucleus. Towards the edge of the nucleus the potential rises smoothly to zero. Such a potential is realistic because a nucleon in the centre of a nucleus is equally attracted in all directions by the remaining nucleons. The potential energy will, therefore, not change if the nucleon moves. Near the edge of the nucleus, however, a nucleon has a greater attraction toward the centre of the nucleus and, therefore, the potential energy must increase further away from the nucleus.

By solving the one body Schroedinger equation one finds that the eigenvalues group closely together in shells and that between shells there are relatively large gaps. From this information we may begin to explain some nuclear properties. Since each level of angular momentum j can contain 2j+1 protons and 2j+1 neutrons, a nucleus that has a shell fully occupied by nucleons will have a large binding

energy per particle, J=0 ground state, and a first excited state high in energy. Such nuclei are called magic nuclei because of their stability and have 2, 8, 20, 28, 50, 82, 126 protons or neutrons in the nucleus. This model is also very successful in describing nuclei that have one more or one less nucleon than the magic number. With this additional nucleon, the nucleus is described in this model by the properties of the level occupied in the next higher shell. Similarly in the absence of a nucleon, the nuclear properties are described by the properties of the level unoccupied (hole state) in the shell.

For nuclei with two neutrons or two protons more or less than the magic number, the model is unable to make predictions without further assumption. Experimentally, these nuclei all have zero angular momentum ground states though the two individual nucleons have angular momentum. They must, therefore, be coupled in opposite directions to produce a total angular momentum of zero. This preference, which is a property of the N-N force, is called the pairing effect. For 3 extra nucleons, this simple model predicts that the ground state angular momentum will again be given by that of the unpaired nucleon. This, in fact, is most often the case. The model, however, is unable to explain the excited states for such nuclei.

In shell model considerations, one often uses the wave functions of the harmonic oscillator as those of the

single nucleon states. Although the average nuclear field may be better represented by a Woods-Saxon Well, it does not possess the simplicity in determining wave functions as does the three dimensional harmonic oscillator. This approximation to the average field was first employed by Talmi (1952) and exhibits the shell properties of the more realistic WS potential.

By including a one body spin-orbit term in the nuclear hamiltonian, the states of given orbital angular momentum ℓ are no longer degenerate, but split up as shown in Fig. 1.1. For our purposes, these single particle states are identified by the integers from 1 to 21 and also by their quantum members $n\ell j$. n is the principal quantum number, ℓ the orbital angular momentum and j represents the coupling of the spin and orbital angular momentum to a total single particle angular momentum.

The size of the well is determined by the oscillator energy $\hbar\omega$ or alternatively by the size parameter b. They are related according to

$$\hbar\omega = \frac{\hbar^2}{mb^2} \quad . \qquad (1.1)$$

$\hbar\omega$ may be estimated by $\hbar\omega = \hbar^2/mA^{1/3}$ where A is the mass number of the nucleus and m is the nucleon mass. The size parameter is proportional to the radius of the nucleus. It

Fig. 1.1: The sequence of single particle states in the harmonic oscillator. The various levels are identified by the integers from 1 to 21. The various spaces are appropriate for the oxygen region.

Fig 1.1

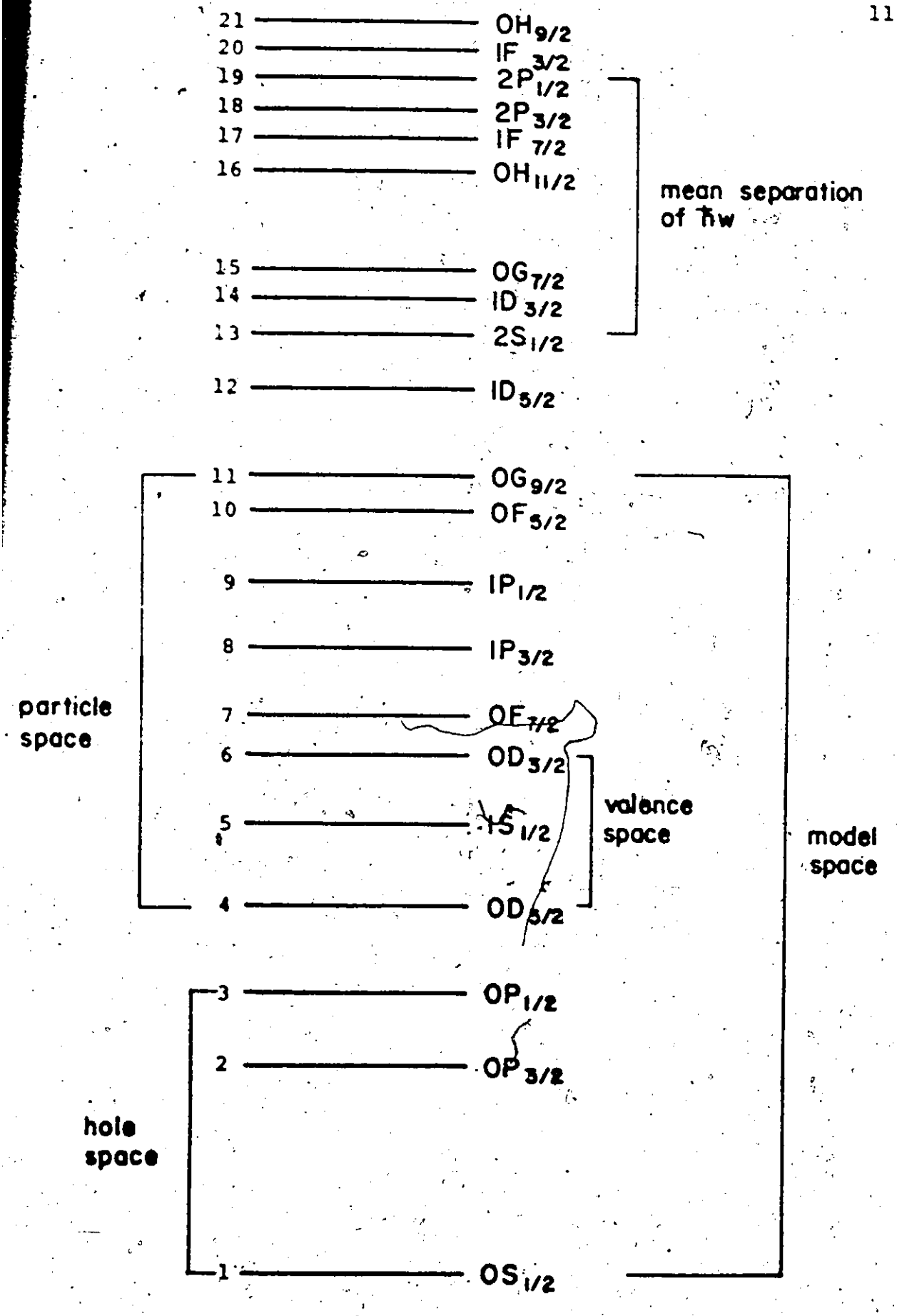
21 $0H_{9/2}$
20 $1F_{3/2}$
19 $2P_{1/2}$
18 $2P_{3/2}$
17 $1F_{7/2}$
16 $0H_{11/2}$
mean separation of $\hbar\omega$
15 $0G_{7/2}$
14 $1D_{3/2}$
13 $2S_{1/2}$
12 $1D_{5/2}$
11 $0G_{9/2}$
10 $0F_{5/2}$
9 $1P_{1/2}$
8 $1P_{3/2}$
7 $0F_{7/2}$
6 $0D_{3/2}$
5 $1S_{1/2}$
4 $0D_{5/2}$
3 $0P_{1/2}$
2 $0P_{3/2}$
1 $0S_{1/2}$
particle space
valence space
model space
hole space

is convenient to remember that $\hbar^2/m = 41.47$ MeV-fm^2. Thus, $b = A^{1/6}$ fm.

The magic nucleus ^{16}O would correspond to having the first three shells fully occupied. Additional nucleons must occupy states in the S-D shell and these are called valence nucleons in the valence model space for ^{18}O. Similarly a deficiency of nucleons in a magic nucleus form hole states. The valence space and nearby states available for occupation by nucleons from the valence space form the particle space. All states considered for the nucleus form the model space.

In general, for more than one valence nucleon, the excited states or the ground state of the nucleus are not adequately described without including a residual or effective interaction between the particles in the valence space. From what we have said, this residual force should exhibit the pairing property. One approach by de Shalit and Talmi (1963) was to parametrize the many particle calculation by the basic set of two body interaction matrix elements required. No assumption is made about the residual interaction apart from that it is a two body force. Determined by a least square fit of the two body matrix elements to the observed spectra, these matrix elements constitute the effective shell model interaction. From this point of view, one need not postulate a two body force which will yield the given matrix elements.

At a more fundamental level one can attempt to start from the free space scattering data and compute the effective interaction matrix elements. One approach uses perturbation theory and is more completely described in Section 2.1. This thesis is concerned with the application of perturbation theory to the fundamental calculation of the effective interaction.

1.3 The Effective Interaction in the Nucleus

According to the shell model, the permitted energy levels of the individual nucleons in the nucleus cluster in shells with a roughly uniform energy spacing between shells which depends on the size of the nucleus. For a light nucleus, the spacing is larger than for a heavy nucleus. To construct a nucleus in this model, one adds neutrons and protons which fill the lowest single particle states first, then the next lowest and so on while satisfying the Pauli exclusion principle. Since each nucleon may have spin up or spin down, each single particle state may contain up to 4 nucleons. The properties of the nucleus as a whole depend on the properties of those states last occupied. In the more advanced version of the shell model, the motion of these last few nucleons, called valence nucleons, is not taken as

uncorrelated. The nuclear properties are defined by the model space and the residual interaction between the particles. This residual interaction cannot be the same as the bare interaction because most of the bare interaction is already taken into account to produce the overall field in which the nucleons move. Secondly, because of the presence of other particles, certain states of the free interaction are not permitted by the Pauli principle. Obviously the effective interaction is model dependent and should be calculated from the bare interaction and the model itself.

Early theorists lacked the prescription to calculate the effective interaction and, therefore, postulated simple analytic forms with adjustable parameters. The most common interactions contained Yukawa or gaussian radial dependence with various space, spin, isospin exchange components. Various degrees of success were obtained with this approach for a given nucleus, but the optimum parameters changed from one nucleus to another. A few of these calculations are now described.

One of the earliest shell model calculations was performed by Kurath (1956) in the 1P shell using a gaussian interaction. Reasonably good results were obtained by including a spin-orbit parameter but its strength changed by a factor of two over nuclei in the 1P shell.

In the S-D shell, Redlich (1955) considered 1, 2, 3 valence nucleons using a gaussian potential and found good agreement as was obtained by Elliott and Flowers (1955) using the Rosenfeld force for mass -18 nuclei. For closed shell nuclei, calculations were done for the odd parity excited states in mass -16 by Elliott and Flowers (1957) and in mass -12 and 16 by Gillet (1964, 1966, 1967) and Gillet and Vinh Mau (1964). Since these early calculations, many attempts have been made to extend the shell model calculations over a wider range of nuclei using even more general phenomenological potentials.

1.4 Microscopic Approach to the Effective Interaction

The more fundamental approach to the effective interaction treats the individual nucleons in constructing the effective interaction. For this reason it is called the microscopic approach. Because of the large number of particles in the nucleus, it is not possible to treat all nucleons equally. In fact, it is hoped that the effect of the nucleons in the core may be small compared to that of the outermost nucleons. Because we have divided the nucleons in the nucleus into two parts (the core and valence nucleons), the interaction between valence nucleons will

consist of two parts. The first is a direct interaction between the valence nucleons. This will, however, be different from the free interaction because of the presence of the other particles. This interaction is hoped to form the larger part of the effective interaction. The second type of interaction involves one valence nucleon interacting with nucleons in the core. The result is an excited core which then interacts with the other valence nucleon. This indirect interaction between the valence nucleons can have a larger range, of the order of the nuclear size, and is likely to have quite different character from the first kind of interaction.

Even though a nucleus will remain in as low an energy state as possible, it may happen that the nucleus spends part of the time in an excited state. These states are not physically observable in a nucleus at rest but quantum mechanically, they may occur provided that their appearance is very brief. The uncertainty principle $\Delta E \Delta t \sim \hbar$ allows this. Such states are called virtual states because they would violate the conservation of energy for a real, observable state.

The interaction between valence nucleons and the core will promote a nucleon in the core to a higher state called a particle state. The unoccupied state remaining is called a hole state. Because of this redistribution of a nucleon from the core, the nucleus has undergone a density

change. This form of interaction is commonly called core polarization for these reasons.

The manner in which we take account of these virtual particle-hole (p-h) excitations, interacting with the valence nucleons and other p-h pairs in the core, leads to different approximations for the core polarization corrections.

The interaction of the p-h pairs with the valence nucleons is called vertex renormalization. The name vertex is used for an elementary two particle interaction. The interaction between p-h pairs is called propagator renormalization. The reason for this name is that the strength of the interaction will determine how the p-h pairs will propagate in the nucleus, i.e., how their wave function varies in time.

The first attempt to calculate the core polarization contribution to the effective interaction was made by Bertsch (1965). He considered the core polarization as consisting of excited single p-h pairs in the core and summed over all possible such pairs. Because only one p-h pair is involved at a time and because of its graphical representation, this approximation is known as the p-h or "bubble" approximation. The large effect that Bertsch found stimulated a more detailed calculation of the effect by Kuo and Brown (1966) and Brown and Kuo (1967) for mass

18 nuclei. Kuo's results for the spectra dramatically approach the experimental values.

Since this early work by Bertsch and Kuo, the theory of the effective interaction has become more and more involved. Here I will briefly outline chronologically the main developments which bear on this work. These are described in more detail in subsequent chapters.

If one bubble gave significant renormalization, then what would the effect of a coherent series of such p-h excitations be? By coherent, we mean that many p-h pairs are excited simultaneously and a disturbance of one p-h pair is felt by all the p-h pairs. This approximation is called the Tamm-Dancoff (TDA) approximation and was calculated by Kuo (1967) with the result that the ground state was lowered and high excited states were raised.

When further correlations are included as in the random phase approximation (RPA), Osnes et al. (1969) and Ellis and Siegel (1970) found the ground state of ^{18}O to be further depressed much below the experimental value. The same result was obtained by Osnes et al. (1971) for mass 42 nuclei. This rather unsatisfactory state of affairs was depressing after the initial success of the one bubble calculation. It appeared that the particle-hole (p-h) force as used, was too strong and that a weakening was required.

A possibility was raised by Osnes et al. (1971), who considered the p-h interaction itself renormalized by bubble core polarization. This effect in electron gas calculations tended to reduce the p-h force and for this reason is now called screening of the p-h interaction. The expectations of Osnes were confirmed when the screened RPA calculation reduced the effective residual interaction to the previous TDA result. This was confirmed by Kirson (1971) who argued that this is physically reasonable. It was apparent that many other physical processes exist which would further renormalize the effective interaction. Kirson and Zamick (1970) considered the renormalization of the coupling between the valence particle and the core to second order in perturbation theory and later (Kirson 1971) to all orders.

This vertex renormalization (black box vertex) is repulsive and raises the ground state energy. The result was that the ground state of ^{18}O was shifted upwards by 3 MeV compared to the RPA interaction. The most sophisticated calculation by Kirson is called self consistent coupled equations (SCCE) because the vertices in the screened propagators are renormalized by TDA propagators and the TDA propagators are renormalized by modified vertices. These are done self consistently (but the results are known to be slightly in error as found by

the present author). Nevertheless the trend is probably correct in that SCCE is very close to the bare interaction.

In addition to the renormalization of the p-p interaction in the valence shell, several calculations have been done to renormalize the p-h interaction between shells. These interactions produce odd parity states of closed shell nuclei. The first was done on ^{16}O by de Takacsy (1967) who found that the core polarization raised the 1^- state much closer to the experimental value but did not change the 3^- significantly. A similar calculation for He^4 was done by Barrett (1968).

Blomquist and Kuo (1969) tried to simulate these effects by using a scaling factor to renormalize the effective interaction. This was necessary because the RPA solutions gave imaginary eigenvalues indicating a lack of self consistency in the assumed ground state wave function. This factor was very nucleus dependent, changing by a factor of 5 between Helium and Lead. A perturbative treatment of p-h states in ^{40}Ca was attempted by Dworzecka and McManus (1971) who included lowest order p-p and h-h interactions in addition to the p-h core polarization process. Using the Sussex matrix elements, the odd parity energy levels of ^{40}Ca were too high and the transition strengths too low. The same result was obtained by Gerace and Green (1968) and Osnes (1971) using the Kuo matrix elements for both the TDA and RPA but the RPA was closer to the experimental levels.

From these papers we see that the RPA fails to bring the ground state low enough in p-h calculations but brings the ground state too low in p-p calculations.

Other processes must be involved which will diminish these drastic results in RPA. One suggestion was made by Osnes et al. (1971) and by Kirson (1971) that the virtual p-h excitations may interact via core polarization itself. This has been called screening of the p-h interaction because the p-h force becomes weaker. The result found by these authors is that for even parity states, the screened RPA reduces to the unscreened TDA result.

When both screening and vertex renormalization are considered self consistently and to all orders, the result is essentially unchanged from those of the bare interaction alone.

CHAPTER II

THEORETICAL METHODS

In this chapter, we briefly describe the tools that are used in this thesis. The use of perturbation theory is described in Section 2.1 and the use of angular momentum algebra in Section 2.2. Finally we describe the two types of bare interactions used for this calculation in Section 2.3.

2.1 Perturbation Theory for the Effective Interaction

In this section, neither a detailed nor rigorous derivation of the perturbative expansion for the effective interactions will be given. This may be found in Bloch and Horowitz (1958), Brandow (1966, 1967, 1970), and Johnson and Baranger (1971). The purpose of this section will be to briefly review the application of perturbation theory through the use of operators for two body interactions and many particle states. The expectation value for the effective interaction leads naturally to contractions and graphical or diagrammatic representations for the processes involved.

The compact Hugenholtz (1957) diagram is used but its relation to the Feynman-Goldstone (1949) diagrams is exhibited, as well as the question of hermiticity, to the core polarization diagrams. Finally we briefly discuss possible, hopefully negligible, improvements in the application of the theory.

The purpose of this theory is to obtain a solution of the many body problem which may not be very different from an exact solution of many non-interacting particles. The many body hamiltonian for A particles is given by

$$H_A = \sum_{i=1}^{A} T_i + \sum_{i\,j}^{A} V_{ij} \quad . \tag{2.1}$$

T_i is the kinetic energy operator for the i^{th} particle and V_{ij} is a two particle interaction between particles i and j. One asks for a solution of the Schroedinger equation given as

$$H_A \psi_A = \varepsilon_A \psi_A \tag{2.2}$$

where ψ_A is the many body wavefunction which determines all observable physical properties for the system. ε_A is the true or physically observable energy of a state of the A particles.

Because of the tremendously large number (3A-3) of degrees of freedom in the realistic nucleus, this equation

cannot be solved exactly. Instead one attempts to isolate those few degrees of freedom which are thought to contribute the most to a given effect and to treat these processes perturbatively in a truncated model space. The success of this approach depends largely on the choice of our unperturbed model for the nucleus. Because of its simplicity and success, the shell model previously described forms the most common zero order model of the nucleus.

The many body hamiltonian is modified to

$$H_A = \sum_i (T_i + U(i)) + \sum_{i<j} V_{ij} - \sum_i U(i) \tag{2.3}$$

$$= H_0 + \sum_{i<j}^{A} V_{ij} - \sum_i U(i) \tag{2.4}$$

where

$$H_0 = \sum_i^A (T_i + U(i)) \quad . \tag{2.5}$$

One may think of U(i) as the usual WS or HO potential well. The hamiltonian H_0 is separable and represents the unperturbed hamiltonian of A non-interacting particles in a central field. The remainder of the hamiltonian H_A will represent a perturbation to the hamiltonian H_0. The Schroedinger equation satisfied by H_0 is

$$H_0\phi_i = \epsilon_i\phi_i \tag{2.6}$$

where ϕ_i is the i^{th} state of A particles with energy ϵ_i and is a Slater determinant of A single particle states. Since the $\{\phi_i\}$ form a complete set, the true many body wavefunction may be expanded in terms of them.

$$\psi_A = \sum_{i=1}^{\infty} a_i\phi_i \tag{2.7}$$

In practice, this series is truncated. The single particle states or orbitals, which are used to construct ϕ_i, can be divided into three classes: a) A fully occupied states, b) A states not fully occupied and the unoccupied states are in the valence space, and finally c) A states not fully occupied, and the unoccupied states are above the valence space in energy. The model space consists of the first two classes.

We define a projection operator P_d by

$$P_d\psi_A = \psi_d \tag{2.8}$$

where ψ_d is the many body wavefunction restricted to the model space. In other words, the expansion of ψ_A consists of states of the first two classes.

In this light, the problem is to find an effective many body hamiltonian H_{eff} with the property that

$$H_{eff}\psi_d = \epsilon\psi_d \quad . \tag{2.9}$$

Then the Schroedinger equation for the effective hamiltonian in a truncated model space will lead to the same energy as the exact hamiltonian in the entire space.

The effective hamiltonian depends on the model of the nucleus and as such depends on the model hamiltonian given by

$$H_{eff} = H_0 + V_{eff} \quad . \tag{2.10}$$

The problem then is the determination of the effective model interaction V_{eff}.

The theoretical derivation of V_{eff} will not be given here since it may be found in many places. For example, from Barrett (1971), and Barrett and Kirson (1972), we have

$$V_{eff}(E) = V + V \frac{Q}{E-H_0} V_{eff}(E) \quad . \tag{2.11}$$

V is the free space two body interaction, E the exact eigenvalue of the true hamiltonian and Q is a projector outside the model space. It ensures that the intermediate states are orthogonal to the states in the model space.

Unfortunately the exact eigenvalue E that we are seeking is needed to find the effective interaction which depends on the energy E. This unsatisfactory state was

remedied by Goldstone (1957) and Brandow who showed that one could replace Eq. (2.11) by

$$V_{eff}(E_0) = V + V\{\frac{Q}{E_0-H_0} V_{eff}(E_0)\}_{linked} \quad . \qquad (2.12)$$

In the perturbation expansion, one must include only those terms that are represented by linked diagrams, including folded diagrams. This is known as the Linked Cluster Theorem.

The convergence of the expansion in Eq. (2.12) depends on the strength of the interaction V which is probably very strong at short ranges. This interaction strength may cause the valence particles to scatter into highly excited states which are not a part of the model space. This effect was calculated approximately by Brueckner et al. (1954, 1955, 1958) to obtain a G-matrix defined by

$$G(E_0) = V + V \frac{Q_{2p}}{E_0-H_0} G(E_0) \quad . \qquad (2.13)$$

This equation will be discussed in more detail in Section 2.3. The G-matrix so obtained is much weaker than the bare interaction at short range. When it is used in the expansion for V_{eff} as in Eq. (2.14)

$$V_{eff}(E_0) = G + G \frac{\tilde{Q}}{E_0-H_0} V_{eff}(E_0) \quad , \qquad (2.14)$$

one hopes that only a few terms are necessary for convergence. The operator $\tilde{Q}$ now allows intermediate states which do not include two particle ladders. Equation (2.14) is an operator equation but the terms in it have both a graphical and algebraic interpretation. The algebraic formalism is based on the convenient notation of "second quantization". Each of the operators G can be written in the form

$$G(r) = \frac{1}{2} \sum_{\alpha\beta\gamma\delta} \langle\alpha\beta|G|\gamma\delta\rangle_{N.A.} \; a_\alpha^\dagger a_\beta^\dagger a_\delta a_\gamma \qquad (2.15)$$

where the two body matrix elements $\langle\alpha\beta|G|\gamma\delta\rangle_{N.A.}$ are not antisymmetrized. The Greek letters represent single particle states. The operators $a_\mu^\dagger$, a_μ are single particle creation and annihilation operators, and satisfy the usual anti-commutation relations for fermions.

$$\{a_i, a_j^\dagger\}_+ = \delta_{ij} \; . \qquad (2.16)$$

The matrix elements of G have a graphical representation in terms of Feynman-Goldstone diagrams shown in Fig. 2.1. The interpretation of Fig. 2.1 is that two particles in initial states γ,δ at time t_1, interact at time t_2 and scatter into the final states α,β at t_3. Since the G interaction is scalar, the total angular momentum and parity are conserved.

Fig 2.1

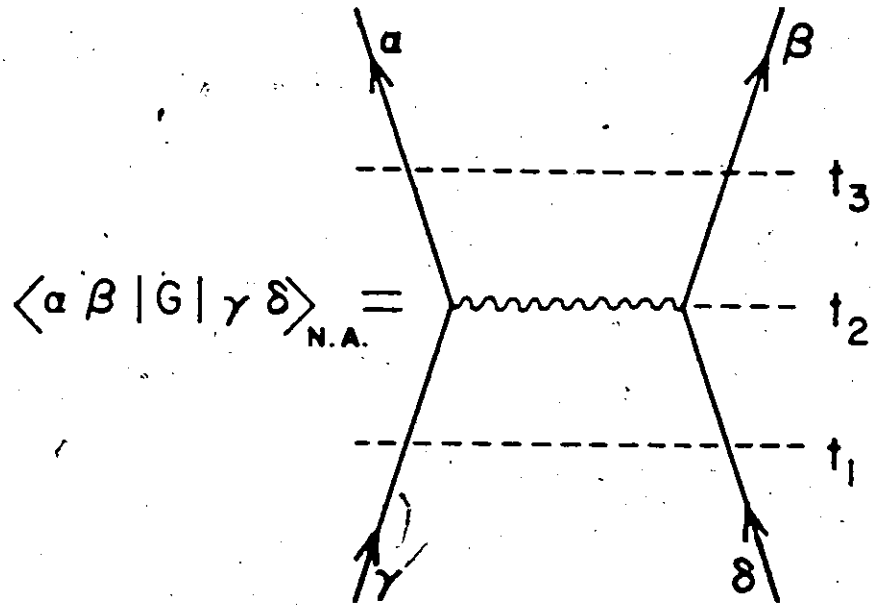

Diagrammatic representation for a G-matrix element that is not antisymmetrized.

The upward arrows imply that the states are occupied by particles.

In order to satisfy the antisymmetry property of many particle wavefunctions, it is convenient to define an antisymmetrized two body matrix element $\langle \alpha\beta|G|\gamma\delta\rangle_{A.S.}$ as shown in Fig. 2.2. The second diagram on the right is preceded by a minus sign due to the interchange of the two annihilation operators a_β and a_γ. The antisymmetrized G interaction is now represented by a dot. This is called a Hugenholtz diagram.

For A particles in the nucleus, we would need A creation operators. However, in our perturbative approach, only the nucleons near the Fermi surface are involved and these usually form a small fraction of the total number of nucleons in the nucleus. Therefore, we will simplify the discussion by omitting consideration of any particles which remain in their normal position. The normal state of the nucleus is then considered to be like the vacuum state of quantum electrodynamics. Instead of a vacuum state of no particles, we use a state containing a finite number of particles. This state will usually represent a magic nucleus. For example, instead of writing

$$|^{18}O\rangle = \prod_i^{18} a_i^\dagger |0\rangle \qquad (2.17)$$

Fig 2.2

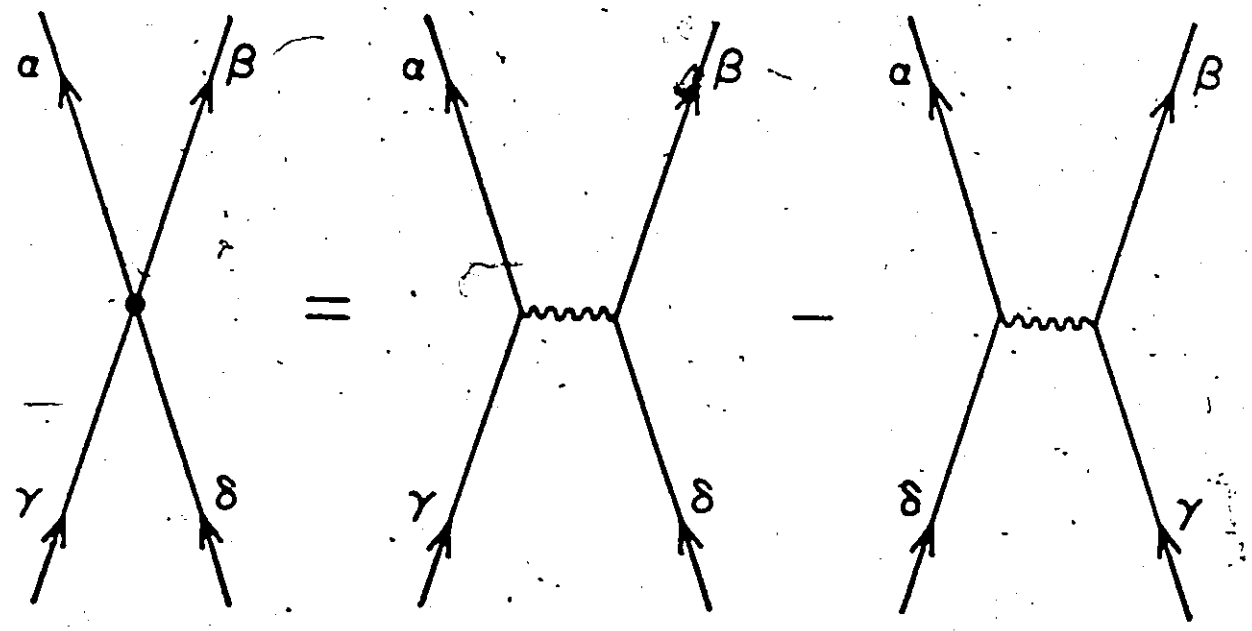

Hugenholtz representation of an antisymmetrized G interaction.

where $|0\rangle$ is the state of no particles, we have

$$|^{18}O\rangle = \prod_{i=1}^{2} a_i^\dagger \, |\tilde{0}\rangle \tag{2.18}$$

where the vacuum state $|\tilde{0}\rangle$ now represents $|^{16}O\rangle$. Characterizing the state $|\tilde{0}\rangle$ is its Fermi energy ε_F. Orbitals whose energies are greater than the Fermi energy are called particle states. Graphically they are indicated by an upward arrow. Orbitals whose energies are smaller than the Fermi energy are called hole states. When a particle is removed from such a state, it is identified by downward pointing arrows. With the new definition of vacuum state, it is no longer true that for all i

$$a_i|\tilde{0}\rangle = 0 \quad . \tag{2.19}$$

It is true only if i represents an empty state in $|\tilde{0}\rangle$. The operator a_i is said to "create a hole state".

To see how to obtain the graphical representation for the effective interaction, consider the second order matrix element $\langle P_3P_4|G\frac{Q}{e}G|P_1P_2\rangle$ shown in Fig. 2.3. The initial state is given by

$$|P_1P_2\rangle = a_{P_1}^\dagger \, a_{P_2}^\dagger \, |\tilde{0}\rangle \tag{2.20}$$

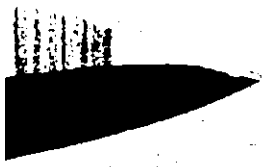

Fig. 2.3: Location of initial and final states, and two G interactions before contractions are made.

Fig 2.3

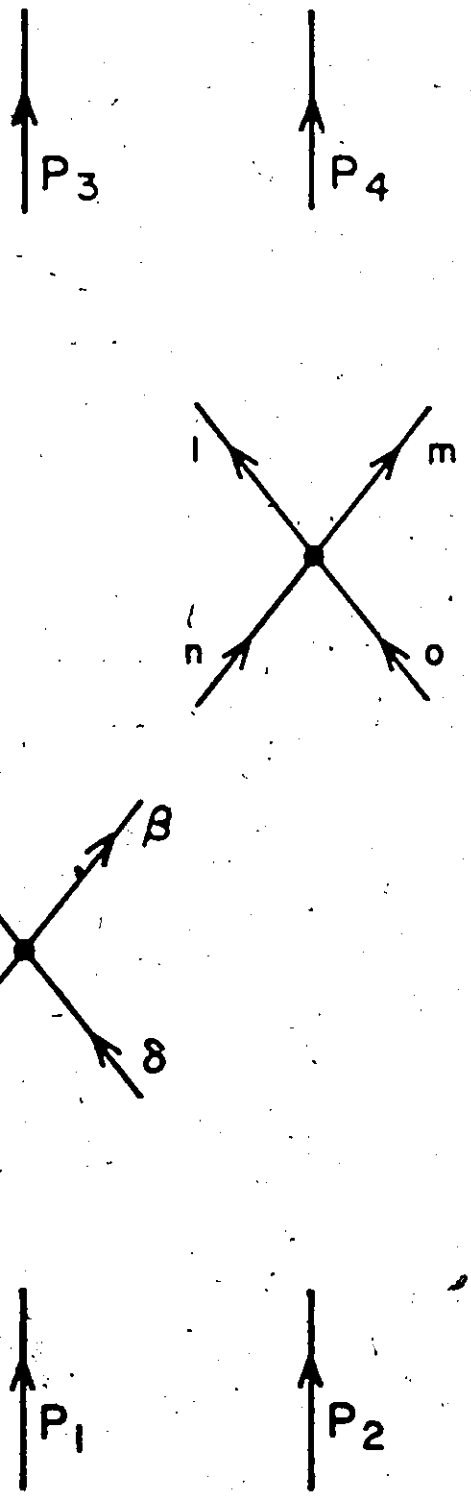

According to Wick's Theorem, the expectation value of a product of operators is given by the sum of all possible contractions of pairs of operators. In Fig. 2.3, a contraction is equivalent to joining two lines together whose arrows are pointing in the same direction and having the same label.

In our case $|\tilde{0}\rangle$ is not a true vacuum so Wick's Theorem must be modified. As shown in Gillet (1966a), for example, one has

$$\begin{aligned}
&\overbrace{a_\alpha a_\beta^\dagger} = \delta_{\alpha\beta} && \text{if } \epsilon_\alpha > \epsilon_F \ , \\
&\overbrace{a_\alpha a_\beta} = 0 && \text{otherwise} \ , \\
&\overbrace{a_\alpha^\dagger a_\beta} = \delta_{\alpha\beta} && \text{if } \epsilon_\alpha < \epsilon_F \ , \\
&\overbrace{a_\alpha^\dagger a_\beta^\dagger} = 0 && \text{otherwise} \ .
\end{aligned} \tag{2.21}$$

In order to illustrate all diagrams in second order as they are obtained from contractions, we represent the interaction G by  . The raised portion contains the two creation operators and the other portion contains two annihilation operators. All topologically distinct contractions in second order are shown in Fig. 2.4. Contractions involving two operators in the same portion of  are equivalent because they correspond to

Fig. 2.4: All possible contractions in second order and their diagrammatic representation obtained from Fig. 2.3.

Fig 2.4

a)

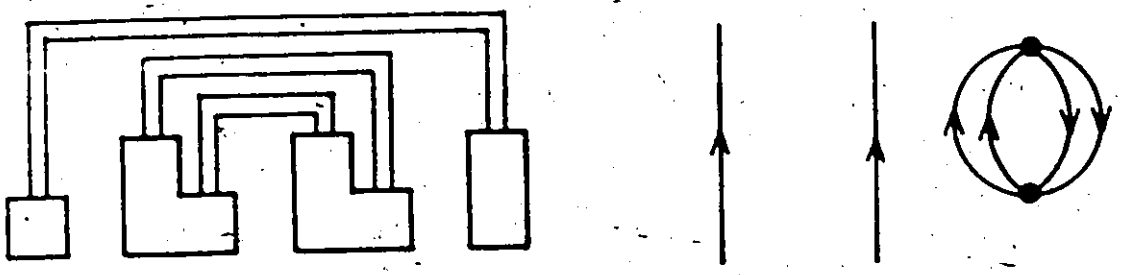

b)

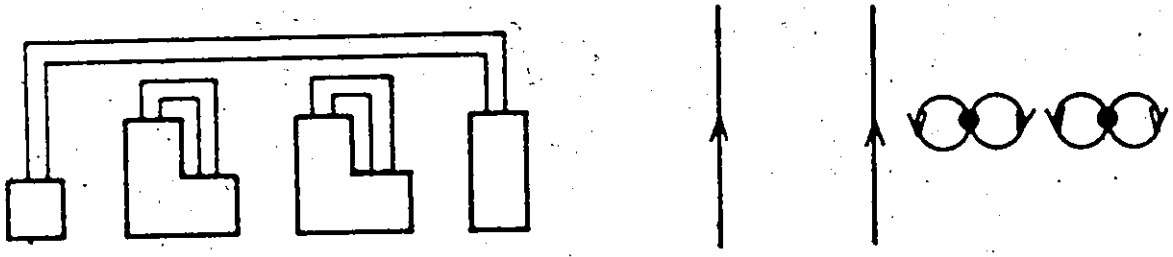

c)

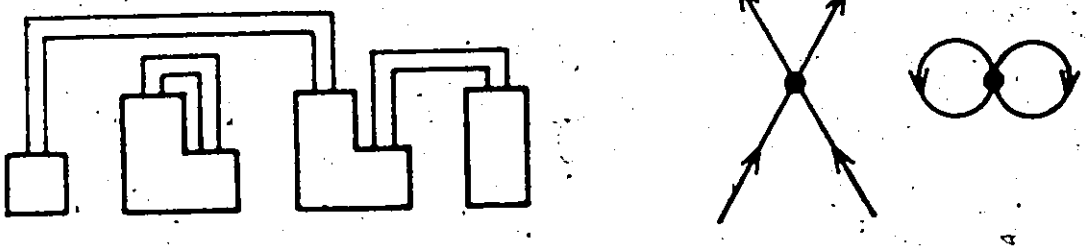

d)

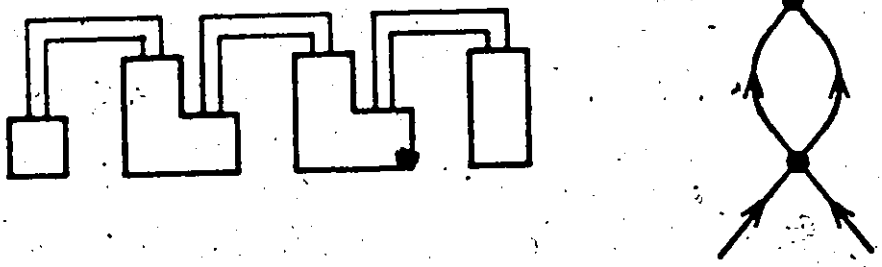

Fig 2.4

e)

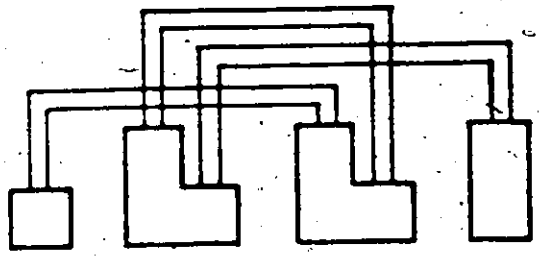

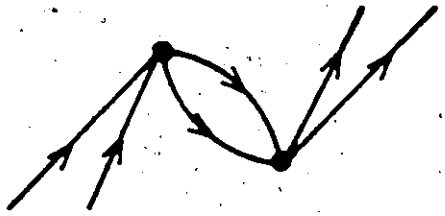

f)

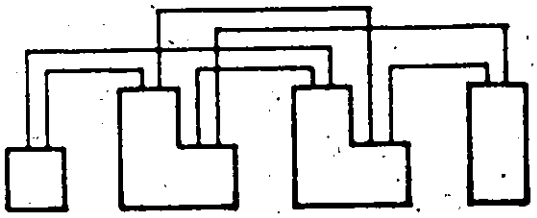

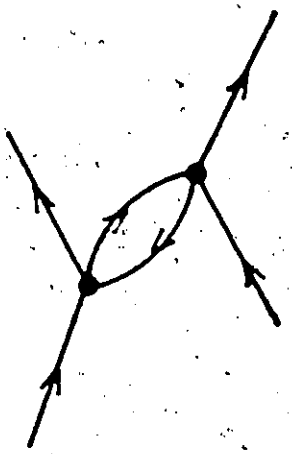

g)

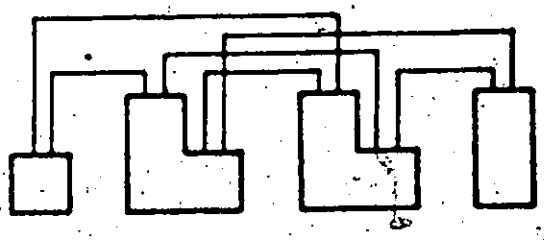

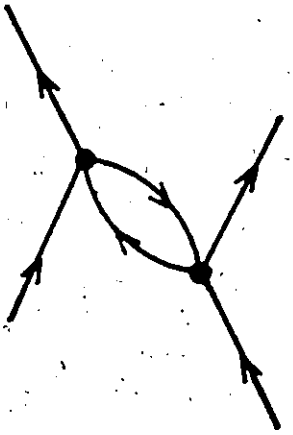

antisymmetrized diagrams. Not all diagrams in Fig. 2.4 are contained in the expansion of V_{eff} to second order. Because of the famous "Linked Cluster Theorem" proved originally by Goldstone, one need not include the contributions from unlinked diagrams.

Figures 2.4(a), (b), (c) are the unlinked graphs in second order, and must not be included in the effective interaction. They actually represent contributions to the energy of our vacuum state. Figures 2.4(d), (e), (f), (g) are second order linked diagrams. However, in Fig. 2.4(d), the intermediate state is a two particle state and has already been included in the G-matrix. Thus ladders of G-matrices between two particles must not be counted. Figure 2.4(e) is topologically equivalent to Fig. 2.4(d), but has an intermediate state of 4p-2h and is a legitimate contribution to the effective interaction. By topologically equivalent diagrams, we mean a diagram that can be twisted or stretched to yield a second diagram. If you stretch Fig. 2.4(e) by pulling on the initial and final states, you will obtain Fig. 2.4(d). By pulling on the contractions shown in Fig. 2.4(e), one will also "unwrap" the contractions to get those contractions of Fig. 2.4(d). In Fig. 2.4(f) are shown the lowest order core polarization diagrams. The intermediate state consists of 3p-1h. Figure 2.4(g) is topologically equivalent to Fig. 2.4(f). By interchanging the order of the two middle interactions

and pulling along the lines of contraction, you obtain the same set of contractions. In this thesis, we will consider only diagrams of the core polarization type. Although neither Fig. 2.4(f) nor Fig. 2.4(g) produce an effective interaction that is hermitian, their sum is hermitian. In graphology, hermiticity is ensured when the diagrams are invariant with respect to the direction in which time travels in the diagram. Since these are Hugenholtz diagrams, each diagram actually represents all the possible exchange diagrams as well. For example, Fig. 2.5 shows all the exchange diagrams of Fig. 2.4(f) which are included when antisymmetrized matrix elements are used. To check this result, compress all the interaction lines into a dot, now all the exchange diagrams should be identical to the Hugenholtz form. In an n^{th} order diagram with n dots, each dot can be stretched in two ways. There are 2^n exchange diagrams. The sign of a diagram depends on the type of matrix elements one is using. If only two particle matrix elements are used, then Brandow has given rules to determine the sign of the diagram. However, we will be using essentially p-h matrix elements and these have a sign opposite to the p-p matrix elements. It has been the author's practice to determine the sign of a diagram by writing down the possible contractions and using Wick's Theorem. When the contractions are written in normal order,

Fig 2.5

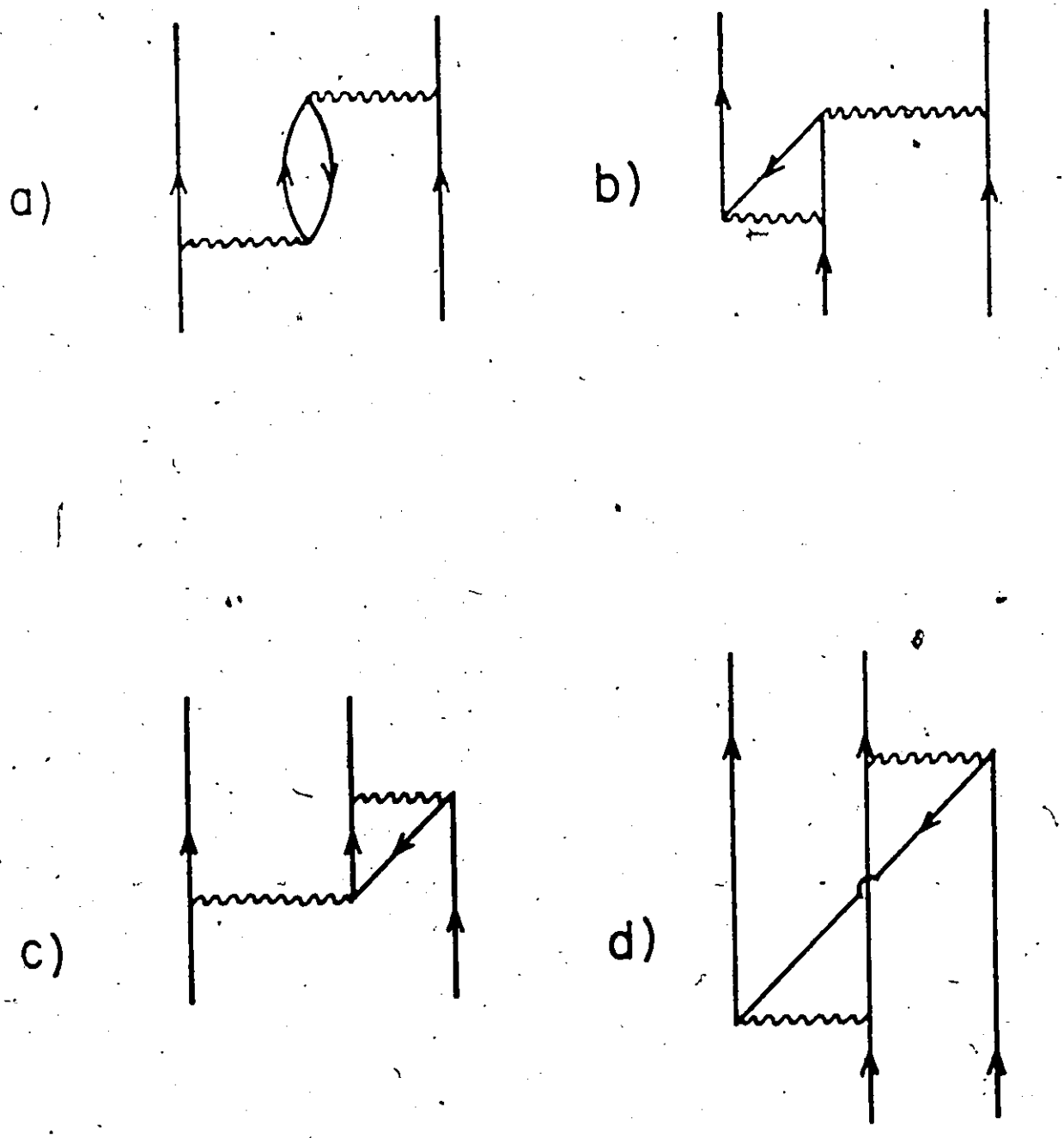

The four exchange diagrams obtained from Fig. 2.4(f) when antisymmetrized matrix elements are used.

the sign of the diagram is equal to the sign of the ___ contractions.

Another technical point concerns the type of G-matrices used in the expansion. When the G-matrix elements are calculated, the energy denominator

$$\frac{1}{E_0-H_0} \tag{2.22}$$

depends on the energy of the initial state as well as the entire intermediate state. When the G-matrix elements are calculated using only the energies of the initial state and of the 2p intermediate state, we say the G-matrix element is "on the energy shell". When the energy denominator depends on other states as well, we say the G-matrix element is "off the energy shell". Both Kirson and ourselves use G-matrix elements which are on the energy shell. Nothing is done about off the energy shell variation. However, not all G-matrix elements inside a deep diagram need be off the shell. Brandow has shown that in some cases, G-matrix elements can be put on shell by a procedure he calls generalized time ordering.

Another problem ignored in our application of perturbation theory is the possible Pauli violation in the intermediate states. Brandow has proven that the Pauli principle will be satisfied in total when all diagrams of a given order are summed even though in individual diagrams

it is violated. The problem arises when the summation over particle states from p-h excitations of the core occurs in the same shell as the valence shell. The core polarization contributions that we have calculated, which are not the complete order by order calculation, should not be seriously in violation of the Pauli principle. Firstly, there are only a couple of valence nucleons in the valence shell and so any given single particle state has low probability of occupancy. This would not be true if the shell were more than half full. Secondly, the next higher shell which contains more single particle states than the valence shell also contributes to the core polarization. These do not violate the Pauli principle and are much greater in number than the violating terms.

2.2 Angular Momentum Algebra

When we begin a study of perturbation theory we are immediately faced with extensive use of angular momentum algebra. The reason is that nuclear forces are invariant under a rotation in real space which implies that angular momentum is conserved. This means that in nuclear structure calculations one can consider the states of given total angular momentum, J, separately from states of other J.

This simplifies the calculation by reducing the dimensionality of the space where one is working. In order to exploit this simplification, angular momentum algebra has been invented.

The simplest problem is that of adding two angular momenta to get the state of good total, $\vec{J} = \vec{j}_1 + \vec{j}_2$. Even in this simplest problem, a phase convention (Condon-Shortley (1959)) has to be adopted in order to have consistent results. Alternatively, everyone must use the same Clebsch-Gordon coefficients. When several particles are involved, the necessity for consistent phase conventions is even greater. In this section our phase conventions will be established and angular momentum algebra applied to the reduction of a perturbation diagram into its simplest two body components.

A given multi-particle, multi-hole wavefunction coupled to total angular momentum J and z component M may be written as

$$|JM\rangle = [\pi_i \xi^{\dagger}_{j_i m_i}]^{JM} |\tilde{0}\rangle \quad . \tag{2.23}$$

The single particle operator $\xi^{\dagger}_{j_i m_i}$ either creates a particle or hole of angular momentum j_i, m_i. In this section we will omit the isospin quantum numbers for the sake of simplicity, but they may easily be included later.

For the hole states, the phase convention shown below is identical to that of Mavromatis et al. (1967) and

Dieperink et al. (1968) but differs from that of Gillet. These operators are replaced according to the following transformation after they have been uncoupled

$$\text{particle states} \quad \left.\begin{aligned} \xi^{+}_{\alpha m_\alpha} &= a^{+}_{\alpha m_\alpha} \\ \xi_{\alpha m_\alpha} &= a_{\alpha m_\alpha} \end{aligned}\right\} \text{ if } \epsilon_\alpha > \epsilon_F \tag{2.24}$$

$$\text{hole states} \quad \left.\begin{aligned} \xi_{\alpha m_\alpha} &= (-)^{\alpha+m_\alpha} a^{+}_{\alpha -m_\alpha} \\ \xi^{+}_{\alpha m_\alpha} &= (-)^{\alpha+m_\alpha} a_{\alpha -m_\alpha} \end{aligned}\right\} \text{ if } \epsilon_\alpha < \epsilon_F .$$

This application will be demonstrated later in this section when hole states appear.

In our model the single particle or single hole states are the states in the harmonic oscillator. Each particle has orbital angular momentum l and z component m; as well, the nucleons are fermions of total spin $S = \frac{1}{2}$ and z component $+\frac{1}{2}$ or $-\frac{1}{2}$. The total angular momentum j is obtained by coupling the orbital to spin angular momentum in that order. For two particles, the total angular momentum is the coupling of the two single particle momenta. For this reason, it is called the j-j coupling scheme.

$$\vec{j}_1 = \vec{l}_1 + \vec{s}_1$$

$$\vec{j}_2 = \vec{l}_2 + \vec{s}_2 \qquad (2.25)$$

$$\vec{J} = \vec{j}_1 + \vec{j}_2 \ .$$

The single particle state in the harmonic oscillator may be written as (Brody and Moshinsky (1960))

$$|nlsjt\rangle = R_{nl}(r)\,[Y^{l}_{m}(\Omega)\,\chi^{s}_{ms}]^{j}_{m}\,\phi^{t}_{mt} \ , \qquad (2.26)$$

where ϕ^{t}_{mt} represents the isospin wavefunction. For a two particle harmonic oscillator state, the angular momentum may be coupled to good total J and total isospin T. The product wavefunction may be rewritten in terms of a center of mass wavefunction times a wavefunction in the relative coordinate according to the Moshinsky transformation. This is very convenient since the nuclear force is given in terms of the relative coordinate. A two body matrix element may then be written as a sum over relative matrix elements only. The required expression has been given by Shakin et al. (1967) and is shown below. The two body matrix elements are normalized and antisymmetrized.

$$\langle (n_1 \ell_1 \tfrac{1}{2}) j_1 (n_2 \ell_2 \tfrac{1}{2}) j_2 JM_J TM_T | V | (n_3 \ell_3 \tfrac{1}{2}) j_3 (n_4 \ell_4 \tfrac{1}{2}) j_4 JM_J TM_T \rangle$$

$$= \frac{1}{\sqrt{(1+\delta_{n_1 n_2}\delta_{\ell_1 \ell_2}\delta_{j_1 j_2})(1+\delta_{n_3 n_4}\delta_{\ell_3 \ell_4}\delta_{j_3 j_4})}} \sum_{\substack{\lambda\lambda' J' nn' \ell\ell' \\ NLS}}$$

$$\times (-)^{\lambda+\lambda'} \hat{J}\hat{\lambda}\hat{\lambda}'\hat{S}\sqrt{\hat{j}_1\hat{j}_2\hat{j}_3\hat{j}_4}$$

$$\times \langle n_1 \ell_1 n_2 \ell_2 \lambda | n \ell N L \lambda \rangle \langle n_3 \ell_3 n_4 \ell_4 \lambda | n' \ell' N L \lambda' \rangle$$

$$\times \begin{Bmatrix} \ell_1 & \ell_2 & \lambda \\ \frac{1}{2} & \frac{1}{2} & S \\ J_1 & J_2 & J \end{Bmatrix} \begin{Bmatrix} \ell_3 & \ell_4 & \lambda' \\ \frac{1}{2} & \frac{1}{2} & S \\ J_3 & J_4 & J \end{Bmatrix} \cdot \begin{Bmatrix} L & \ell' & \lambda' \\ S & J & J' \end{Bmatrix} \begin{Bmatrix} L & \ell & \lambda \\ S & J & J' \end{Bmatrix}$$

$$\times \left(\frac{1 - (-)^{\ell+s+T}}{2}\right) \langle (n\ \ell\ s) J' | V | (n'\ \ell'\ s) J' \rangle \quad . \qquad (2.27)$$

The symbol $\hat{x} = 2x + 1$. The $\langle n_1 \ell_1 n_2 \ell_2 \lambda | n \ell N L \lambda \rangle$ are defined in Brody. The $\begin{Bmatrix} \ell, \ell, L \\ s, s, S \end{Bmatrix}$ and $\begin{Bmatrix} \ell, \ell, \lambda \\ s, s, S \\ J, J, J \end{Bmatrix}$ symbols are defined in Talmi (1963). The matrix elements $\langle (n\ \ell\ s) J' | V | (n'\ \ell'\ s) J' \rangle$ in the relative coordinate are the fundamental quantities in this calculation. They contain all we need to know about the two body force in the structure calculation.

Shown in Fig. 2.6 are all possible two body vertices in the Hugenholtz notation. Figure 2.6(a) is the basic two

Fig. 2.6: Various types of elementary two body vertices and angular momentum coupling.

Fig 2.6

a) $\langle (ab)JT|G|(cd)JT\rangle$ =

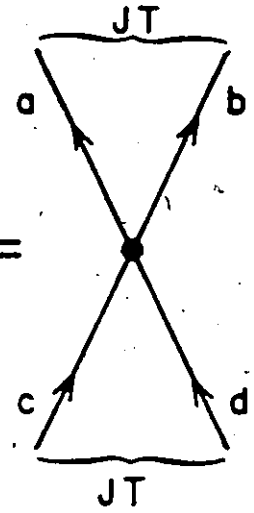

b)

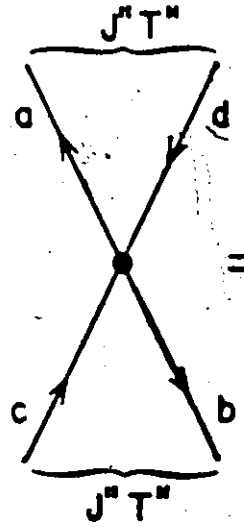

= $\langle (ad^{-})J"T"|G|(cb^{-})J"T"\rangle$

c) $\langle \{b(ad^{-})J'T'\}ct|G|ct\rangle$ =

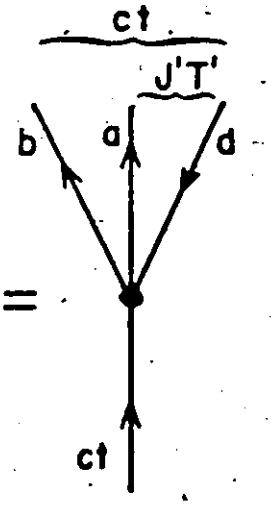

Fig 2.6

d) $\langle (ad^-)JT(bc^-)JT\}00|G|0\rangle =$

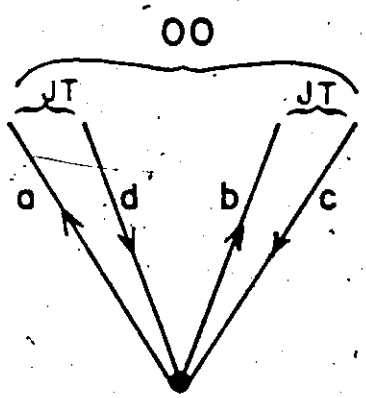

e)

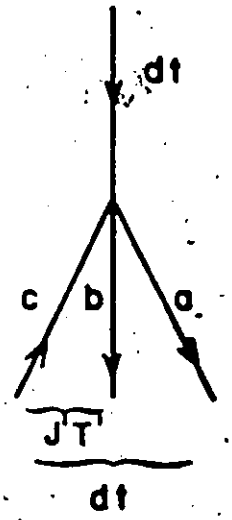

$= \langle d^-t|G|\{a^-(cb^-)J'T'\}dt\rangle$

body p-p matrix element defined as in Eq. (2.27) in terms of the relative matrix elements. The particle-hole vertex in Fig. 2.6(b) may be obtained from the p-p matrix elements as will be shown in Appendix C. The transformation is given below as well as in Dieperink et al. (1968) and Kirson (1971).

The application of angular momentum algebra and the contractions leading to these transformations and phase conventions is given in Appendix C.

$$\langle (ad^{-})J''T''|G|(cb^{-})J''T''\rangle = -\sqrt{(1+\delta_{cd})(1+\delta_{ab})}$$

$$\times \sum_{JT} \hat{J}\hat{T} \begin{Bmatrix} a & d & J'' \\ c & b & J \end{Bmatrix} \begin{Bmatrix} \frac{1}{2} & \frac{1}{2} & T'' \\ \frac{1}{2} & \frac{1}{2} & T \end{Bmatrix}$$

$$\times \langle (ab)JT|G|(cd)JT\rangle \quad (2.28)$$

In Fig. 2.6(c) is a 1p-2p-1h vertex which is related by a factor to the p-h vertex as follows:

$$\langle (b(ad^{-})J'T')ct|G|ct\rangle = \sqrt{\frac{\hat{J}'\cdot\hat{T}'}{\hat{c}\hat{t}}}\,\langle (ad^{-})J'T'|G|(cb^{-})J'T'\rangle. \quad (2.29)$$

In Fig. 2.6(d) is shown a 2p-2h vertex which is related to the p-h vertex as follows:

$$\langle\{(ad^-)JT(bc^-)JT\}00|G|0\rangle = (-)^{b+c+1+J+T}\sqrt{\hat{J}\hat{T}}$$

$$\times \langle(ad^-)JT|G|(cb^-)JT\rangle \quad . \tag{2.30}$$

In Fig. 2.6(e) is a 1h-2h-1p vertex which is related to the p-h vertex as follows:

$$\langle d^-t|G|\{a^-(cb^-)J'T'\}dt\rangle = (-)^{a+d+1+J'+T'}\sqrt{\frac{\hat{J}'\cdot\hat{T}'}{\hat{d}\hat{t}}}$$

$$\times \langle(ad^-)J'T'|G|(cb^-)J'T'\rangle \quad . \tag{2.31}$$

The diagrams in Fig. 2.6 are given a slightly different notation and value by Kirson to facilitate sums. The relationship between his definition and mine is given below

$$\langle(ab)JT|G|(cd)JT\rangle = G(abcd,JT)$$

$$\langle(ad^-)JT|G|(cb^-)JT\rangle = f(ad,cb,JT)$$

$$\langle\{b(ad^-)JT\}ct|G|ct\rangle = \frac{(-)^{b+\frac{1}{2}}}{\sqrt{\hat{c}\hat{t}}}\,v(c,b(ad)JT)$$

$$\langle\{(ad^-)JT(bc^-)JT\}00|G|0\rangle = (-)^{J+T}\sqrt{\hat{J}\hat{T}}\,B(ad,bc,JT)$$

$$\langle d^-t|G|\{a^-(cb^-)JT\}dt\rangle = \frac{(-)^{d-\frac{1}{2}+J+T}}{\sqrt{\hat{d}\hat{t}}}\,v'(a,d(cb)JT) \quad . \tag{2.32}$$

Once these basic vertices are defined, it is immediately possible to calculate higher order perturbation diagrams. Shown in Fig. 2.7 are the four core polarization diagrams required to produce an antisymmetrized and hermitian matrix element of the effective interaction. The interior bubble represents some description of the core polarization. The analytic expression for Fig. 2.7(a) when the core is represented by a single bubble is

$$\langle (p_2p_4)JT | G_{c\text{-}p} | (p_1p_3)JT \rangle = \frac{(-)^{p_3+p_4+J+T}}{\sqrt{(1+\delta_{p_1p_3})(1+\delta_{p_2p_4})}}$$

$$\times \sum_{\substack{\text{Ph} \\ J''T''}} \begin{Bmatrix} p_1 & p_2 & J'' \\ p_4 & p_3 & J \end{Bmatrix} \begin{Bmatrix} \frac{1}{2} & \frac{1}{2} & T'' \\ \frac{1}{2} & \frac{1}{2} & T \end{Bmatrix}$$

$$\times v(p_1,p_2(ph)J''T'') \frac{1}{\epsilon}$$

$$\times v(p_4,p_3(ph)J''T'') \quad (2.33)$$

The quantity ϵ is the energy denominator and is defined for Fig. 2.7(a) as

$$\epsilon = \epsilon_{p_2} + \epsilon_p - \epsilon_h - \epsilon_{p_1} \quad (2.34)$$

where ϵ_a are the unperturbed single particle energies in the model.

Fig. 2.7: The four distinct diagrams required to produce an antisymmetrized and hermitian core polarization interaction. The black areas indicate different approximations to the core vibrations.

Fig 2.7

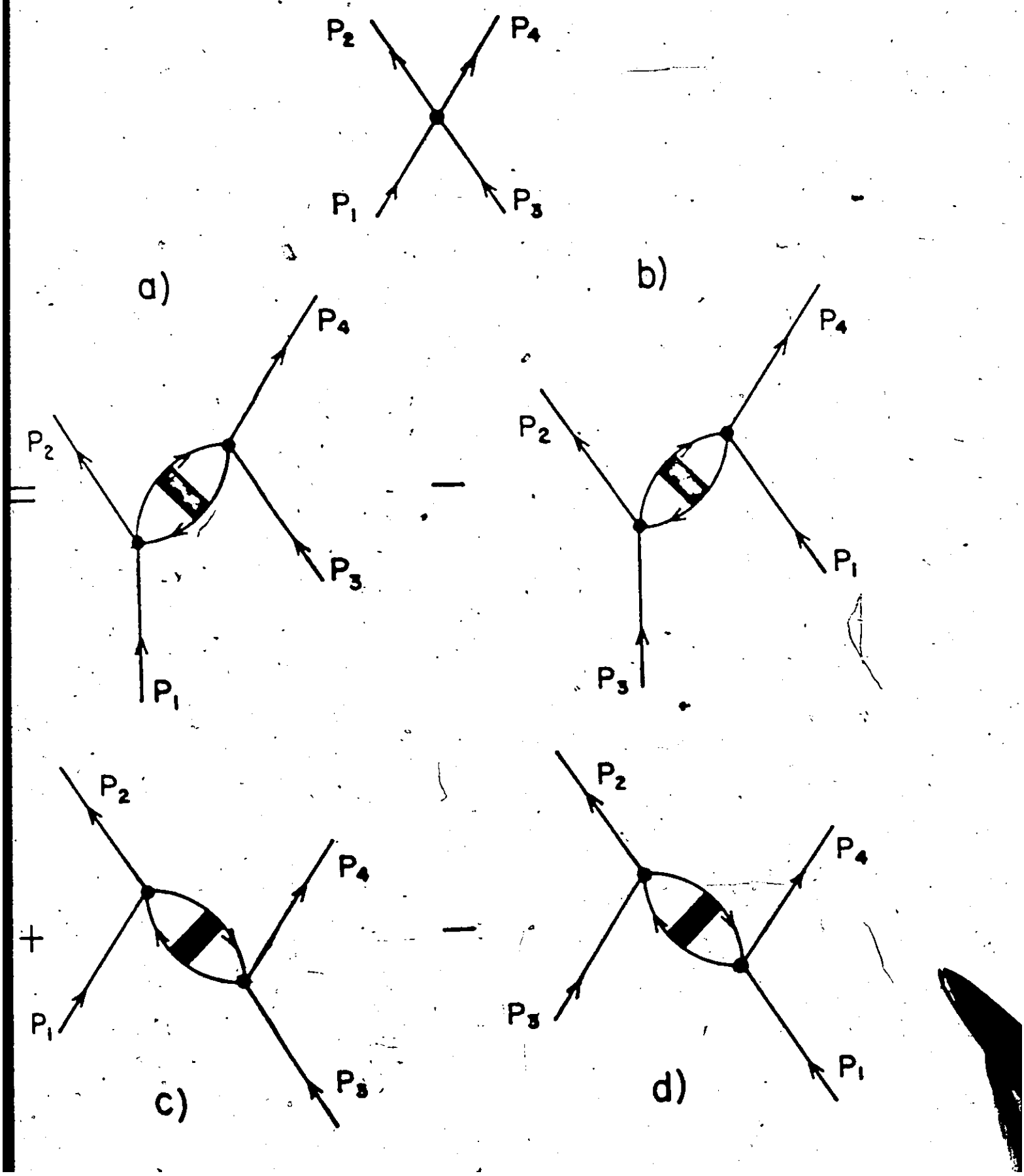

The analytic expression for Fig. 2.7(c) is different from Eq. (2.33) because of the time reversal of the interior bubble. However, it is easily shown that Fig. 2.7(c) is related to Fig. 2.7(a) as shown in Fig. 2.8. Equation (2.33), therefore, may be used for all diagrams in Fig. 2.7 with an appropriate relabelling of the external lines.

In addition to renormalization of the effective p-p interaction, the coupling of the valence particle to the core excitations may themselves be renormalized.

The renormalized vertex is called the "black box" vertex, denoted by the subscript bb. As shown in Fig. 2.9, the equation for TDA screening of the p-h interaction is

$$
\begin{aligned}
v_{bb}(P_1,P_2(Ph)J''T'') = {} & v(P_1,P_2(Ph)J''T'') + \sum_{\substack{P'h' \\ JT}} (-)^{J''+T''+J+T} \sqrt{\hat{J}''\hat{T}''\hat{J}\hat{T}} \\
& \times \begin{Bmatrix} P_1 & P_2 & J'' \\ h & P & J \end{Bmatrix} \begin{Bmatrix} \frac{1}{2} & \frac{1}{2} & T'' \\ \frac{1}{2} & \frac{1}{2} & T \end{Bmatrix} \\
& \times \{ v(P_1,P(P'h')JT)\,[\varepsilon+\mathfrak{f}^{JT}]^{-1} f^{JT}(P_2h,P'h',JT) \\
& + v(P,P_1(P'h')JT)\,[\varepsilon+\mathfrak{f}^{JT}]^{-1} B(P'h',P_2h,JT) \}.
\end{aligned}
\tag{2.35}
$$

A corresponding expression exists for v'_{bb}, but a relation to v_{bb} was discovered and this was used in the actual calculation. It depends on the fact that

Fig 2.8

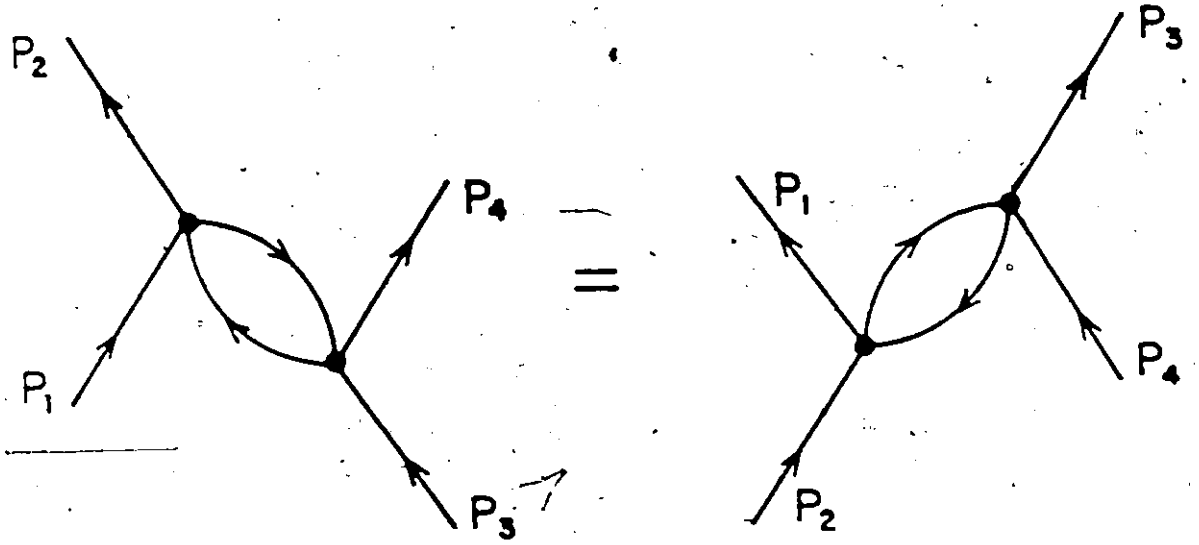

Equality of second order diagrams based on angular momentum algebra.

Fig. 2.9: Typical sequence of diagrams defined for the black box vertex. Higher order diagrams contain greater number of bubbles between the external vertices.

Fig 2.9

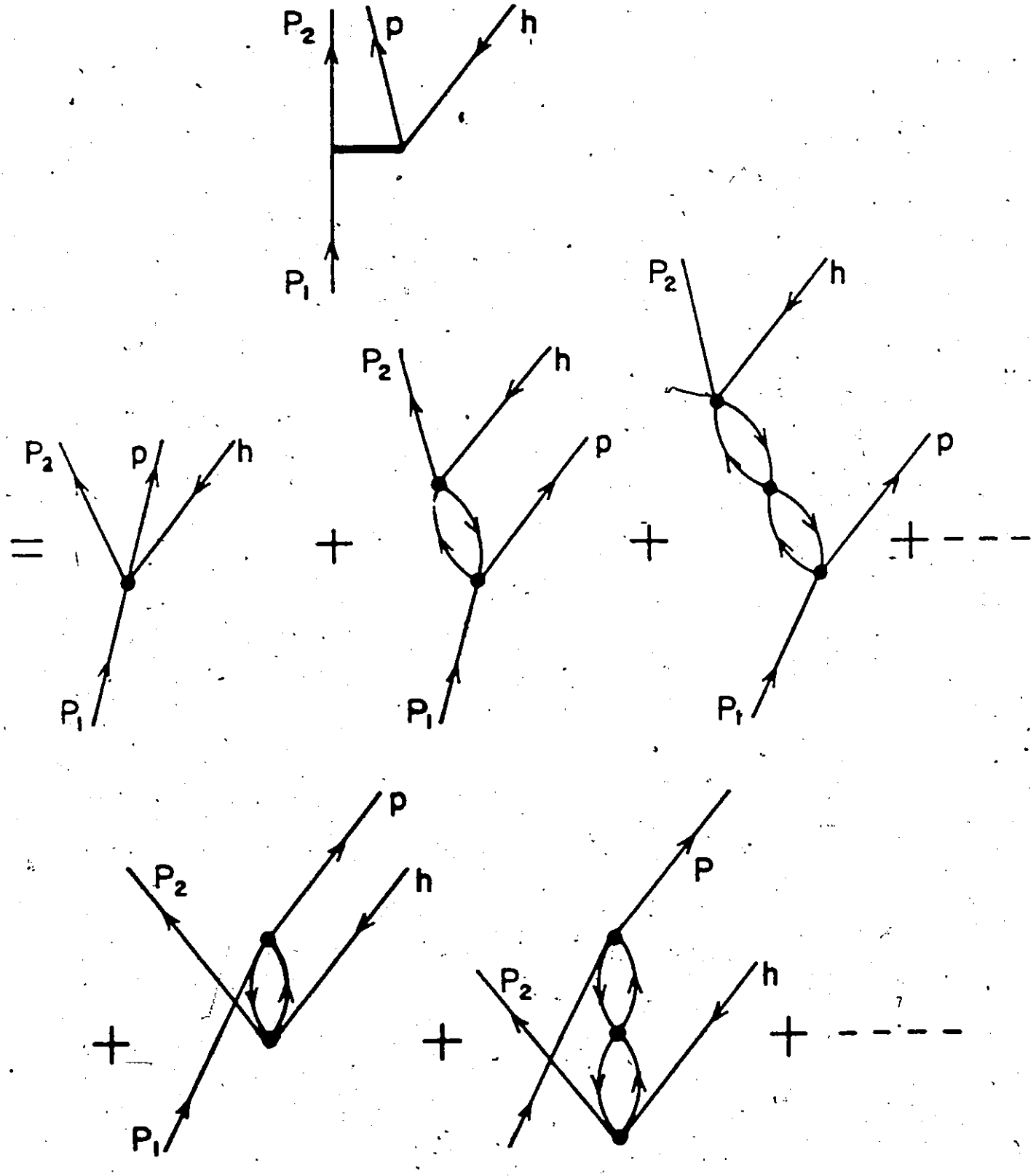

$$v'(a,b(Ph)JT) = (-)^{a+b}\, v(a,b(Ph)JT) \qquad (2.36)$$

as shown in Fig. 2.10. In other words, by twisting the lines a,b in opposite directions, one obtains the v' vertex apart from a phase. This observation is applied to the renormalized vertex v_{bb} as shown in Fig. 2.11. By switching the external lines a,b again as shown, one obtains the v'_{bb} renormalized vertex. A precaution involves the energy denominator ϵ in Eq. (2.35). The energy denominator appropriate to the v'_{bb} vertex must be used in the equation for v_{bb}. This relationship was verified for this example and for others where two diagrams, whether bare or higher order, are related by a factor.

One may demonstrate angular momentum recoupling using the graphical technique of Brink and Satchler (1968). A modification must be made to take into account the properties of hole states and this is illustrated in Appendix B.

2.3 The Nuclear Reaction Matrix

The motion of nucleons in a nucleus is governed in part by the free nucleon-nucleon interaction. Because of the strong short range repulsion of the force, the

Fig 2.10

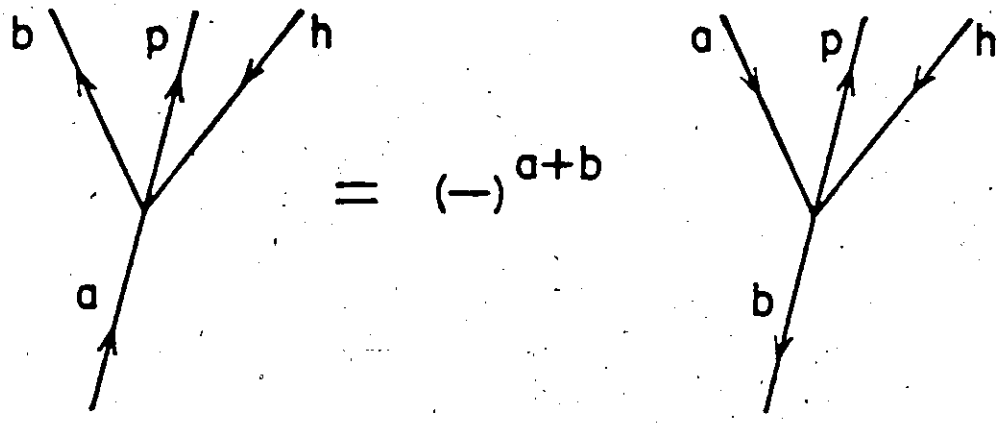

Relation between two elementary vertices.

Fig 2.11

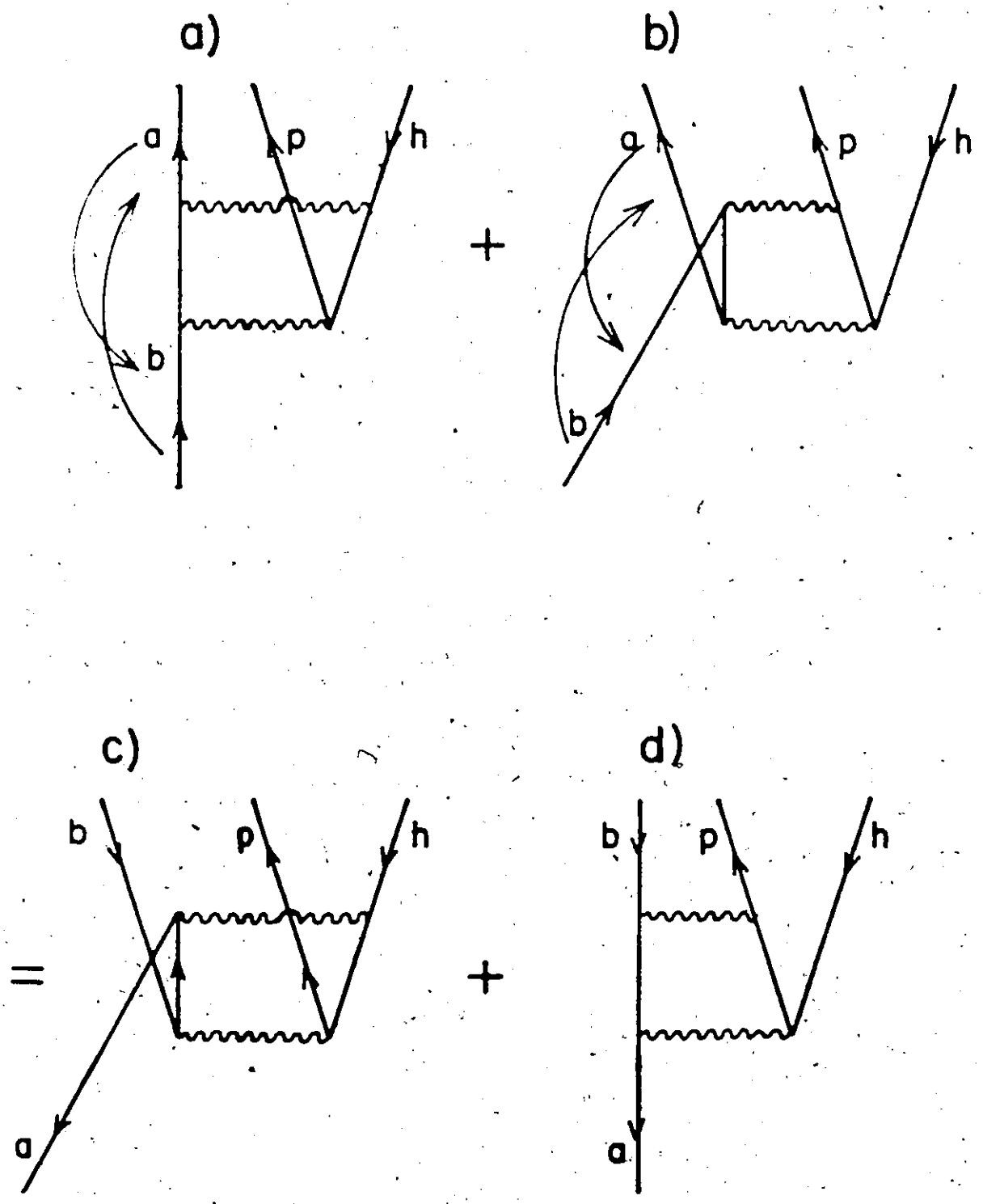

Relation between second order vertices of the black box type.

perturbation expansion for the effective interaction may not converge. The nuclear reaction matrix G was introduced in Section 2.1 and will be described in more detail here. The definition of G involves the free nucleon interaction and for the calculations in this thesis we have used two different forces. A brief comparison of the forces will be given.

The G-matrix is defined by

$$G(E_0) = V + V \frac{Q_{2p}}{E_0 - H_0} G(E_0) \quad . \tag{2.37}$$

The free interaction is denoted by V and Q_{2p} is a projection operator which ensures that the intermediate states are two particle states and that not both of them are in the valence space simultaneously. E_0 is the unperturbed energy of the initial state when matrix elements of $G(E_0)$ are taken.

In principle, one may use a complete set of unoccupied states which are available to the valence nucleons. The higher orbitals may be populated since the nuclear force is "infinitely" repulsive at short range. This approach soon becomes unfeasible because of the large number of orbitals involved for an exact calculation. To circumvent this difficulty, Brueckner showed how to take into account these higher excited states through perturbation theory. The G-matrix consists of a series of ladder diagrams shown in Fig. 2.12 where the initial and final two body states are in the valence shell. One of the pioneering calculations of G

Fig 2.12

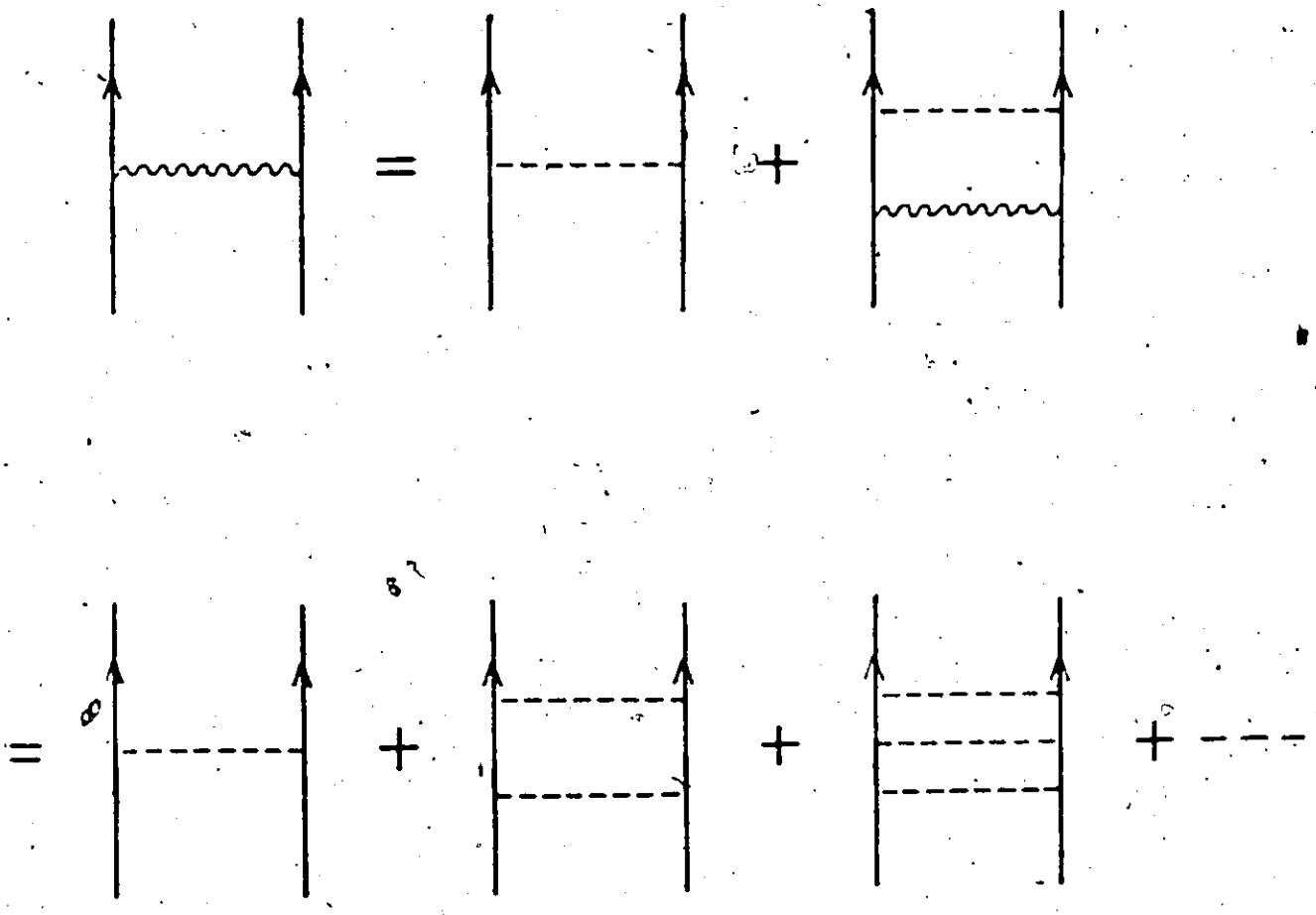

Ladder sequence of bare interactions contained in the G interaction denoted by a wavy line.

was done by Dawson et al. (1962), Kallio and Koltveit (1964), and Kuo and Brown (1966). These calculations showed that the G-matrix became much less repulsive at short range. The shell model spectrum from the G-matrix still left the experimental spectrum unexplained. One of the common forces available is the G-matrix elements of Kuo-Brown. Even though they are known to contain errors, they have been extensively used in shell model and effective interactions calculations. Since then, a method has been developed by Barrett et al. (1971) for computing G with an exact Pauli operator. These matrix elements were obtained from Barrett for oxygen but those for calcium were in the process of calculation. Unfortunately these could not be obtained at that time.

Because we wished to compare the calculations for oxygen and calcium, we required a force that was available for both nuclei. One of these is the separable, two term potential of Kahana, Lee and Scott (1969), expressed in momentum space:

$$\langle k|V|k'\rangle = \sum_{\substack{i\ell\ell' \\ JSm_\tau}} g^i_{\ell\ell'}(J) v^i_\ell(k) v^i_{\ell'}(k') [Y^{Jm}_{\ell s}(\hat{k}\sigma)^* Y^{Jm}_{\ell' s}(\hat{k}'\sigma)] P_\tau \qquad (2.38)$$

$$Y^{Jm}_{\ell s}(\hat{k}\sigma) = [Y_{\ell m}(\hat{k}) \chi^s(\sigma)]^{Jm} \qquad (2.39)$$

The quantities k', k are the relative momenta of the two interacting particles in the initial and final states respectively. ℓ' and ℓ are the relative orbital angular momenta and s is the total spin. J is the total angular momentum.

$$\vec{J} = \vec{\ell} + \vec{s} \quad \text{and} \quad \vec{J} = \vec{\ell}' + \vec{s} \ . \tag{2.40}$$

For example, the $^1S_0$ potential has the form

$$\langle k|V|k'\rangle = \sum_i^2 g_{00}^i(0) v_0^i(k) v_0^i(k') \ . \tag{2.41}$$

One term in the sum is attractive; the other is repulsive. The form factor v_0^1 of the attractive potential is

$$v_0^1(k) = \frac{1}{k^2 + a_1^2} \tag{2.42}$$

and the repulsive term in the S state is

$$v_0^2(k) = \frac{1}{k^2 + a_2^2} \ . \tag{2.43}$$

In the $^3D_1$ channel, we have

$$v_2^1(k) = \frac{k^2}{(k^2 + (a_2^1)^2)} \tag{2.44}$$

and

$$v_2^2(k) = \frac{k^2}{(k^2 + (a_2^2)^2)} \quad . \tag{2.45}$$

For all remaining channels, they have

$$v_l^1(k) = \frac{k^l}{(k^2 + a_l^2)^{l+\frac{1}{2}}} \tag{2.46}$$

and

$$v_l^2(k) = \frac{k^{l+2}}{(k^2 + a_l^2)^{2+\frac{l}{2}}} \quad . \tag{2.47}$$

All parameters in these form factors are determined by a fit to the scattering data. This data is contained in the free reaction matrix

$$T_P(\varepsilon) = V + V \frac{P}{\varepsilon - t} T_P(\varepsilon) \tag{2.48}$$

In this equation, t is the relative kinetic energy operator for the scattered nucleons, ε is the initial relative kinetic energy of the two particles, P is the principal value operator. The free reaction matrix is directly related to the scattering phase shifts. In the $^1S_0$ channel, we have

$$\frac{\pi}{2} \langle k|T_F(\varepsilon)|k\rangle = \frac{-\hbar^2}{mk} \tan \delta_0(k) \quad . \qquad (2.49)$$

The nucleon mass is m and the S state phase shift is $\delta_0(k)$.

The coupled $^3S_1$-$^3D_1$ channel has a similar expression involving the coupling parameter ρ_1 and the $^3S_1$ and $^3D_1$ phase shifts.

Once the free reaction matrix is determined, the Brueckner G-matrix can be obtained by

$$G(E) = T_F(\varepsilon) + T_F(\varepsilon)\left(\frac{Q}{E-H_0} - \frac{P}{\varepsilon-t}\right)G(E) \quad . \qquad (2.50)$$

For a separable potential, one can go directly from V to G without finding T_F. This equation was solved for several approximations for Q. They provided similar results.

The second interaction that was used is called PSA and provides relative matrix elements of the free reaction matrix in a Born approximation. These are a first approximation to the reaction matrix and it will be interesting to compare the effects of these differences.

The second interaction used in our calculations is based on an elegant suggestion by Elliott et al. (1967). Their method is to extract shell model matrix elements of the nuclear interaction directly from an integral over the experimentally determined phase shifts. Although their derivation was stated in terms that the nuclear force be weak enough for the Born approximation to hold, this is not

an essential restriction. Rather, one could regard the V(r) in question as a local free reaction matrix whose Born approximation must by definition give the correct phase shifts for a particular state of given quantum numbers ℓ, s, J. From this point of view, the basic approximation is that a good approximation to the free reaction matrix, that is local in r, should exist. It was discussed by Brink (1967) that such an approximation may not be useful in calculating total binding energies of nuclei but that it may well be useful for calculating spectra. In this case, only nucleons near the Fermi energy are involved and these tend to be located in a low density region of the nucleus.

The procedure that is followed is the construction of the reduced or relative matrix elements of the nuclear interaction between harmonic oscillator single particle states, diagonal in ℓ for a scalar interaction.

$$\langle n\ell|V_\ell(r)|n'\ell\rangle = \sum_{\mu=0}^{n+n'} B(n,\ell,n',\ell,\ell+\mu)\, I(\ell,\mu) \quad . \qquad (2.51)$$

The quantities $I(\ell,\mu)$ are the Talmi integrals defined as

$$I(\ell,\mu) = \frac{2}{\Gamma(\ell+\mu+\frac{3}{2})} \int_0^\infty \left(\frac{r^2}{q^2}\right)^{\ell+\mu} e^{-r^2/q^2}\, V_\ell(r)\, \frac{r^2}{q^2}\, \frac{dr}{q} \quad . \qquad (2.52)$$

The quantity $q = \sqrt{2}\, b$ is expressed in terms of the usual oscillator parameter given by

$$b = \sqrt{\frac{\hbar}{m\omega}} \quad . \tag{2.53}$$

The relative coordinate of an interacting pair of nucleons is

$$\underset{\sim}{r} = \underset{\sim}{r}_1 - \underset{\sim}{r}_2 \quad . \tag{2.54}$$

If the potential were the same in all states, one could revert to the usual notation I_p with $p = \ell + \mu$. The coefficients $B(n,\ell,n',\ell,\ell+\mu)$ are the Talmi coefficients.

Once the relative matrix elements are known, they may be used to construct the shell model matrix elements as given in Eq. (2.27). From Slater (1960), one uses a general integral over products of hypergeometric functions to obtain

$$\int_0^\infty e^{-k^2q^2} j_\ell^2(kr)\, {}_1F_1(-\ell-1-\mu, \tfrac{1}{2}-\ell; k^2q^2)\, k^2 dk$$

$$= \frac{(-\frac{\pi}{2})}{2q^3} \frac{2^\mu}{\Gamma(\ell+\frac{1}{2})} \frac{(r^2/q^2)}{(2\mu+1)!!} e^{-r^2/q^2} \sum_{\nu=0}^{\beta} \frac{(-)^\nu}{(\mu-\nu)!} \frac{\mu!\,\ell!}{(\ell+\nu)!\,\nu!} \left(\frac{r^2}{q^2}\right)^{\mu-\nu} \tag{2.55}$$

where $\beta = \min(\mu,\ell)$. One now operates on Eq. (2.55) with

$$\frac{2}{\Gamma(\ell + \mu + \frac{3}{2})} \int_0^\infty V_\ell(r) \frac{r^2}{q^2} \frac{dr}{q} \quad . \tag{2.56}$$

The R.H.S. becomes a series of Talmi integrals and the L.H.S., after rearrangement contains an integral over the Born phase shifts given below

$$\tan \delta_\ell^B(k) = \frac{-mk}{\hbar^2} \int_0^\infty j_\ell^2(kr) V_\ell(r) r^2 dr \quad . \tag{2.57}$$

One has a recursive relation now for obtaining the different Talmi integrals by letting $\mu = 0, 1, \ldots$, etc. The final relation is given by Eq. (3.5) in Srivastava et al. (1969).

Because the nuclear force contains tensor components, the relative matrix elements need not be diagonal in ℓ but can differ by two units of angular momentum. For this case a generalized Talmi integral involving the total angular momentum is required which is diagonal in J.

$$I_T(J,\mu) = \frac{2}{\Gamma(J + \mu + \frac{3}{2})} \int_0^\infty U_T(r) e^{-r^2/q^2} r^{2J+2\mu+2} dr \quad . \tag{2.58}$$

In the tensor case, according to Stapp et al. (1957), the phase shifts are given in the Born approximation as

$$\delta^J_{\ell=J\pm1} \sim - \langle J\pm1, J|V|J\pm1, J\rangle$$

and (2.59)

$$\varepsilon^J \sim - \langle J-1, J|V|J+1, J\rangle \quad .$$

The matrix elements diagonal in ℓ can be treated by the methods given above. For the other case, involving coupling of different ℓ, one requires a representation for the product of two spherical Bessel functions differing in ℓ.

From Rainville (1960), one obtains

$$j_{\ell-1}(kr)\, j_{\ell+1}(kr) = \frac{\frac{\pi}{4}\left(\frac{kr}{2}\right)^{2\ell}}{\Gamma(\ell+\frac{1}{2})\,\Gamma(\ell+\frac{5}{2})} \times {}_2F_3\left[\begin{matrix}\ell+1,\ \ell+\frac{3}{2}\\ \ell+\frac{5}{2},\ \ell+\frac{1}{2},\ 2\ell+2,\end{matrix}\ -k^2r^2\right]. \qquad (2.60)$$

Using similar methods as above, one may obtain a recursive procedure as given in Eq. 4.11 and 4.12 of Srivastava et al. (1969). Shown in Table 2.1 are a few of the relative matrix elements required for the calculations done in this thesis using the phase shifts of Seamon et al. (1968). Looking at Table 2.1, in comparing the two forces, the matrix elements diagonal in ℓ and n are qualitatively similar. The PSA matrix elements off diagonal in n differ more from the KLS but not unreasonably so. The biggest difference in the two forces occurs for the off diagonal in ℓ cases. The PSA matrix elements are a factor of 5 smaller than those of the KLS and this indicates that the Born approximation is inadequate for treating the strong tensor component of the free nucleon-nucleon interaction.

TABLE 2.1

RELATIVE MATRIX ELEMENTS

State n1n'l'SJ	Oxygen KLS	Oxygen PSA	Calcium KLS	Calcium PSA
000000	- 7.077	-7.522	-4.760	-6.044
001000	- 5.923	-3.923	-4.457	-3.473
010101	2.100	1.591	1.039	.909
011101	2.696	1.776	1.354	.968
020202	- .624	- .589	- .260	- .297
021202	- .795	- .654	- .362	- .391
030303	-	.342	-	.207
031303	-	.233	-	.163
000011	-10.490	-9.41	-6.805	-7.850
001011	- 9.607	-3.983	-6.719	-3.800
010110	- 2.463	-2.134	-1.383	-1.443
010111	2.353	1.783	1.216	1.03
010112	- 1.208	-1.314	- .599	- .680
011110	- 2.149	-1.438	-1.470	-1.212
011111	2.753	1.880	1.51	1.105
011112	- 1.513	-1.631	- .792	- .897
020211	2.457	1.897	1.135	.994
020212	- 2.890	-2.952	-1.364	-1.589
020213	- .165	- .304	- .058	- .141
021211	2.752	1.945	1.421	1.094
021212	- 3.225	-2.876	-1.707	-1.686
021213	- .252	- .365	- .150	- .187
030312	-	- .120	-	- .066
030313	-	.303	-	.160
030314	-	- .100	-	- .041
000211	- 5.304	- .740	-2.889	- .418
001211	- 5.852	-1.08	-3.587	- .623
010312	-		-	.442
011312	-		-	.610

CHAPTER III

APPLICATION TO THE SCHEMATIC MODEL AND CORE POLARIZATION

In this chapter, we will apply the theoretical methods of Chapter II to the schematic model of Brown and Bolsterli (1959). A review of this model as an explanation of the giant dipole resonance will be given to form a basis for some extensions of the schematic model. This model will be complemented by a detailed discussion of the core polarization processes given in Sprung and Jopko (1972).

3.1 The Giant Dipole Resonance

During the photoexcitation of a nucleus, the proton struck by the incident γ-ray may be excited to a higher energy state. If only a single proton is involved, the process happens quickly and the lifetime of the state will be short, corresponding to a large width. On the other hand, if the incident energy is shared among all nucleons in the nucleus, the lifetime will be long and the state will be narrow. Both kinds of resonances occur in the real nucleus. The giant dipole resonance occurs throughout the

table of elements. In oxygen, the excitation energy is approximately 15 MeV and has a width of a few MeV. It is called the giant dipole resonance because this resonance carries nearly all the transition strength to the ground state compared to other dipole states, and levels excited strongly involving γ-rays of these energies are likely to be dipole ones, since the wavelengths of the γ-rays are still of the order or greater than the nuclear radius (Brown (1967)).

3.2 The Particle-Hole Approximation

If we try to explain the dipole resonance from the view of only one participating proton, one finds difficulty. From the shell model, there are unoccupied states approximately 4 MeV above the last occupied state. If we include a further 2 MeV pairing energy that is released when one nucleon is excited, the single particle model would predict an excitation energy of approximately 6 MeV. This is less than one half of the observed value. This is called the p-h approximation because only a single particle is involved and when it is excited to a higher energy state, it leaves behind an unoccupied or hole state. This approximation will be considered as a polarization of the core because the density profile of the nucleus has been changed. The diagram

representing this process is shown in Fig. 3.1. When this process is considered to renormalize the effective interaction between a pair of valence particles, it is called 3p-1h because it involves two valence particles in addition to the p-h pair.

If the basic nuclear p-p interaction is attractive, then the p-h interaction should be repulsive. This happens because a hole represents a loss of interaction with the missing particle. In general the p-h interaction may be written as

$$V_{ph} = \sum_{ij} |i\rangle V_{ij} \langle j| \qquad (3.1)$$

where i and j represent different p-h states. In the schematic model it was argued that the probability amplitude of a given p-h pair interacting with another p-h pair should be given by the product of the individual amplitudes. This seems reasonable when the excitation of p-h pairs occur at random and are independent events. In addition, the realistic p-h force is well fitted by the separable interaction which has the form

$$V_{ph} = \sum_{ij} \lambda |i\rangle D_i D_j \langle j| \qquad (3.2)$$

where we have replaced V_{ij} with $\lambda D_i D_j$ and λ is a strength parameter.

Fig. 3.1: Diagrammatic representation of the p-h approximation to core polarization.

Fig. 3.2: Diagrammatic representation of the TDA approximation to core polarization.

Fig 3.1

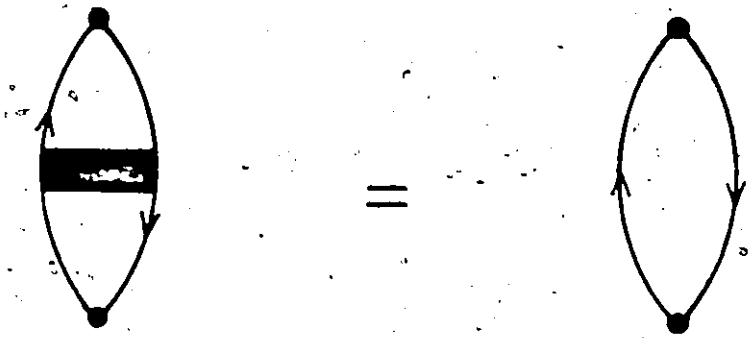

Fig 3.2

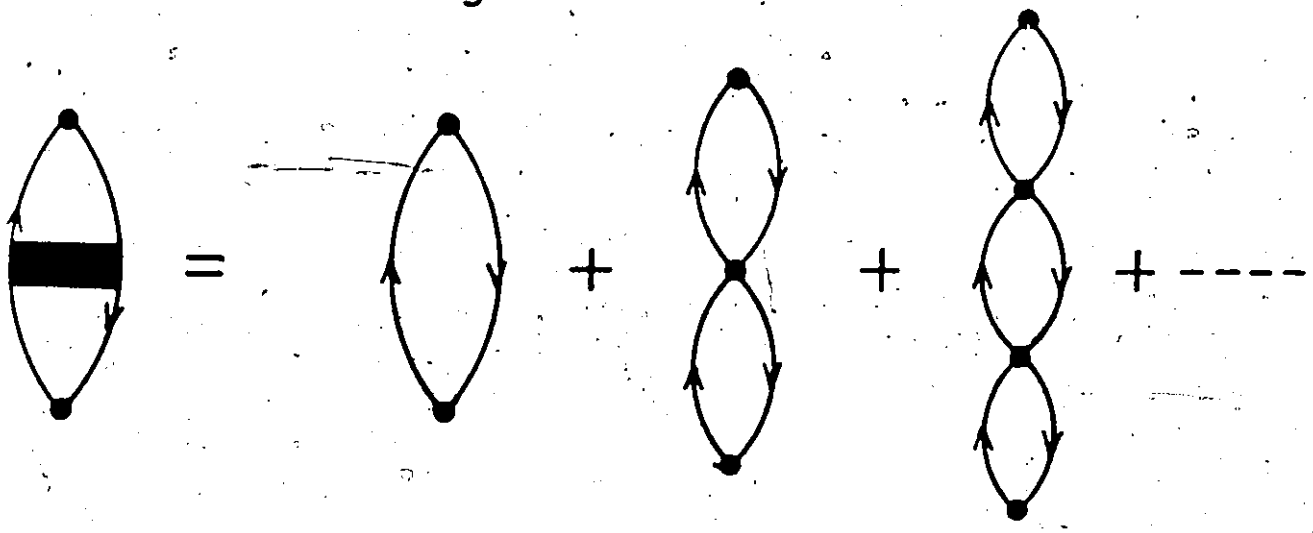

Let us define $|D\rangle = \sum_i D_i |i\rangle$ so we can write

$$V_{ph} = |D\rangle\lambda\langle D| \quad . \tag{3.3}$$

The ket $|D\rangle$ can be normalized to unit length. Its significance will become clear in a moment. It is convenient to introduce another energy parameter c, related to the "average" p-h excitation energy by the relation

$$\sum_i \lambda \frac{D_i^2}{\epsilon_i} = \frac{\lambda}{c} \quad . \tag{3.4}$$

ϵ_i is the excitation energy of the $p_i h_i$ pair. In this schematic model we will choose the p-p interaction to be identical to the p-h interaction, except for sign.

The 3p-1h contribution to the effective interaction is, therefore,

$$|D\rangle\lambda_{eff}\langle D| = |D\rangle\lambda\langle D| + |D\rangle\lambda\langle D| \frac{1}{\epsilon} |D\rangle\lambda\langle D| \quad . \tag{3.5}$$

But

$$\langle D| \frac{1}{\epsilon} |D\rangle = \frac{1}{c} \quad . \tag{3.6}$$

Therefore,

$$\lambda_{eff} = \lambda + \frac{\lambda^2}{c} \quad . \tag{3.7}$$

We define an amplification factor S for the p-p interaction (or p-h interaction) according to

$$\lambda_{eff} = S\lambda \quad . \tag{3.8}$$

Then

$$S^{ph} = 1 + \frac{\lambda}{c} \quad . \tag{3.9}$$

In this and subsequent sections, we take the Γ, ν, ν' vertices to be equal and the $\bar{\nu}$, B vertices equal but different from the first three vertices. These assignments follow from the transformation properties of the actual vertices and are defined in Eq.(2.32).

3.3 The Tamm-Dancoff Approximation

Since the p-h approximation cannot explain the dipole resonance, a collective description of the nucleus was sought. Such a classical attempt was made by Goldhaber et al. (1948) using the two fluid model. In this model, all the protons in the nucleus behave as a simple viscous fluid and all the neutrons behave as a fluid. An incident γ-ray interacts with the positively charged proton fluid and sets up an oscillation between the proton and neutron fluids.

The energy of the interaction depends, of course, on the classical "spring constant" between the fluids. Because this constant could not be calculated from fundamental principles, this model is unable to explain the dipole resonance on a fundamental basis.

Returning to the microscopic model, Brown and Bolsterli demonstrated collective effects from the microscopic approach. They postulated that since there are many nearly degenerate p-h states in the nucleus, the p-h pair may interact with many other p-h pairs. This is shown in Fig. 3.2. In the following discussion, we will assume that there are three p-h states. The unperturbed p-h hamiltonian has the form

$$H_0^{Ph} = \begin{pmatrix} \epsilon_1 & 0 & 0 \\ 0 & \epsilon_2 & 0 \\ 0 & 0 & \epsilon_3 \end{pmatrix} . \qquad (3.10)$$

The separable p-h interaction has the form

$$V^{Ph} = \begin{pmatrix} V_1V_1 & V_1V_2 & V_1V_3 \\ V_2V_1 & V_2V_2 & V_2V_3 \\ V_3V_1 & V_3V_2 & V_3V_3 \end{pmatrix} . \qquad (3.11)$$

The eigenstates of the system are the solutions of the Schroedinger equation

$$(H_0^{ph} + V^{ph})\psi^{ph} = E^{ph}\psi^{ph} \qquad (3.12)$$

For this simple model, the equation may be obtained exactly and analytically. To illustrate this, let us take the degenerate case with $\epsilon_i = \epsilon$. Then using $H_0^{ph} = \epsilon\underline{1}$ and $V_{ph} = |D\rangle\lambda\langle D|$, the Schroedinger equation in a p-h basis is

$$(\epsilon\underline{1} + |D\rangle\lambda\langle D|)|\psi\rangle = E|\psi\rangle \qquad (3.13)$$

It is obvious that one solution is $|\psi\rangle = |D\rangle$ with

$$(\epsilon + \frac{\lambda\epsilon}{c})|D\rangle = E|D\rangle \qquad (3.14)$$

This eigenvalue has been shifted by the amount $\frac{\lambda\epsilon}{c} = Tr(V_{ph})$ from the unperturbed position. Because the sum of the eigenvalues is $Tr(H_0^{ph}) = N\epsilon$, it is evident that the other (N-1) eigenvalues are caught at the unperturbed value ϵ. Thus, this one "dipole state" $|D\rangle$ has captured all the strength of the p-h interaction. This demonstrates the significance of the ket $|D\rangle$.

Even in the non-degenerate case, the solution will have the form

$$\psi^{ph} = \alpha|1\rangle + \beta|2\rangle + \gamma|3\rangle \qquad (3.15)$$

It was found that of the N solutions (here 3), all eigenvalues remained close to the unperturbed energy ϵ_i except one which either greatly increased or decreased in energy according to whether the p-h interaction was repulsive or attractive. The amplitudes of the basis states for this eigenfunction tend to be of the same sign so that the transition strength would be many times the single p-h value. This energy shift and collectivity are precisely the properties required for the dipole state. This approximation is known as the Tamm-Dancoff approximation (TDA).

In terms of the effective interaction, the TDA series may be summed as a geometric series as shown by Kirson. The expression has the schematic form

$$V^{TDA} = v + v \frac{1}{\epsilon+t} v \quad . \qquad (3.16)$$

In our model, the corresponding equation is

$$|D\rangle\lambda^{TDA}_{eff}\langle D| = |D\rangle\lambda\langle D| + |D\rangle\lambda\langle D| \frac{1}{\epsilon+t} |D\rangle\lambda\langle D| \quad . \qquad (3.17)$$

By expanding the denominator in a power series, it may be shown that

$$\langle D| \frac{1}{\epsilon+t} |D\rangle = \frac{1}{\epsilon+\lambda} \qquad (3.18)$$

$$\lambda_{eff}^{TDA} = \lambda + \frac{\lambda^2}{(c+\lambda)} \tag{3.19}$$

and

$$S^{TDA} = 1 + \frac{\frac{\lambda}{c}}{1 + \frac{\lambda}{c}} = \frac{1 + \frac{2\lambda}{c}}{1 + \frac{\lambda}{c}} \tag{3.20}$$

The detailed expression for the TDA may be obtained from Eq. (2.33) by replacing

$$\nu \frac{1}{\epsilon} \nu \rightarrow \nu \frac{1}{\epsilon+f} \nu \tag{3.21}$$

This may be seen by expanding the denominator as follows

$$\begin{aligned} \nu \frac{1}{\epsilon+f} \nu &= \nu \frac{1}{\epsilon} \left(1 + \frac{f}{\epsilon}\right)^{-1} \nu \\ &= \nu \frac{1}{\epsilon} \left(1 - \frac{f}{\epsilon} + \frac{f^2}{\epsilon^2} - \frac{f^3}{\epsilon^3} + \ldots\right) \nu \\ &= \nu \frac{1}{\epsilon} \nu - \nu \frac{1}{\epsilon} f \frac{1}{\epsilon} \nu + \nu \frac{1}{\epsilon} f \frac{1}{\epsilon} f \frac{1}{\epsilon} \nu + \ldots \end{aligned} \tag{3.22}$$

Each additional f vertex introduces another bubble in the series and the signs alternate because the f vertex introduces a minus sign as a part of the overall sign of the diagram.

3.4 The Random Phase Approximation

The microscopic approach in the TDA leads to a partial form of collectivity between the p-h pairs. This collectivity was extended by Thouless (1961) to take into account further correlations between the nucleons in the nucleus. This approach has been called the Random Phase Approximation (RPA) because of certain operators which are replaced by their average. The RPA equations have been redeveloped and better understood through time dependent Hartree-Fock theory (Rowe (1966)), equations of motion and linearization. These approaches will not be described here.

Clearly if the TDA produces a large effect both in the dipole resonance and effective interaction, it is of interest to investigate the effect of the RPA. The diagrammatic series for the RPA is shown in Fig. 3.3 and contains both forward and backward going TDA strings of bubbles and with all possible relative time orderings for the vertices. This series requires a new vertex where the TDA strings change direction. The vertex is denoted by B in Kirson (1971). It contains two p-h pairs interacting simultaneously as shown in Fig. 2.6(d) and it thus represents a correlation between the p-h pairs.

A more complete discussion of the usual RPA and a version due to Kirson (denoted RKA) and its application to the schematic model are given in Appendix D.

Fig 3.3

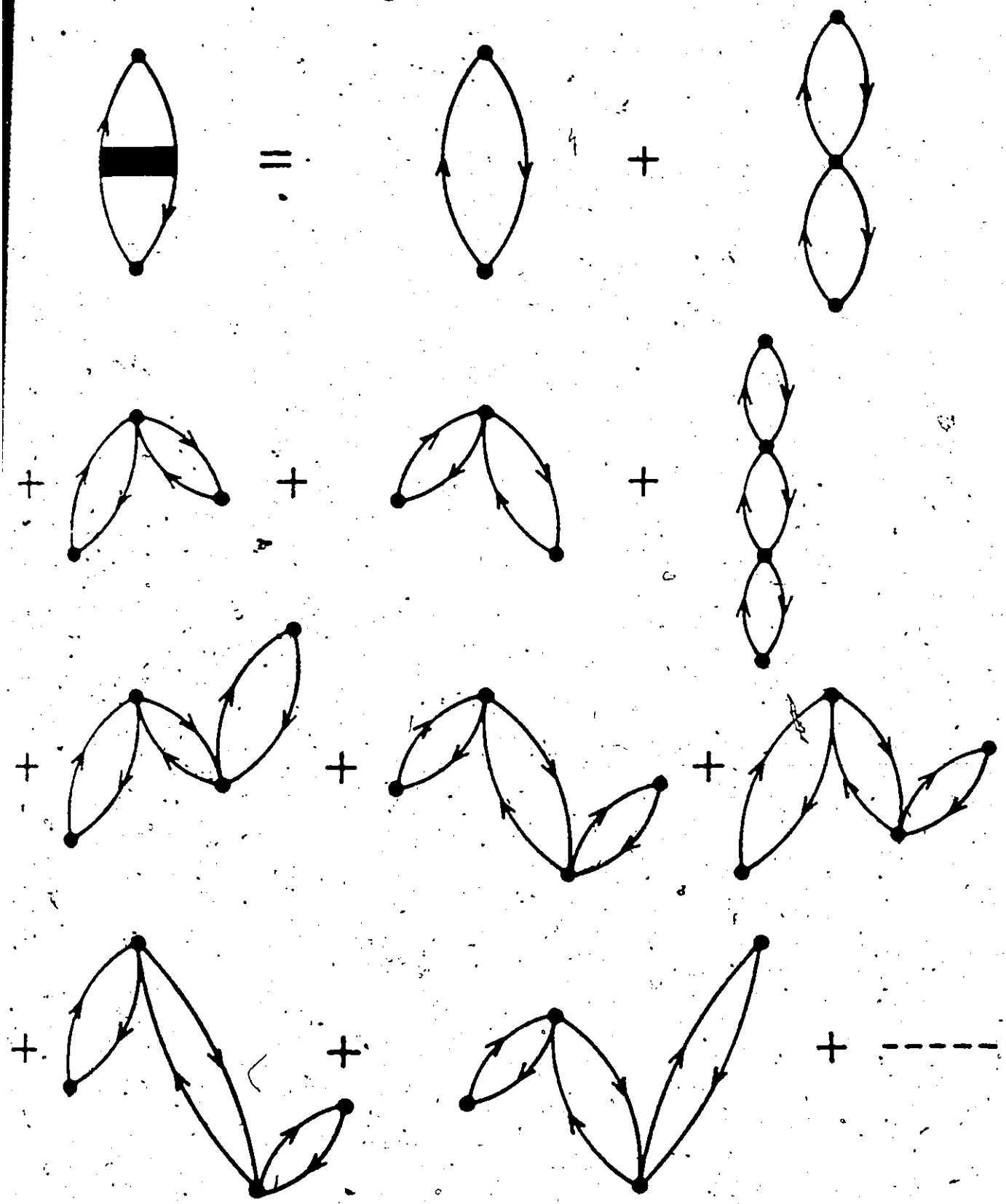

Diagrammatic representation of the RPA approximation to core polarization.

The RPA series was summed by Kirson. His solution is obtained by replacing $v \frac{1}{\epsilon} v$ in Eq. (2.33) by

$$v[\mathcal{A} - B\mathcal{A}^{-1}B]^{-1}[v - B\mathcal{A}^{-1}\tilde{v}] \tag{3.23}$$

where $\mathcal{A} = \epsilon + f$.

For the effective interaction, it is shown in Appendix D that it is a good approximation to take

$$B = |D><D| \equiv \tilde{v} \ . \tag{3.24}$$

The only difference from the f vertex is in the strength constant μ rather than λ. It turns out that a realistic value for μ is $\frac{1}{2}\lambda$.

The RPA contribution to the effective interaction in the schematic model is

$$V_{eff} = v + v[\mathcal{A} - B\mathcal{A}^{-1}B]^{-1}[v - B\mathcal{A}^{-1}\tilde{v}] \tag{3.25}$$

$$|D>\lambda^{RPA}_{eff}<D| = |D>\lambda<D| + |D>\lambda<D| \frac{1}{\mathcal{A} - B\mathcal{A}^{-1}B} \times [|D>\lambda<D| - |D>\mu<D| \frac{1}{\mathcal{A}} |D>\mu<D|] \tag{3.26}$$

$$\lambda^{RPA}_{eff} = \lambda + \frac{\lambda \cdot c}{(\lambda+c)^2 - \mu^2}\left[\lambda^2 - \frac{\lambda\mu^2}{c+\lambda}\right] \tag{3.27}$$

so that the amplification factor is

$$S^{RPA} = \frac{1 + \frac{3\lambda}{c} + 2(\lambda^2-\mu^2)/c^2}{1 + \frac{2\lambda}{c} + (\lambda^2-\mu^2)/c^2} \qquad (3.28)$$

In Appendix D it will be shown that the S^{RPA} is even larger than S^{TDA} and may easily diverge.

3.5. Screening of the Interaction

Since it appeared that the addition of more and more bubbles caused the effective interaction to diverge, some other mechanism was sought to prevent this. Such a process, called screening, was first investigated by Blomquist and Kuo (1969). The process is shown in Fig. 3.4 where the p-h interaction is modified by the excitation of a p-h pair. The interaction is called screened because the internal p-h pairs weaken the interaction between the external p-h pairs. Kirson was able to sum the screened interaction, provided the sereening was of the TDA type.

The schematic equation for screening is

$$f_= = f + v \frac{1}{\epsilon + f_=} v \qquad (3.29)$$

where $f_=$ denotes the screened p-h vertex, f the simple p-h vertex considered up to now. In our model we make the ansatz that $f_= = |D\rangle\kappa\langle D|$. The constant κ measures the

Fig. 3.4: Diagrammatic representation of the screened interaction. Each external bubble may be a part of the RPA diagram but each internal bubble is a part of TDA diagrams only.

Fig 3.4

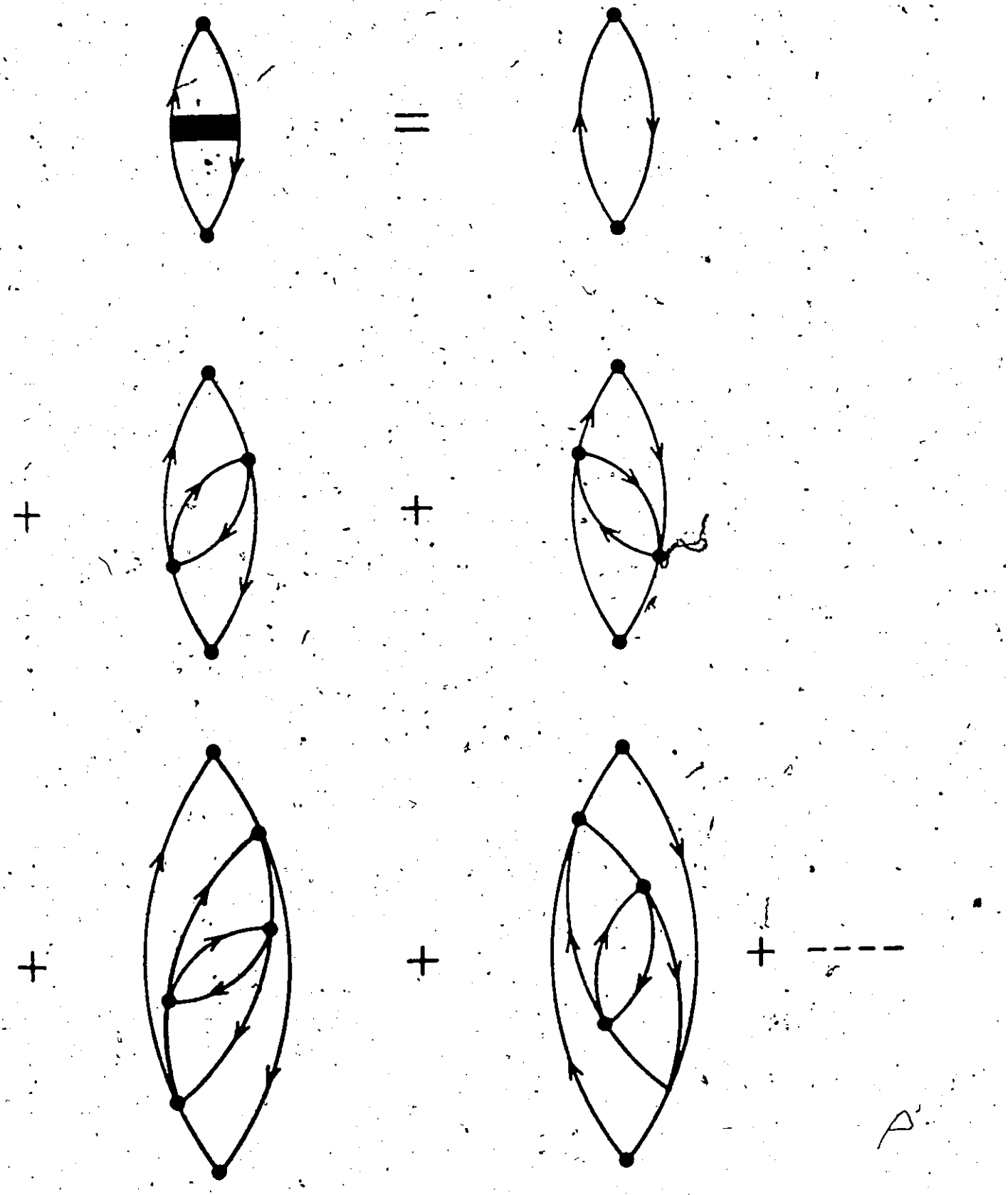

strength of the screened interaction. Equation (3.29) becomes

$$|D>\kappa<D| = |D>\lambda<D| + |D>\lambda<D| \frac{1}{\varepsilon + \varepsilon_\infty} |D>\lambda<D| \qquad (3.30)$$

then

$$\kappa = \lambda + \frac{\lambda^2}{c+\kappa} \quad \text{or} \quad \frac{\kappa}{c} = \frac{\lambda}{c} + \frac{\lambda^2/c^2}{1 + \frac{\kappa}{c}} \; . \qquad (3.31)$$

The solution for $\frac{\kappa}{c}$ is

$$\frac{2\kappa}{c} = \frac{\lambda}{c} - 1 + (1 + \frac{2\lambda}{c} + 5(\frac{\lambda}{c})^2)^{1/2} \qquad (3.32)$$

so for weak forces

$$\frac{\kappa}{c} = \frac{\lambda}{c} (1 + \frac{\lambda}{c}) \; . \qquad (3.33)$$

The screening of the RPA propagator thus corresponds to an increased coupling strength for repulsive forces but a decreased coupling strength for attractive forces.

In fact Eq. (3.32) is not completely correct because the ε in the denominator is not really a constant but represents the excitation energy of the intermediate state. In an iterative solution, this is taken into account by solving for κ_0/c in the equation below:

$$\frac{\kappa_n}{c} = \frac{\lambda}{c} + \frac{\lambda^2/c^2}{n + 1 + \frac{\kappa_{n+1}}{c}} \quad . \tag{3.34}$$

The starting value of κ_{n+1} is λ. The increase of $\varepsilon \to (n+1)\varepsilon$ represents the energy of n additional p-h pairs. Equation (3.34) was solved by iteration for 20 times but does not differ greatly from the previous result for small λ/c.

An interesting property for the asymptotic values of $\frac{\kappa}{c}$ is that for large positive $\frac{\lambda}{c}$, $\frac{\kappa}{c}$ approaches ϕ. For large negative $\frac{\lambda}{c}$, $\frac{\kappa}{c}$ approaches $-\frac{1}{\phi}$ where ϕ is the golden ratio and is an irrational number equal to $\frac{1+\sqrt{5}}{2} = 1.618\cdots$.

From Eq. (3.33), we have approximately

$$S^{nRPA} = (1 + \frac{\lambda}{c} + \ldots) \quad . \tag{3.35}$$

These are the same two terms as in S^{TDA} and so the schematic model confirms the detailed calculation of Kirson. To use the screened RPA (nRPA), we solve Eq. (3.36) for f_∞ and this is used

$$\begin{aligned} \langle (p_2h_2^-)JT|f_{n+1}|(p_1h_1^-)JT\rangle &= \langle (p_2h_2^-)JT|f|(p_1h_1^-)JT\rangle \\ &+ (-)^{J+T+1} \sum_{phJ''T''} (-)^{J''+T''} \\ &\times \begin{Bmatrix} p_1 & p_2 & J'' \\ h_2 & h_1 & J \end{Bmatrix} \begin{Bmatrix} \frac{1}{2} & \frac{1}{2} & T'' \\ \frac{1}{2} & \frac{1}{2} & T \end{Bmatrix} \\ &\times \nu(p_1p_2(ph)J''T'') \left(\frac{1}{\varepsilon+f_n}\right) \nu'(h_1h_2(ph)J''T'') \end{aligned} \tag{3.36}$$

in $\mathcal{E}_\infty = \varepsilon + f_\infty$ to replace $\mathcal{E}$ previously defined. The actual iteration procedure is quite complicated and lengthy to compute. A small error was discovered in Kirson's version of the iteration procedure. The correct procedure and its results will be described in Chapter IV.

3.6 Vertex Renormalization

In all the approximations discussed so far, we have considered different approximations for the core excitations. Besides this propagator renormalization there is a vertex renormalization shown in Fig. 2.9. This is a modification of the interaction between the valence nucleon and the core vibrations. As shown in Fig. 2.9, the valence particle may interact any number of times with the hole state from the p-h pair. Kirson calls this vertex a black box (bb) vertex and it is defined in Eq. (2.35). To get the bb vertex renormalized to all orders, one uses $\varepsilon + f$ in place of ε. Clearly this vertex may be used with all the propagator renormalizations. With the p-h approximation we have bb3plh. The other approximations we consider are bbRPA and bbnRPA.

In the schematic model we have

$$v_{bb} = v + v \frac{1}{\varepsilon+f} f + \bar{v} \frac{1}{\varepsilon+f} B \qquad (3.37)$$

$$|D>\lambda\tau<D| = |D>\lambda<D| + |D>\lambda<D| \frac{1}{\varepsilon+\xi} |D>\lambda<D|$$

$$+ |D>\mu<D| \frac{1}{\varepsilon+\xi} |D>\mu<D| \qquad (3.38)$$

$$\tau = 1 + \frac{(\lambda^2+\mu^2)/c^2}{\frac{\lambda}{c}(1 + \frac{\lambda}{c})} \qquad (3.39)$$

where τ measures the renormalization of the bare vertex. The amplification factor becomes

$$S^{bbnRRA} = \frac{1 + \frac{2\kappa}{c} + \frac{\lambda\tau^2}{c} + [\frac{\kappa^2}{c^2} + \frac{\lambda\kappa\tau^2}{c} - \frac{\mu^2}{c^2}(1 + \dot{\tau}^2)]}{1 + \frac{2\kappa}{c} + [\frac{\kappa^2}{c^2} - \frac{\mu^2}{c^2}]} . \qquad (3.40)$$

This may be specialized in several ways. If one calculates the vertex correction using the unscreened p-h interaction f, we replace κ by λ. If the bare vertex is used, then $\tau = 1$.

The vertex renormalization may be extended by including the bb vertices in the diagrammatic expansion for the bb vertex. One obtains the following renormalized vertex ν_-:

$$\nu_- = \nu + \nu_- \frac{1}{\varepsilon+\xi_-} f_- + \tilde{\nu}_- \frac{1}{\varepsilon+\xi_-} B \quad . \qquad (3.41)$$

Making the usual substitution according to the schematic model, we obtain

$$\tau_- = 1 + \tau_-\kappa<D| \frac{1}{\varepsilon+\xi_-} |D> + \frac{\mu^2\tau_-}{\lambda} <D| \frac{1}{\varepsilon+\xi_-} |D> \quad . \qquad (3.42)$$

The solution is

$$\tau_- = (1 + \frac{\kappa}{c})/(1 - \frac{\mu^2}{\lambda c}) \quad . \tag{3.43}$$

This may also be called a bb vertex and the amplification factor S is the same as in Eq. (3.40) but $\tau \to \tau_\infty$. This answer for τ_- above is analytic but the actual situation involves an iteration with changing energy denominators. This cannot be done analytically but corresponds to the SCCE solution of Kirson. We iterate three equations. These are the screened p-h interaction f_∞; and the renormalized vertices v_- and v'_-. A computer program was written to obtain numerical values for τ_- and κ self consistently.

3.7 Results of the Schematic Model

The amplification factor S in the various approximations is presented in Figs. 3.5 and 3.6. For the p-h case, the amplification factor is linear with respect to the force strength $\frac{\lambda}{c}$. As the value of $\frac{\lambda}{c}$ becomes more negative, the TDA factor deviates from the p-h case and, actually diverges at $\frac{\lambda}{c} = 1$. The TDA approximation occurs when there is no B vertex. ($\mu = 0$ in our model, Eq. (3.34).)

Fig. 3.5: The amplification factor S in the schematic model for the p-h, TDA, and RKA approximations.

Fig 3.5

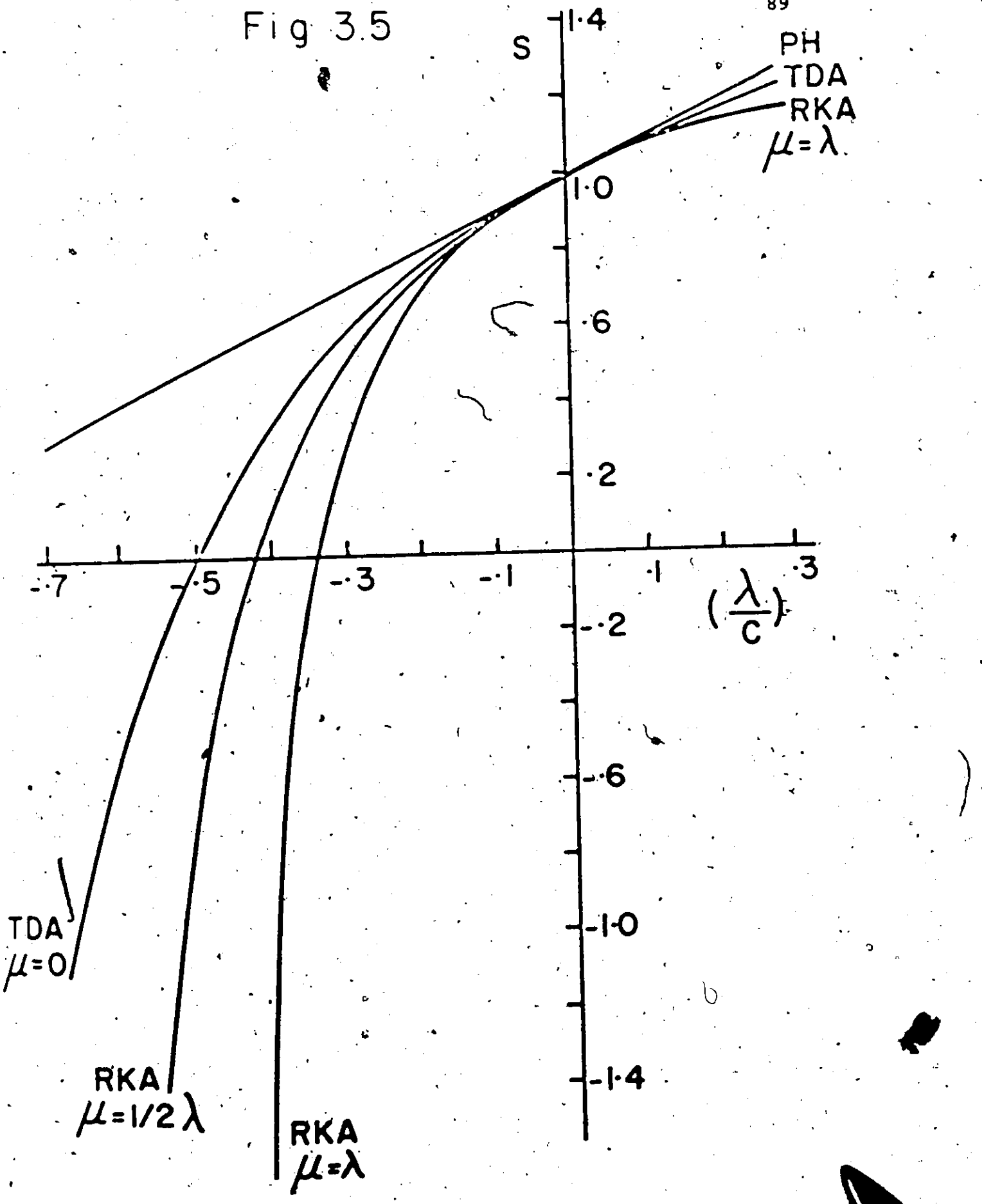
S
1·4
1·0
·6
·2
-·2
-·6
-1·0
-1·4
-·7
-·5
-·3
-·1
·1
·3
$(\frac{\lambda}{c})$
PH
TDA
RKA
$\mu=\lambda$
TDA
$\mu=0$
RKA
$\mu=1/2\lambda$
RKA
$\mu=\lambda$

Fig. 3.6: The amplification factor S in the schematic model for the p-h, nRKA, bbRKA, bbnRKA, and SCCE approximations for $\mu = \frac{1}{2}\lambda$.

Fig 3.6

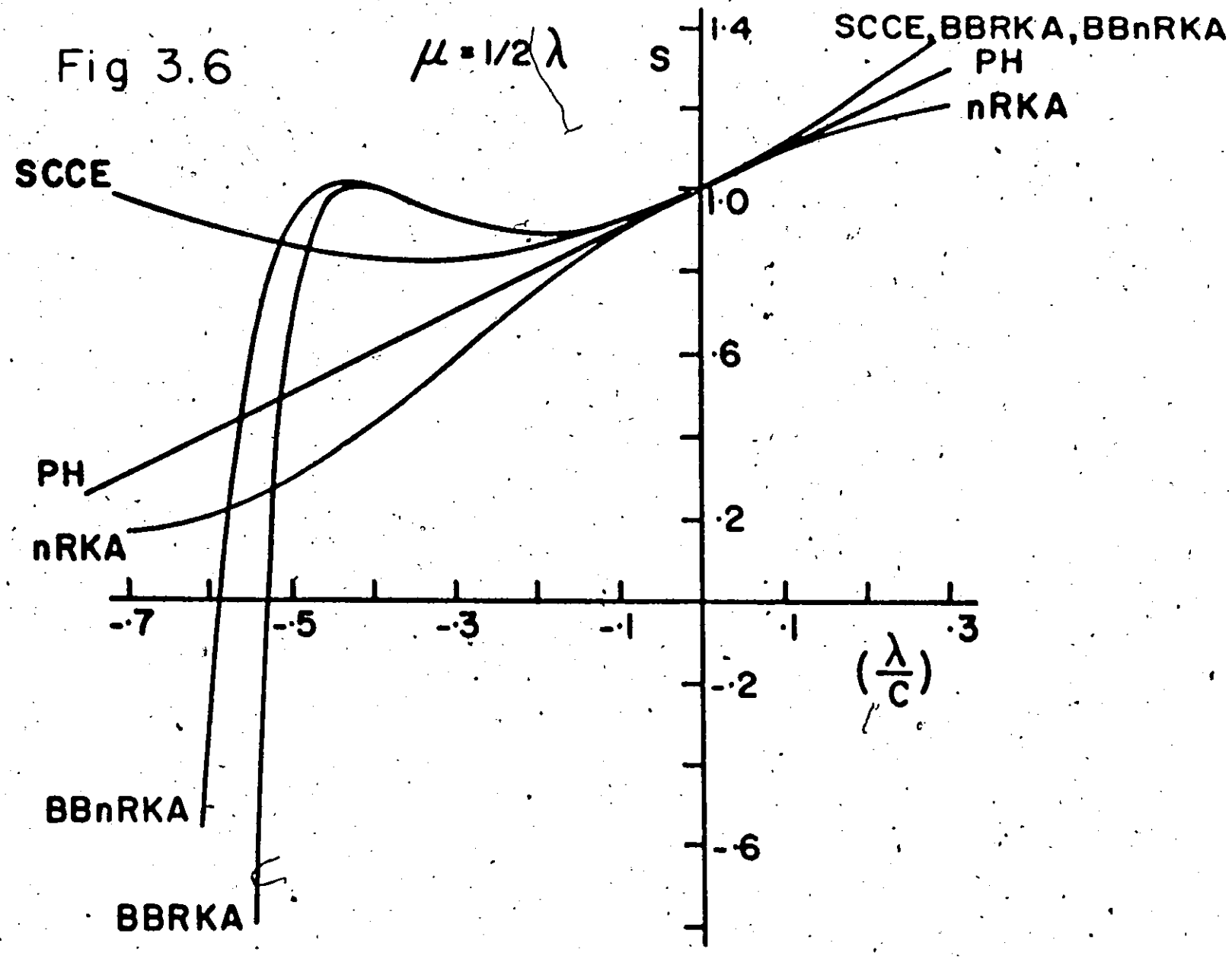
μ = 1/2 λ
S
1·4
1·0
·6
·2
-·2
-·6
SCCE, BBRKA, BBnRKA
PH
nRKA
SCCE
PH
nRKA
BBnRKA
BBRKA
-7
-5
-3
-1
·1
·3
(λ/c)

When $\mu \neq 0$, we have the RPA approximation. From a least squares fit to the Kuo-Brown force (as shown in Appendix D), a realistic value for μ is $\frac{1}{2}\lambda$. If we assume that $\mu = \lambda$, then we have an extreme version of the RKA. From Fig. 3.5, the factor S for extreme RPA diverges at $\frac{\lambda}{c} = -\frac{1}{2}$ but diverges less quickly in the more realistic case.

When screening is included, the amplification factor S^{nRPA} no longer diverges and is only slightly weaker than the p-h case. For $\frac{\lambda}{c} > -\frac{1}{2}$, the factor closely follows the TDA result. Including the vertex renormalization, the amplification factor varies slightly from unity for $\frac{\lambda}{c} > -\frac{1}{2}$ but eventually diverges for more attractive forces. The results for bbRKA and bbnRKA are nearly the same except the screened case diverges less quickly.

When vertex and propagator renormalizations are carried out self consistently, the amplification factor is nearly unity for all force strengths and is denoted by SCCE in Fig. 3.6.

The separable approximation of Table D.1 was rounded off to give $-\lambda\Sigma D_r^2 = -15.6$, $c = 2\hbar\omega = 31.2$ MeV and $\mu = \frac{1}{2}\lambda$. This implies that $\frac{\lambda}{c} = -\frac{1}{2}$ for the realistic case. This is quite a strong interaction since in the extreme RKA it would be at the critical strength, S^{ph} becomes $\frac{1}{2}$ and the p-h interaction is, therefore, $\frac{1}{2}$ as large for the p-h approximation. Under TDA, the amplification factor is

reduced to zero and for RKA ($\mu = \frac{1}{2}\lambda$), the factor is $-\frac{2}{3}$. This is a strong effect since it has changed the sign of the interaction leaving the strength nearly the same. When screening is included, Eq. (3.34) yields $\frac{\kappa}{c} = -.16$, a considerable weakening of the effective coupling constant. The amplification factor for nRKA becomes 0.38 which is weaker than the zero result for TDA.

Including the bb vertex, the factor τ becomes $-\frac{1}{4}$. This is a strong effect since it changes the sign of the original vertex. When τ is calculated from Eq. (3.43) which uses the bb vertices and the screened propagators, we have $\tau_\infty = 0.74$. This implies that the bb vertex is now slightly weaker than the bare vertex but still has the same sign. The amplification factor using this value of τ becomes .43 for bbRKA and .77 for bbnRKA. When τ_∞ and κ are calculated self consistently, we have $\frac{\kappa}{c} = -0.3$ and $\tau_\infty = 0.57$. These yield an amplification factor for SCCE of 0.87 which is only slightly weaker than the bare force.

The general conclusion to be drawn is that in the degenerate schematic model, the various higher order diagrams summed by Kirson do act to reduce the effective coupling constant and thereby mitigate the extremely large renormalization effects that can be found for attractive forces in the RPA calculation. The precise amount of core polarization effect is sensitive to details of the force, but at least for $-.4 < \frac{\lambda}{c} < 0$, there is a clear tendency for the net result to

be a very small change in the unperturbed force. This is in agreement with Kirson's conclusion that the sum of all these higher order processes gives almost no renormalization.

CHAPTER IV

RESULTS OF CALCULATION

In this chapter, we will describe in detail the correction to Kirson's sequence of iterations for the screened p-h vertex f_∞, given in Jopko and Sprung (1973). The shell model spectra for mass 18 and 42 nuclei will be shown for the various forms of core polarization approximations. These are calculated using the two different bare interactions, and the results are compared.

4.1 Calculation of the Screened p-h Vertex

The principal difference between our calculation and that of Kirson concerns the treatment of energy denominators inside deeply nested p-h bubbles such as in Fig. 4.1. One aspect of this problem is discussed on page 636-7 of Kirson (1971). While we were including this effect, we noticed an additional complication which we shall now explain.

Suppose we are calculating a nested propagator f_∞ as in Fig. 4.1 to be used as a core polarization correction

Fig 4.1

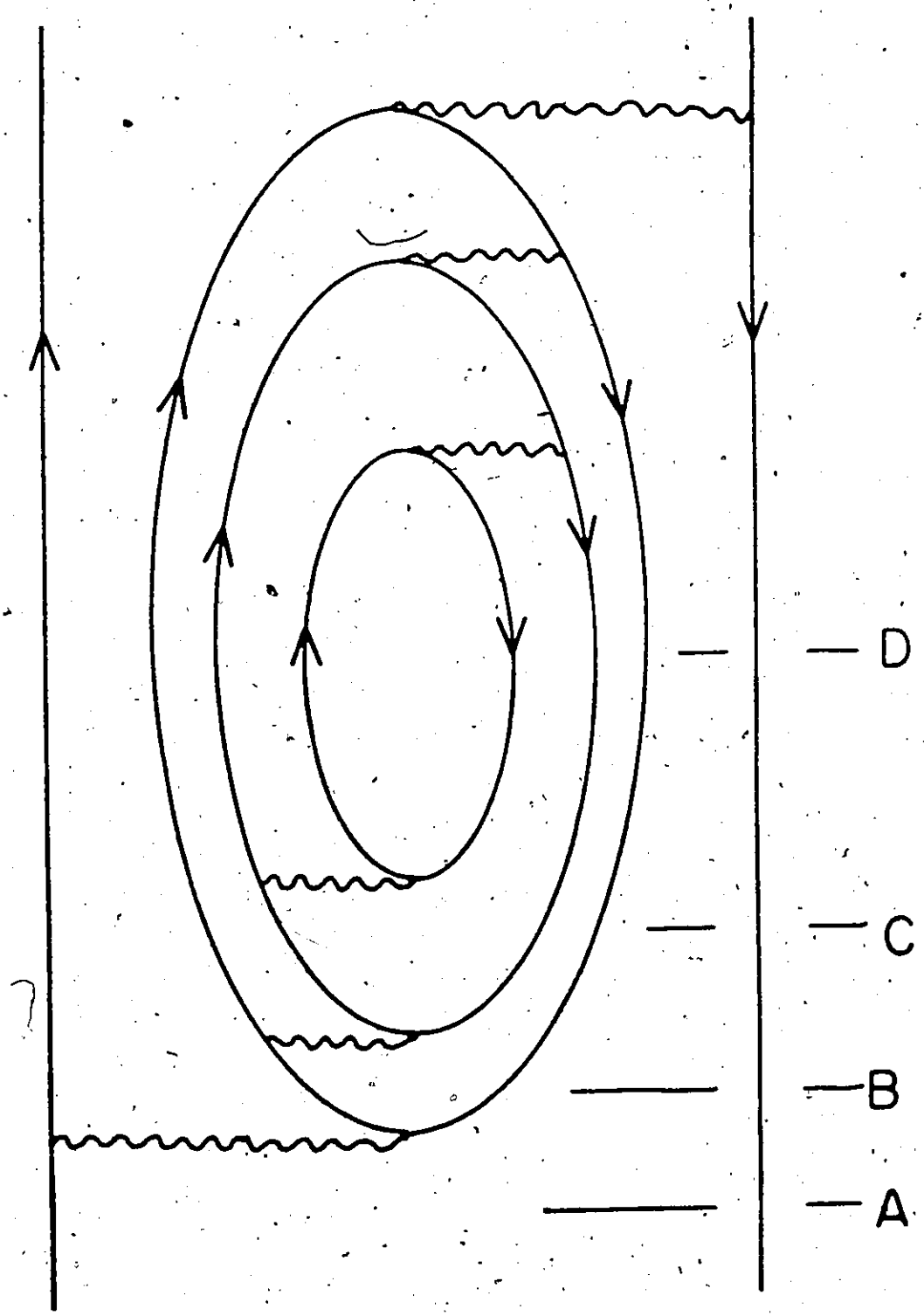

Example of Nested Particle-Hole Propagator.

to the p-p interaction. At level A there exists an excitation energy of $\varepsilon = 2\hbar\omega$. On a naive view, the excitation energies at levels B and C would be 4 and 6 $\hbar\omega$ respectively; however, as pointed out by Kirson, they may in fact be only 4 or 2 $\hbar\omega$. Kirson's point is that during the process of iteration one generates a sequence of f matrices according to

$$f_{n+1} = f + v \frac{1}{\varepsilon + f_n} v' \quad . \tag{4.1}$$

At each stage ε is the excitation energy (excess over the initial energy). In discussing f_∞ in this section, we will omit all complicating factors such as 6-j symbols and summations such as over J" and T".

If one is going to iterate four times as in Fig. 4.1, the first iteration for f_∞ represents the innermost bubble (level D) and so $\varepsilon = 8\hbar\omega$ (or, as we shall see, 6 or 4 $\hbar\omega$). To start f is f_0 or the bare p-h propagator. The reason why the excitation energy may not increase is the existence of odd parity phonons. Consider Fig. 4.2(a) and 4.2(b) which show respectively

$$\langle (Sd)^2 p^{-1} | V | pf \rangle \tag{4.2}$$

and

$$\langle pf, Sd, p^{-1} | V | Sd \rangle \quad .$$

Fig 4.2

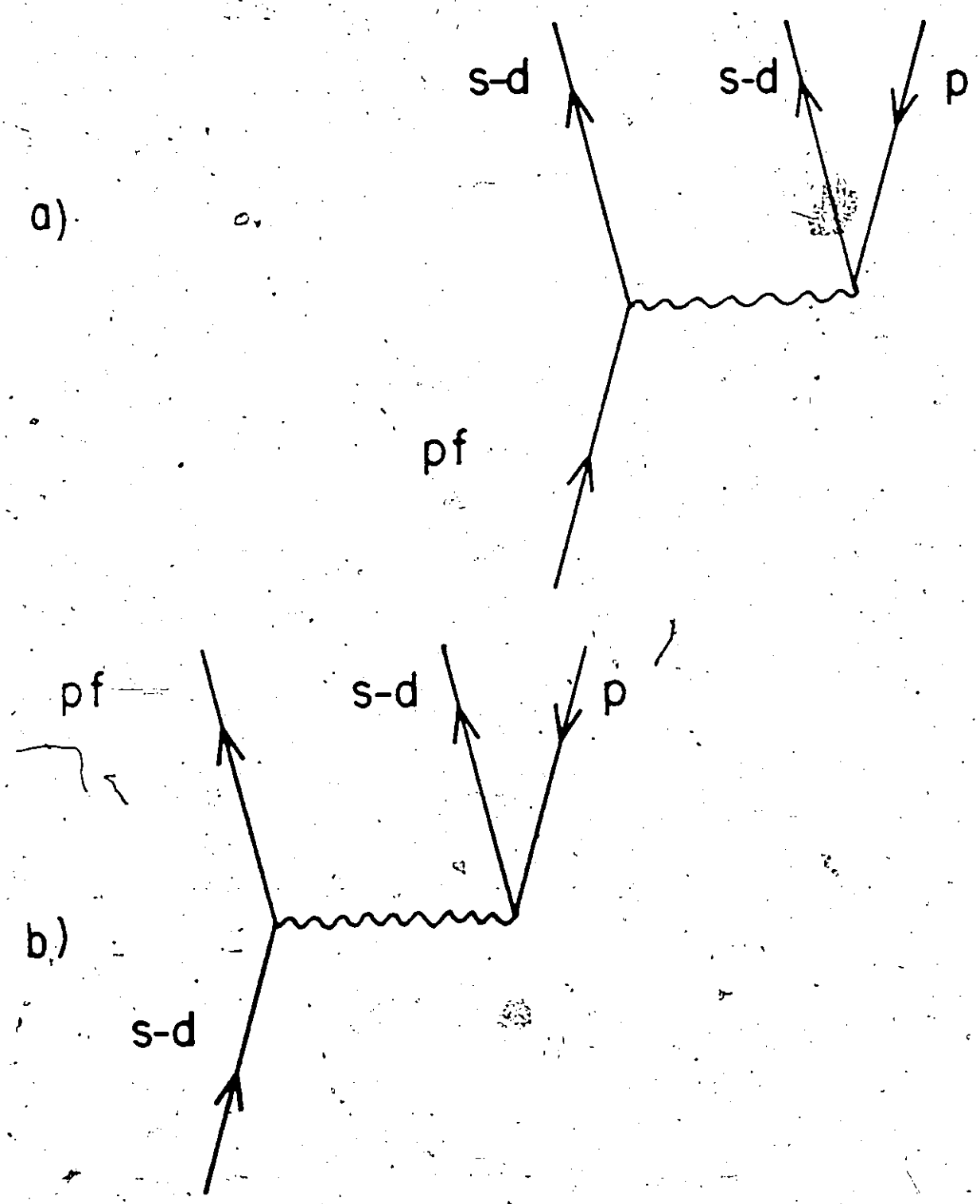

Vertices which have (a) 0 $\hbar\omega$ and (b) 2 $\hbar\omega$ excitation.

We have in mind the oxygen region but clearly the argument can be applied in calcium as well. The odd parity phonon carries 1 $\hbar\omega$ energy so in Figs. 4.2(a) and 4.2(b) the increase in excitation energy from below the interaction to above it is

$$\epsilon_a = 1\ \hbar\omega + \epsilon(sd) - \epsilon(pf) = 0\ \hbar\omega$$
$$\epsilon_b = 1\ \hbar\omega + \epsilon(pf) - \epsilon(sd) = 2\ \hbar\omega \quad . \tag{4.3}$$

Even though these figures may occur in a more complicated diagram, we have ignored the energy of all other particle or hole states since they will be the same before and after the interaction shown.

If we did not have to remember this possible non-increase in excitation energy, we would simply solve the sequence

$$f_1 = f_0 + v \frac{1}{8\ \hbar\omega + f_0} v'$$
$$f_2 = f_0 + v \frac{1}{6\ \hbar\omega + f_1} v' \tag{4.4}$$
$$f_3 = f_0 + v \frac{1}{4\ \hbar\omega + f_2} v' \quad .$$

The propagator in Fig. 4.1 would then be $(2\ \hbar\omega + f_3)^{-1}$. Because of the other possible energy

denominators, one must also consider the sequences

$$\begin{cases} f_1^{\alpha} = f_0 + \nu \dfrac{1}{8\hbar\omega + f_0}\nu' \\ f_1^{\beta} = f_0 + \nu \dfrac{1}{6\hbar\omega + f_0}\nu' \\ f_1^{\gamma} = f_0 + \nu \dfrac{1}{4\hbar\omega + f_0}\nu' \end{cases}$$

$$\begin{cases} f_2^{\alpha} = f_0 + \nu \dfrac{1}{6\hbar\omega + f_1}\nu' \\ f_2^{\beta} = f_0 + \nu \dfrac{1}{4\hbar\omega + f_1}\nu' \end{cases} \qquad (4.5)$$

$$\begin{cases} f_3^{\alpha} = f_0 + \nu \dfrac{1}{4\hbar\omega + f_2}\nu' \\ f_3^{\beta} = f_0 + \nu \dfrac{1}{2\hbar\omega + f_2}\nu' \end{cases}$$

In the energy denominator on the right side of Eq. (4.5) we have omitted the superscripts α,β because the required one depends on which p-h matrix element we are doing. The parity sequences for the bubbles in Fig. 4.1 are listed in Table 4.1. The parity of level A must always be even because the parity of the two valence nucleons is even. For four bubbles, there are five parity sequences. The number of parity sequences is the number of ways that odd parity bubbles may be listed for the four bubbles such that no two of them are consecutive. The reason for

TABLE 4.1

POSSIBLE PARITY SEQUENCES FOR THE INTERMEDIATE STATES OF FIG. 4.1.

Level / Case	A	B	C	D
(a)	+	+	+	+
(b)	+	−	+	+
(c)	+	+	−	+
(d)	+	+	+	−
(e)	+	−	+	−

TABLE 4.2

POSSIBLE SEQUENCES OF ENERGY DENOMINATORS FOR THE CASES IN TABLE 4.1.

Level / Case	A	B	C	D
(a)	2	4	6	8
(b)	2	4	6	8
	2	2	4	6
(c)	2	4	6	8
	2	4	4	6
(d)	2	4	6	8
	2	4	6	6
(e)	2	4	6	8
	2	4	6	6
	2	2	4	6
	2	2	4	4

this is that the particle space (or hole space) of the odd parity phonon has only one parity. Because of parity conservation the next bubble must always have even parity. For n bubbles, it appears that the number of parity sequences is F_n, where $F_0 = F_1 = 1$ and F_n is the n^{th} Fibonacci number given by $F_n = F_{n-1} + F_{n-2}$.

For each of the given parity sequences, there are sequences of energy denominators shown in Table 4.2. Case (a) in Table 4.2 corresponds to the normal case when all bubbles are even parity and there is an increase of $2\hbar\omega$ excitation energy between bubbles.

As an odd parity phonon appears in case (b), we see that there is a situation when the energy denominator remains the same from level A to B.

The number of different sequences of energy denominators for each case is given by 2^m where m is the number of odd parity phonons in that parity sequence for the given case. For example, for case (e) in Table 4.1, we have two odd parity levels and so there are four possible sequences of energy denominators shown in Table 4.2. In each case, the different sequences may be specified by beginning with two and noting that the difference in energy may be 0 or $2\hbar\omega$ for each odd parity bubble but is always $2\hbar\omega$ for even parity bubbles. These observations greatly complicate the numerical calculation because one needs to store in memory the cases α, β, γ for

f_n at each stage of the iteration. Kirson has remarked to us that his prescription will begin to err only when there are more than two levels of nested bubbles. If the calculation converges rapidly, there may be little practical effect from this complication. To verify this, we repeated Kirson's calculation for the oxygen region and found generally very good agreement with his results. In Table 4.3 we provide an example showing the effect of using the proper sequences of f matrices in the calculation. It is seen to be only a few percent. What this will do to the SCCE calculation of Kirson is unknown. Probably the SCCE result will have a larger error but not by much.

4.2 Shell Model Spectra of A = 18, 42 Nuclei

In this chapter, the practical application of the perturbative approach to the shell model residual interaction will be demonstrated. We have chosen to deal with mass 18 and 42 nuclei for the reasons that these nuclei are the simplest for which the residual interaction is required and the region where the perturbative approach may be most successful. No attempt has been made to extend the calculation for nuclei further from the magic nuclei. Reasons for this are the greater complications for three or

TABLE 4.3

THE EFFECT OF CONSIDERING PROPER ENERGY DENOMINATOR SEQUENCES ON THE $|(d_{5/2})^2\ JT\rangle$ CORE POLARIZATION DIAGONAL MATRIX ELEMENT FOR MASS 18, IN nRPA.

J	T	Kirson	Present Work
0	1	-1.333	-1.350
1	0	- .684	- .695
2	1	.067	- .071
3	0	.221	.224
4	1	.573	.578
5	0	- .391	- .398

core active nucleons in a shell model calculation and the possible presence of three body forces arising in the residual interaction, but not considered in this calculation. Further, the results of the renormalization, as we shall see, are unable to explain the low lying spectra in the simple two valence nucleon case, so extension to three or more nucleons seems questionable. The calculation itself becomes less reliable when the valence shell contains many nucleons because of the increasing violation of the Pauli principle for particles excited from the core into the valence space.

Starting with the bare residual interaction, we have performed all the renormalizations discussed in Chapter III for both oxygen and calcium using both the KLS and PSA forces. Using these renormalized matrix elements, shell model calculations were done for each force for each renormalization. The results for the KLS force in oxygen were disappointing and the reason appears to be that the ground state for the bare KLS force is approximately 4 MeV lower than the ground state from the Kuo-Brown force. The spectra for oxygen using the PSA force and for calcium using both forces is presented.

In Table 4.4, the twenty matrix elements in oxygen and fifty-one matrix elements in calcium which are to be renormalized, are presented. When coupling of angular momenta is included, the list expands to sixty-three in

TABLE 4.4

VALENCE SHELL MATRIX ELEMENTS FOR O AND Ca.

THE NUMBERING SYSTEM FOR THE VARIOUS SHELL MODEL ORBITALS WAS DEFINED IN FIG. 1.1.

Oxygen	Calcium	
4444	7 7 7 7	710 8 8
4455	7 7 7 8	710 8 9
4446	7 7 7 9	710 9 9
4455	7 7 710	710 910
4456	7 7 8 8	7101010
4466	7 7 8 9	8 8 8 8
4545	7 7 810	8 8 8 9
4546	7 7 9 9	8 8 810
4556	7 7 910	8 8 9 9
4566	7 71010	8 8 910
4646	7 8 7 8	8 81010
4655	7 8 7 9	8 9 8 9
4656	7 8 710	8 9 810
4666	7 8 8 8	8 9 9 9
5555	7 8 8 9	8 9 910
5556	7 8 810	8 91010
5566	7 8 910	810 810
5656	7 81010	810 9 9
5666	7 9 7 9	810 910
6666	7 9 710	8101010
	7 9 8 8	9 9 9 9
	7 9 810	9 91010
	7 9 910	910 910
	7 91010	9101010
	710 710	10101010

oxygen and three hundred and twenty-five in calcium. Each of these matrix elements is renormalized by excitations from the core. The p-h states which contribute to a given phonon of angular momentum J^π and isospin T^π and parity π are listed in Table 4.5.

4.3 Calculational Procedure

The method and organization of these calculations is presented below. The first step was to determine all those two body matrix elements in the valence shell shown in Table 4.4 in speedometer order. That is, the first digit varies least rapidly, the last digit varies most rapidly. (Not all possible permutations of the states in the valence shell are allowed because in some cases, the two states could not couple to a given total angular momentum which is preserved in the final state since the interaction is a scalar quantity.)

The second step is to list all possible p-h excitations which had 2 $\hbar\omega$ energy for even parity and 1 $\hbar\omega$ energy for odd parity as indicated in Table 4.5. No 3 $\hbar\omega$ or 4 $\hbar\omega$ excitations were considered because of the large increase in size of the matrices required.

Because of the large number of matrix elements required, it was necessary to write a routine that would

TABLE 4.5

THE NUMBER AND LIST OF p-h STATES THAT COUPLE TO ANGULAR MOMENTUM AND PARITY J^{π} IN OXYGEN AND CALCIUM. THE NUMBERING OF STATES IS GIVEN IN FIG. 1.1.

Oxygen

J^{π}	Number	List of p-h states
0^+	3	9-1,8-2,5-1
1^+	7	10-2,9-1,9-2,8-1,8-2,6-1,5-1
2^+	8	10-1,10-2,9-2,8-1,8-2,7-2,6-1,4-1
3^+	6	10-1,10-2,8-2,7-1,7-2,4-1
4^+	3	10-2,7-1,7-2
5^+	1	7-2
0^-	2	6-2,5-1
1^-	5	6-1,6-2,5-1,5-2,4-2
2^-	5	6-1,6-2,5-2,4-1,4-2
3^-	3	6-2,4-1,4-2
4^-	1	4-2

Calcium

0^+	5	14-1,13-2,12-3,9-1,8-2
1^+	13	15-3,14-1,14-2,14-3,13-1,13-2,12-1,12-3,10-2,9-1, 9-2,8-1,8-2
2^+	17	15-1,15-3,14-1,14-2,14-3,13-1,13-3,12-1,12-2, 12-3,11-3,10-1,10-2,9-2,8-1,8-2,7-2
3^+	16	15-1,15-2,15-3,14-1,14-3,13-3,12-1,12-2,12-3, 11-1,11-3,10-1,10-2,8-2,7-1,7-2
4^+	12	15-1,15-2,15-3,14-3,12-1,12-3,11-1,11-2,11-3, 10-2,7-1,7-2
5^+	7	15-1,15-3,12-3,11-1,11-2,11-3,7-2
6^+	3	15-3,11-1,11-3
7^+	1	11-3

TABLE 4.5 - continued

Calcium

J^π	Number	List of p-h States
0^-	3	10-3,9-2,8-1
1^-	8	10-1,10-3,9-1,9-2,8-1,8-2,8-3,7-3
2^-	11	10-1,10-2,10-3,9-1,9-3,8-1,8-2,8-3,7-1,7-2,7-3
3^-	9	10-1,10-2,10-3,9-3,8-1,8-3,7-1,7-2,7-3
4^-	5	10-1,10-3,8-3,7-1,7-3
5^-	3	10-3,7-1,7-3
6^-	1	7-3

locate a matrix element from the four labels specifying it. Up to the p-f-h shell, there are twenty-one different states. Using the fact that

$$\sum_{i-j=1}^{n} 1_{ij} = \frac{n(n+1)}{2} \qquad i,j \text{ integers} \tag{4.6}$$

the number of distinct two particle states is $\frac{21(21+1)}{2} = 231$. The number of distinct two body matrix elements in speedometer order is, therefore, $\frac{231(231+1)}{2} = 26{,}796$ for given J and T.

To locate the matrix element $\langle ab|V|cd\rangle$ in this array where $a \leq c$, $a \leq b$, $c \leq d$, ≤ 21, we used the following procedure. Define

$$K_1 = \frac{(a-1)\times(2N-a)}{2} + b$$

$$K_2 = \frac{(c-1)\times(2N-c)}{2} + d \tag{4.7}$$

$$KK = \frac{(K_1-1)\times(2NN-K_1)}{2} + K_2$$

where N = 21 and NN = 231. The value of KK is the index to locate the matrix element in an array.

The p-h matrix elements that were required have the following form

$$\langle ph^{-}|V|p'h'^{-}\rangle \quad , \quad \langle ph^{-}|V|h'p^{-}\rangle$$

$$\langle val, val^{-}|V|ph^{-}\rangle \quad , \quad \langle val, val^{-}|V|hp^{-}\rangle \tag{4.8}$$

where p, h are particle-hole states and val is a state in the valence space. A program was written that contained an integer array of length 26,796 that was preset to zero. Given the space of p-h excitations and the valence space, the program constructed all p-h matrix elements needed. This matrix element was rewritten in p-p order and then speedometer order. The location of the matrix element in the array was calculated from Eq. (4.7) and if the word were empty, then the integer

$$a \times 10^{6} + b \times 10^{4} + c \times 10^{2} + d \tag{4.9}$$

was stored at that location. If the entry were not zero, then we would skip to the next p-h matrix element. For example, if we require $\langle 62^{-}|V|51^{-}\rangle$ where 2^{-} represents a hole in the state labelled 2, then this is obtained from the p-p matrix element $\langle 61|V|52\rangle$. This is written in speedometer order as $\langle 16|V|25\rangle$ and its location in the array is computed as

$$K_1 = \frac{(1-1)\times(42-1)}{2} + 6 = 6$$

$$K_2 = \frac{(2-1)\times(42-2)}{2} + 5 = 25 \qquad (4.10)$$

$$KK = \frac{(6-1)\times(462-6)}{2} + 25 = 1265 \quad .$$

If the position 1265 in the array were zero, then the integer 01060205 is stored in that location. This procedure is repeated for all p-h matrix elements. At the end of the program, all non zero words in the array are printed and punched out on cards. Once the list of p-p matrix elements is known, another program uses this as input and constructs the coefficients in the expansion of the two body matrix element as given in Eq. (2.27) and stores the coefficient and the six labels n, ℓ, n', ℓ', S, and J for the relative matrix element as well as the number of coefficients in the expansion, the angular momentum J and isospin T. Arrays were assigned to contain the integer

$$n \times 10^{10} + \ell \times 10^{8} + n' \times 10^{6} + \ell' \times 10^{4} + S \times 10^{2} + J \qquad (4.11)$$

and the complete set of relative matrix elements determined. In oxygen, there were one hundred and twenty-seven relative matrix elements required and two hundred and seventy-two in calcium. The time to calculate all these coefficients was approximately ten hours on the CDC 6400. The slowest part

of the calculation seemed to be the Moshinsky brackets. Since that time, a new routine for the Moshinsky brackets was written[I] with an anticipated increase in efficiency of a factor of 10. The number of coefficients calculated is estimated to be 150,000. These coefficients and the corresponding relative matrix elements were used to construct all two body matrix elements.

Each such p-p matrix element may be used twice to construct two different p-h matrix elements, for example,

$$\langle 16|V|25\rangle \rightarrow \langle 15^{-}|V|26^{-}\rangle$$
$$\text{and} \qquad (4.12)$$
$$\langle 61|V|25\rangle \rightarrow \langle 65^{-}|V|21^{-}\rangle \quad .$$

The p-h matrix element $\langle 15^{-}|V|26^{-}\rangle$ appears useless because the particle states are more deeply bound than the hole states. However, from the symmetry of the p-h transformation, it is easily shown that in general

$$\langle ab^{-}|V|cd^{-}\rangle = (-)^{a+b+c+d}\langle ba^{-}|V|dc^{-}\rangle \quad . \qquad (4.13)$$

Therefore,

$$\langle 15^{-}|V|26^{-}\rangle = (-)^{j_1+j_5+j_2+j_6}\langle 51^{-}|V|62^{-}\rangle$$

I by Mr. P. Dunmore.

and the required meaning of particle and hole is obtained.

Because there are approximately six thousand p-p matrix elements required in calcium and each may be used to construct two p-h matrix elements and each of these may be coupled to at most eighteen combinations of total J and T, it was not possible to store all p-h matrix elements in core simultaneously. The core polarization expression is calculated as a sum over J", T" for the p-h excitations. It was convenient then to store all p-h matrix elements for given J" and T" in a block and to read in the next block of six thousand words for the new J", T". Two p-h matrix elements were stored in each computer word. Because of the long (60 bit) word of the CDC computer, each number can still be stored to 6 digit accuracy. In the first half of the word, the p-h matrix element obtained from the p-p matrix element in speedometer order was stored. In the second half of the word, the p-h matrix element obtained from the p-p matrix element not in standard order was stored. The p-h matrix elements were of the f type (Kirson), since the same matrix element may be required in a B vertex or a ν vertex. These may be obtained by multiplying the f vertex by an appropriate factor.

In addition to this large array, another array $\frac{1}{4}$ the size was used to store the location of a p-h matrix element in the six thousand word array. The largest integer required is 26,796 and may be stored in $\frac{1}{4}$ of a

computer word. To save space, then an array of 6,699 only was required.

This procedure was employed in separate programs to calculate the screened vertex f_∞ and the black box vertices bb. These also were fed into the final program in blocks from disc of given J", T". In the final program, all renormalizations of matrix elements in the valence space were performed for all possible J and T and the results stored on tape.

The greatest amount of time spent in the computation occurred in the calculation of the screened vertex f_∞. In oxygen, fifteen minutes was sufficient for four iterations but in calcium, only two iterations were completed in three hours. For four iterations, the estimated time was a prohibitively large ten hours and this would have to be done for each of the two forces used. Also, the systems group of the computer centre was unable to make operative the RESTART feature of the SCOPE operating system. In the event of any failure of the computer, an entire ten hour run would be lost.

In Table 4.6 is shown a comparison of part of the four iteration calculation in calcium with the complete two iteration one. As can be seen, there are only small changes in diagonal matrix elements (though relatively more important changes in the smaller off-diagonal matrix elements) for the 2^+0 phonon, KLS force. A reasonable

TABLE 4.6

COMPARISON OF TWO AND FOUR ITERATION CALCULATIONS, IN ^{40}Ca, FOR SOME TYPICAL f-MATRIX ELEMENTS, 2^+0 PHONON, KLS FORCE. THE LEFT HAND COLUMN IS FROM THE FOUR ITERATION CALCULATION.

$4\hbar\omega + f_2$	$4\hbar\omega + f_0$
42.51	42.50
.64	.85
44.94	45.06
.13	.17
.31	.31
44.01	43.80
- .21	- .22
.50	.59
1.93	2.03
43.81	43.60

level of convergence for two iterations is expected.

The results of the calculation are now presented. Shown in Tables 4.7, 4.8, and 4.9 are the various renormalizations computed using the PSA force in oxygen and calcium and using the KLS force in calcium. The largest renormalizations occur for small J and of all matrix elements in the valence space, those with diagonal two particle states are expected to have the greatest result . The reason is that if the two particle states are different, they will have a different number of nodes in the radial wavefunction and hence the overlap with the effective interaction will likely be smaller. For these reasons we present the J=0, T=1 and J=1, T=0 matrix elements which are diagonal in both the s-d and p-f shell. The bare G-matrix elements are given in the first column as a reference for the magnitude of core polarization corrections in the columns that follow. From the Tables 4.7 to 4.9 the 3p-1h corrections are almost always negative. For the J=0 case, the largest 3p-1h renormalization occurs for the 4444 matrix element. For the J=1 case, the largest 3p-1h correction is for the 4466 matrix element probably because the bare G-matrix element is so large. Similarly, the 7777 matrix element contains the greatest 3p-1h effect. The next column contains the TDA renormalization and again they are almost always negative and even more so than 3p-1h. In particular the TDA result for 8888 and 9999, both J=0 and

TABLE 4.7

CORE POLARIZATION CONTRIBUTIONS FOR VARIOUS VALENCE SPACE MATRIX ELEMENTS IN THE OXYGEN REGION USING THE PSA FORCE.

J=0 / T=1 abcd	G*	p-h	TDA	RPA	nRPA	bbph	bbRPA	bbnRPA
4444	-2.006	-.213	-.567	-1.141	-.605	.667	-.284	.281
4455	- .979	-.104	-.280	- .358	-.256	.065	-.074	-.024
4466	-3.405	.075	-.128	- .206	-.141	.908	.666	.681
5555	-2.768	.124	-.428	-2.104	-.678	.554	-.441	.125
5566	- .799	-.052	-.105	- .119	-.115	.106	.062	.051
6666	- .615	-.087	-.221	- .351	-.226	.213	.088	.154
J=1 / T=0								
4444	- .779	-.186	-.477	-1.01	-.518	.306	-.584	-.022
4455	- .415	-.053	-.175	- .227	-.156	.042	-.058	-.023
4466	2.409	-.266	-.279	- .298	-.248	-.439	-.411	-.385
5555	-3.367	-.123	-.647	-2.309	-.878	.407	-.538	-.024
5566	- .310	.099	.101	.102	.094	.076	.070	.068
6666	- .742	-.143	-.171	- .247	-.173	.082	.009	.069

TABLE 4.8

CORE POLARIZATION CONTRIBUTIONS FOR VARIOUS VALENCE SPACE MATRIX ELEMENTS IN THE CALCIUM REGION USING THE PSA FORCE.

J=0, T=1 a b c d	G	p-h	TDA	RPA	nRPA	bbph	bbRPA	bbnRPA
7 7 7 7	-1.279	-.307	-1.193	-1.43	-.564	.733	.363	.888
7 7 8 8	- .651	-.121	- .370	- .689	-.334	-.059	-.535	-.229
7 7 9 9	- .613	-.021	- .069	- .091	-.071	.103	.044	.062
7 71010	-2.331	.079	- .134	- .345	-.153	1.074	.723	.787
8 8 8 8	-1.410	-.085	-3.425	.093	1.347	3.105	2.418	2.744
8 8 9 9	-1.514	-.019	- .340	- .784	-.338	.773	-.248	.135
8 81010	- .709	-.000	- .054	- .082	-.061	.367	.276	.256
9 9 9 9	- .339	-.123	-2.447	.338	1.064	1.740	1.859	1.907
9 91010	- .325	-.051	- .150	- .252	-.136	.184	.150	.135
10101010	- .606	-.240	- .735	-1.129	-.544	.362	.002	.227
J=1, T=0								
7 7 7 7	- .581	-.258	-1.038	-1.129	-.412	.405	.163	.646
7 7 8 8	- .166	-.116	- .318	- .589	-.284	-.173	-.567	-.304
7 7 9 9	.198	.018	.042	.051	-.040	-.003	.016	.009
7 71010	1.773	-.273	- .316	- .436	-.279	-.529	-.539	-.449
8 8 8 8	- .853	-.149	-3.339	.380	1.435	2.768	2.701	2.801
8 8 9 9	.965	-.020	.135	.336	.135	-.251	.267	.106
8 81010	.133	.010	.013	.009	.018	-.084	-.051	-.046
9 9 9 9	- .947	-.165	-2.490	.295	1.024	1.903	1.922	1.955
9 91010	- .090	-.067	- .132	- .199	-.119	.076	.054	.046
10101010	- .524	-.227	- .562	- .794	-.374	.189	-.018	.136

TABLE 4.9

CORE POLARIZATION CONTRIBUTIONS FOR VARIOUS VALENCE SPACE MATRIX ELEMENTS IN THE CALCIUM REGION USING THE KLS FORCE.

J=0, T=1 a b c d	S	p-h	TDA	RPA	nRPA	bbph	bbRPA	bbnRPA
7 7 7 7	- .848	-.927	-1.695	-4.974	-2.328	.431	-1.120	-.030
7 7 8 8	- .465	-.337	- .646	-1.732	- .832	.137	- .624	-.144
7 7 9 9	- .522	-.171	- .261	- .398	- .334	.229	.121	.130
7 71010	-2.322	-.475	- .811	-1.768	-1.139	1.131	.351	.630
8 8 8 8	-1.012	-.181	-1.321	- .771	.450	.455	.087	.606
8 8 9 9	-1.293	-.192	- .585	-2.284	- .979	.372	- .684	-.074
8 81010	- .587	-.172	- .271	- .421	- .336	.318	.208	.202
9 9 9 9	- .097	-.152	- .800	.392	.780	.079	.328	.473
9 91010	- .191	-.193	- .348	- .759	- .409	.114	- .011	.038
10101010	- .177	-.651	-1.297	-3.817	-1.683	.143	- .878	-.169
J=1, T=0								
7 7 7 7	.099	-.459	-1.077	-3.643	-1.541	.247	-1.028	-.130
7 7 8 8	.081	-.267	- .513	-1.408	- .641	-.097	- .729	-.303
7 7 9 9	.041	.052	.101	.166	.134	-.061	- .004	-.011
7 71010	1.437	-.563	- .577	-1.065	- .603	-.883	-1.063	-.804
8 8 8 8	- .585	-.027	- .995	.327	.943	.431	.472	.724
8 8 9 9	.630	-.056	.146	.902	.326	-.135	.372	.107
8 81010	- .080	.065	.079	.070	.090	-.042	- .029	-.018
9 9 9 9	- .715	-.201	- .953	.306	.702	.078	.273	.418
9 91010	.123	-.114	- .231	- .508	- .268	.031	- .076	-.039
10101010	.496	-.186	- .601	-2.113	- .753	.017	- .659	-.187

1 is extremely large and negative. The next column contains the RPA renormalization and these are even more attractive than TDA.

When screening is included, we obtain the results under the column nRPA and it is seen that they correspond rather closely to the TDA results, but are usually slightly more attractive. For bbph it is immediately apparent, that the renormalizations are repulsive with few negative entries. Using the bb vertex and RPA propagator, more negative corrections are obtained. This is reasonable because the RPA always lowers the spectrum compared to the bare result. When bb vertices are included with screening, the result is more positive since screening raises the spectrum relative to RPA.

The above is quite satisfying but for two exceptions. These are the 8888 and 9999 cases. The TDA result is very large and negative but the RPA result is small and positive and the nRPA is large and positive. When these matrix elements are compared with Kuo and Osnes (1974), one finds that the screened RPA is negative but slightly smaller than the TDA. Although these authors included screening to second order and pp and hh interactions which we did not, this should not be the reason for the discrepancy, since there is good agreement in the other cases. The result stated in this thesis for these two exceptions may be understood in the schematic model.

For an attractive force, it is easily shown that

$$S^{TDA} \leq S^{nRPA} \leq S^{RPA} \quad , \quad \frac{\lambda}{c} \leq 0 \quad . \tag{4.14}$$

This is consistent with the cases excluding the two exceptions because if S^{TDA} is negative, then S^{nRPA} will be larger and hence the correction to the bare interaction will be larger making it even more negative. Similarly, the RPA correction is still more negative than the nRPA result.

For repulsive forces, the schematic model gives

$$S^{TDA} \geq S^{RPA} \geq S^{nRPA} \quad , \quad \frac{\lambda}{c} \geq 0 \quad . \tag{4.15}$$

If the TDA correction is negative, then the RPA correction will be less negative (more repulsive still) and the nRPA result is even more repulsive.

It is claimed that for these two exceptions, the p-h force is repulsive and, therefore, the nRPA result is very different from the TDA. In fact the TDA, RPA, and nRPA corrections satisfy the inequalities in Eq. (4.15) very well. This adds confidence to the results of the realistic calculation and the difference from the result of Kuo and Osnes is unexplained.

The matrix elements in Tables 4.7 to 4.9 consist of a sum over various multipoles of core polarization. The contribution of each multipole is shown in Table 4.10 for

TABLE 4.10(a)

VARIOUS CONTRIBUTIONS BY MULTIPOLES (J"T") TO THE CORE POLARIZATION MATRIX ELEMENT.

$$\langle (0f_{7/2})^2 JT | \Delta G^{KLS}_{c-p} | (0f_{7/2})^2 JT \rangle$$

J=J T=1 BARE= -.848 MEV

J"	T"	3P1H	TDA	RPA	NRPA	BB3P1H	BBRPA	BBNRPA
0	0	-.034	-.067	-.817	-.003	-.036	.029	.079
0	1	-.006	-.005	-.005	-.005	-.014	-.010	-.010
1	0	.050	.046	.047	.044	.093	.090	.084
1	1	.034	.029	.026	.025	.064	.047	.045
2	0	-.620	-1.262	-4.410	-1.863	-.296	-1.869	-.811
2	1	-.110	-.088	-.081	-.077	-.183	-.135	-.128
3	0	.051	.053	.055	.053	.090	.081	.075
3	1	.077	.067	.061	.058	.181	.149	.140
4	0	-.281	-.393	-.562	-.473	-.133	-.160	-.148
4	1	-.087	-.075	-.068	-.066	-.211	-.169	-.164
5	0	.022	.022	.022	.022	.150	.138	.132
5	1	.039	.036	.035	.034	.189	.169	.162
6	0	-.082	-.098	-.099	-.099	-.112	-.108	-.109
6	1	-.042	-.039	-.037	-.037	-.178	-.162	-.163
7	0	.053	.051	.050	.049	.496	.467	.464
7	1	.009	.009	.009	.009	.332	.323	.321
TOTAL		-.927	-1.635	-4.975	-2.329	.432	-1.120	-.030

TABLE 4.10(b)

J=1 T=0 BARE= .099 MEV

J"	T"	3P1H	TDA	RPA	NRPA	BB3P1H	BBRPA	BBNRPA
0	0	-.034	-.067	-.017	-.003	-.036	.029	.079
0	1	.019	.016	.015	.014	.043	.031	.030
1	0	.047	.043	.044	.041	.087	.084	.078
1	1	-.097	-.082	-.074	-.071	-.179	-.133	-.128
2	0	-.502	-1.021	-3.570	-1.508	-.240	-1.513	-.656
2	1	.265	.215	.196	.186	.444	.327	.310
3	0	.032	.033	.034	.033	.056	.050	.046
3	1	-.143	-.124	-.114	-.108	-.337	-.276	-.260
4	0	-.103	-.140	-.205	-.173	-.049	-.058	-.054
4	1	.095	.082	.074	.072	.231	.186	.180
5	0	.001	.001	.001	.001	.007	.007	.006
5	1	-.006	-.005	-.005	-.005	-.027	-.024	-.023
6	0	.027	.033	.033	.033	.037	.036	.036
6	1	-.042	-.039	-.037	-.037	-.178	-.162	-.163
7	0	-.041	-.048	-.039	-.038	-.385	-.363	-.361
7	1	.021	.021	.021	.021	.774	.753	.749
TOTAL		-.460	-1.078	-3.643	-1.542	.247	-1.029	-.130

TABLE 4.10(c)

J=2 T=1 BARE= -.647 MEV

J$^\pi$	T$^\pi$	3P1H	TDA	RPA	NRPA	BB3P1H	BBRPA	BBNRPA
0	0	-.034	-.057	-.017	-.003	-.036	.029	.079
0	1	-.005	-.005	-.005	-.005	-.014	-.010	-.010
1	0	.040	.037	.038	.036	.076	.073	.068
1	1	.028	.024	.021	.021	.052	.038	.037
2	0	-.290	-.589	-2.058	-.870	-.138	-.872	-.378
2	1	-.051	-.041	-.038	-.036	-.085	-.063	-.060
3	0	.002	.003	.003	.003	.004	.004	.004
3	1	.004	.003	.003	.003	.009	.007	.007
4	0	.094	.128	.187	.158	.044	.053	.049
4	1	.029	.025	.023	.022	.070	.056	.055
5	0	-.012	-.012	-.012	-.012	-.079	-.072	-.069
5	1	-.020	-.019	-.018	-.018	-.099	-.089	-.085
6	0	.027	.030	.033	.033	.037	.036	.036
6	1	.014	.013	.012	.012	.059	.054	.054
7	0	.025	.024	.023	.023	.231	.218	.217
7	1	.004	.004	.004	.004	.155	.151	.150
TOTAL		-.145	-.462	-1.800	-.628	.285	-.387	.153

TABLE 4.10(d)

J=3 T=0 BARE= -.255 MEV

J"	T"	3P1H	TDA	RPA	NRPA	BB1P1H	BBRPA	BBNRPA
0	0	-.034	-.067	-.017	-.003	-.036	.029	.079
0	1	.019	.016	.015	.014	.043	.031	.038
1	0	.031	.029	.029	.027	.058	.056	.052
1	1	-.064	-.054	-.049	-.047	-.118	-.088	-.084
2	0	-.030	-.060	-.218	-.089	-.014	-.089	-.039
2	1	.016	.013	.012	.011	.026	.019	.018
3	0	-.021	-.021	-.022	-.021	-.036	-.032	-.030
3	1	.093	.081	.074	.070	.219	.180	.169
4	0	.123	.167	.246	.207	.058	.070	.065
4	1	-.114	-.038	-.089	-.086	-.277	-.222	-.216
5	0	.008	.003	.000	.000	.002	.002	.002
5	1	-.002	-.001	-.001	-.001	-.007	-.007	-.006
6	0	-.042	-.046	-.051	-.051	-.058	-.056	-.056
6	1	.065	.061	.057	.057	.275	.251	.251
7	0	-.011	-.011	-.011	-.010	-.105	-.099	-.098
7	1	.006	.005	.006	.006	.211	.205	.204
TOTAL		.035	.012	-.012	.083	.239	.249	.340

TABLE 4.10(e)

J=4 T=1 BARE= -.287 MEV

J^π	T^π	3P1H	TDA	RPA	NRPA	BB3P1H	BBRPA	BBNRPA
0	0	-.034	-.067	-.017	-.003	-.036	.029	.079
0	1	-.005	-.005	-.005	-.005	-.014	-.010	-.010
1	0	.018	.017	.017	.016	.034	.033	.031
1	1	.013	.011	.010	.009	.023	.017	.017
2	0	.207	.421	1.470	.621	.099	.623	.270
2	1	.037	.029	.027	.026	.061	.045	.043
3	0	-.022	-.023	-.024	-.023	-.039	-.035	-.033
3	1	-.034	-.029	-.027	-.025	-.079	-.065	-.061
4	0	-.031	-.043	-.062	-.053	-.015	-.018	-.016
4	1	-.010	-.008	-.008	-.007	-.023	-.019	-.018
5	0	.018	.018	.010	.010	.067	.062	.059
5	1	.017	.016	.015	.015	.084	.075	.072
6	0	.027	.030	.033	.033	.037	.036	.036
6	1	.014	.013	.012	.012	.059	.054	.054
7	0	.004	.004	.004	.003	.035	.033	.033
7	1	.001	.001	.001	.001	.023	.023	.023
TOTAL		.218	.375	1.455	.630	.316	.882	.577

TABLE 4.10(f)

J=5 T=0 BARE= -.590 MEV

J^π	T^π	3P1H	TDA	RPA	NRPA	BB3P1H	BBRPA	BBNRPA
0	0	-.036	-.067	-.017	-.003	-.036	.029	.079
0	1	.019	.015	.015	.014	.043	.031	.030
1	0	.002	.002	.002	.002	.004	.004	.004
1	1	-.005	-.004	-.004	-.004	-.009	-.007	-.006
2	0	.325	.651	2.310	.976	.155	.979	.425
2	1	-.172	-.139	-.127	-.120	-.287	-.212	-.201
3	0	.001	.001	.001	.001	.001	.001	.001
3	1	-.003	-.003	-.002	-.002	-.007	-.006	-.005
4	0	-.126	-.171	-.251	-.211	-.059	-.071	-.066
4	1	.116	.100	.091	.088	.282	.227	.228
5	0	-.008	-.008	-.008	-.008	-.054	-.050	-.048
5	1	.043	.040	.038	.037	.205	.184	.177
6	0	-.010	-.011	-.012	-.012	-.014	-.013	-.014
6	1	.016	.015	.014	.014	.066	.060	.060
7	0	-.001	-.001	-.001	-.001	-.008	-.008	-.008
7	1	.000	.000	.000	.000	.016	.016	.016
TOTAL		.162	.431	2.048	.771	.298	1.163	.664

TABLE 4.10(g)

J=6 T=1 BARE= -.169 MEV

J^π	T^π	3P1H	TDA	RPA	NRPA	BB3P1H	BBRPA	BBNRPA
0	0	-.034	-.067	-.017	-.003	-.036	.029	.079
0	1	-.006	-.005	-.005	-.005	-.014	-.010	-.010
1	0	-.017	-.015	-.016	-.015	-.031	-.030	-.028
1	1	-.011	-.010	-.009	-.008	-.021	-.016	-.015
2	0	.207	.421	1.478	.621	.099	.623	.270
2	1	.037	.029	.027	.026	.061	.045	.043
3	0	.026	.027	.029	.027	.046	.042	.039
3	1	.048	.034	.032	.030	.093	.077	.072
4	0	.096	.128	.187	.158	.044	.053	.049
4	1	.029	.025	.023	.022	.070	.056	.055
5	0	.003	.003	.003	.003	.019	.017	.016
5	1	.005	.004	.004	.004	.023	.021	.020
6	0	.002	.002	.003	.003	.003	.003	.003
6	1	.001	.001	.001	.001	.005	.004	.004
7	0	.000	.000	.000	.000	.001	.001	.001
7	1	.000	.000	.000	.000	.001	.001	.001
TOTAL		.374	.578	1.731	.863	.362	.915	.599

TABLE 4.10(h)

J=7 T=0 BARE=-2.137 MEV

J'	T'	3P1H	TDA	RPA	NRPA	BB3P1H	BBRPA	BBNRPA
0	0	-.034	-.067	-.017	-.803	-.036	.029	.079
0	1	.019	.016	.015	.014	.043	.031	.030
1	0	-.039	-.036	-.037	-.034	-.073	-.070	-.065
1	1	.080	.068	.062	.059	.149	.110	.106
2	0	-.290	-.589	-2.058	-.870	-.138	-.872	-.378
2	1	.153	.124	.113	.107	.256	.189	.179
3	0	-.011	-.011	-.012	-.011	-.019	-.017	-.016
3	1	.049	.043	.039	.037	.115	.095	.089
4	0	-.020	-.027	-.040	-.033	-.008	-.011	-.018
4	1	.018	.016	.014	.014	.045	.036	.035
5	0	-.000	-.000	-.000	-.000	-.002	-.002	-.002
5	1	.002	.002	.002	.002	.009	.008	.008
6	0	-.000	-.000	-.000	-.000	-.000	-.000	-.000
6	1	.000	.000	.000	.000	.001	.001	.001
7	0	-.000	-.000	-.000	-.000	-.000	-.000	-.000
7	1	.000	.000	.000	.000	.000	.000	.000
TOTAL		-.072	-.462	-1.919	-.718	.339	-.475	.055

the 7777 matrix element only. Similar results are obtained for 4444 in oxygen.

We have ordered Table 4.10 to correspond to a similar table in Kirson's paper. Looking first at the columns labelled 3p-1h, TDA and RPA we see that the most important collective vibrations contributing to renormalization are the 2^+0 and 4^+0 ($J^\pi T$) phonons. The 0^+0 phonon seems to be less important in calcium than in oxygen where Kirson found it to contribute as much as the 2^+0 and usually more than the 4^+0. In calcium, the 0^+0 is comparable to the 6^+0 and both are rather weak. In the nRPA calculation (nested RPA), we find the same trend in calcium as in oxygen. The nesting screens the p-h interaction so as to reduce the strong collectivity found in RPA. The result is that nRPA is very similar to TDA, a conclusion noted by Osnes et al. (1969) and Kirson (1971) in oxygen. When the bare p-h vertex is converted to the black box vertex as in bb3p1h, there is a complete redistribution of the coupling strength between the valence nucleons and the phonons. The contributions of 2^+0 and 4^+0 phonons are tremendously reduced, those of 0^+0 and 6^+0 increase and the 7^+0 and 7^+1 become predominant for the J=0, T=1 matrix element. This strength reduces with increasing J. The overall effect of the bb vertex, comparing 3p1h and bb3p1h matrix elements, is to make the interaction between valence particles much more repulsive. In the bbRPA calculation,

we find great similarity to bb3p1h except for the 2^+0 phonon which is much enhanced. In addition the total correction is in many cases similar to the 3p1h calculation. This very satisfying picture is destroyed, however, when we go on to bbnRPA. As was found in oxygen, the total correction in bbnRPA is small, so the renormalized matrix element differs little from the bare one.

Using the PSA force, one finds results similar to those of KLS. The major difference is that with PSA, the RPA renormalization is only slightly more attractive than the TDA. A possible explanation for this follows from Vary et al. (1973) that the poor convergence of the p-h diagram is caused by the strong tensor component of the nuclear force. In the PSA, the tensor coupling is rather weak even compared to the Sussex (Elliott et al. (1967)) matrix elements. Perhaps the central component of the force is also weak giving us a force too weak to produce much collectivity. In oxygen, Kirson found that the 5^+ phonon made a very large contribution to the bbRPA calculation as compared to RPA. We have identified the 1^-0 phonon as responsible. When the black box vertex is computed omitting the 1^-0 phonon, the 5^+0 phonon contribution is reduced to its original value (as in RPA). A similar comparison between bb3p1h and 3p1h is true. In calcium, one sees a similar large contribution by the 7^+ phonons in the black box vertex. In Table 4.11 we confirm the

TABLE 4.11

$\langle (0f_{7/2})^2 JT | \Delta G_{c-p} | (0f_{7/2})^2 JT \rangle$

J	T	7^+0 Phonon		
		3p1h	bb3p1h	bb3p1h (No 1^-0)
0	1	.052	.496	.059
1	0	-.041	-.385	-.046
2	1	.025	.231	.028
3	0	-.011	-.105	-.013
4	1	.004	.035	.004
5	0	-.001	-.008	-.001
6	1	.000	.001	.000
7	0	.000	.000	.000

J	T	RPA	bbRPA	bbRPA (No 1^-0)
0	1	.049	.467	.057
1	0	-.039	-.363	-.044
2	1	.023	.218	.026
3	0	-.011	-.099	-.012
4	1	.004	.033	.004
5	0	-.001	-.008	-.001
6	1	.000	.001	.000
7	0	.000	.000	.000

contributions with and without the 1^-0 phonons in the black box vertex for the 7^+0 phonon, KLS force.

In ^{16}O the 1^-0 phonon is known to be spurious in that it represents a motion of the center of mass of the nucleus. In ^{18}O the 1^-0 phonon in the core is no longer entirely spurious, for the ^{16}O core can vibrate against the two valence nucleons. Lacking a proper treatment of center of mass motion, one cannot accurately compute the renormalization effects when using black box vertices.

As a more meaningful test of the renormalized interaction, a shell model calculation was carried out for mass 18 and 42 nuclei. In presenting the results, one must first locate the theoretical ground state relative to the experimental spectrum. The problem is to determine what the binding energy of ^{18}O is relative to ^{16}O since ^{16}O is our reference state. We can then compare our position of the calculated ground state of ^{18}O with experiment. This has been done by Dawson et. al. who argued that the binding energy of ^{18}O is equal to the binding energy of ^{16}O plus the two neutron single particle energies and the two neutron interaction energies. This can be estimated from the valence nucleon interaction energy as follows for oxygen.

$$BE(^{18}O) + BE(^{16}O) - 2BE(^{17}O) = +\ 3.905\ \text{MeV} \qquad (4.16)$$

$$BE(^{18}F) + BE(^{16}O) - BE(^{17}F) - BE(^{17}O) = 5.0\ \text{MeV}$$

and for calcium

$$BE(^{42}Ca) + BE(^{40}Ca) - 2BE(^{41}Ca) = 3.11 \text{ MeV}$$

$$BE(^{42}Sc) + BE(^{40}Ca) - BE(^{41}Ca) - BE^{41}Sc) = 3.20 \text{ MeV} \quad . \tag{4.17}$$

The ground state binding energy, including single particle and valence interaction energy, of ^{18}O relative to ^{16}O is - 3.905 MeV.

The oscillator energy was chosen as 14 MeV in oxygen and 11 MeV in calcium. Therefore, the even parity excitations in oxygen have an energy of 28 MeV and the odd parity excitations are 14 MeV in energy. For the single particle energies in the valence shell, one may use the oscillator energy but a more realistic value may be obtained from experiment by measuring the energy for removal of a nucleon through pick-up reactions. The resulting energy levels for the valence shell in oxygen are given by Clement and Baranger (1968) and in calcium by Kuo et al. (1968). For oxygen and calcium,

$$\varepsilon(d_{5/2}) = 0, \quad \varepsilon(s_{1/2}) = 0.78 \text{ MeV}, \quad \varepsilon(d_{3/2}) = 5.08 \text{ MeV} \tag{4.18}$$

and

$$\varepsilon(f_{7/2}) = 0, \quad \varepsilon(p_{3/2}) = 2.1 \text{ MeV}, \quad \varepsilon(f_{5/2}) = 6.5 \text{ MeV},$$

$$\varepsilon(p_{1/2}) = 4.1 \text{ MeV} \quad ,$$

respectively. The T=0, 1$^-$ spectrum of oxygen is shown in

Figs. 4.3 and 4.4 respectively for the PSA force. The T=0, 1 spectra for calcium are shown in Figs. 4.5 and 4.6 for the PSA force and Figs. 4.7 and 4.8 for the KLS force.

Looking at the spectra, the 3p1h calculation is an improvement over the bare force but this trend is overamplified by TDA and RPA which push the ground state progressively lower. The bb3p1h spectrum has the states far too high; bbRPA brings them down toward the experimental value. Nesting of the propagators mitigates the strong collectivity by pushing bbnRPA spectrum upwards toward the result of the bare force. This is in agreement with Kirson's finding in oxygen using the Kuo-Brown force.

We now compare the two forces. Looking at Figs. 4.3 to 4.8 one sees that the PSA T=1 matrix elements show much less tendency to collective behaviour. Especially the similarity of the TDA and RPA calculations distinguishes the PSA from the KLS force. The order of levels is quite consistent among the various calculations. This is not the case for the T=0 states. The KLS force is more successful in putting the J=1 level as the ground state, but both forces suffer from the feature that the bb matrix elements put the J=1 level about 0.5 to 1.5 MeV above the J=7 level. The calculated level density is reasonable except for the RPA and nRPA calculations with the KLS force. It was conjectured above that the PSA matrix elements tend to be too small, especially in tensor force coupling.

Fig. 4.3: Low lying T=0 spectrum in ^{18}F using the PSA force for various approximations.

Fig. 4.4: Low lying T=1 spectrum in ^{18}O and ^{18}F using the PSA force for various approximations.

Fig. 4.5: Low lying T=0 spectrum in ^{42}Sc using the PSA force for various approximations.

Fig. 4.6: Low lying T=1 spectrum in ^{42}Ca and ^{42}Sc using the PSA force for various approximations.

Fig. 4.7: Low lying T=0 spectrum in ^{42}Sc using the KLS force for various approximations.

Fig. 4.8: Low lying T=1 spectrum in ^{42}Ca and ^{42}Sc using the KLS force for various approximations.

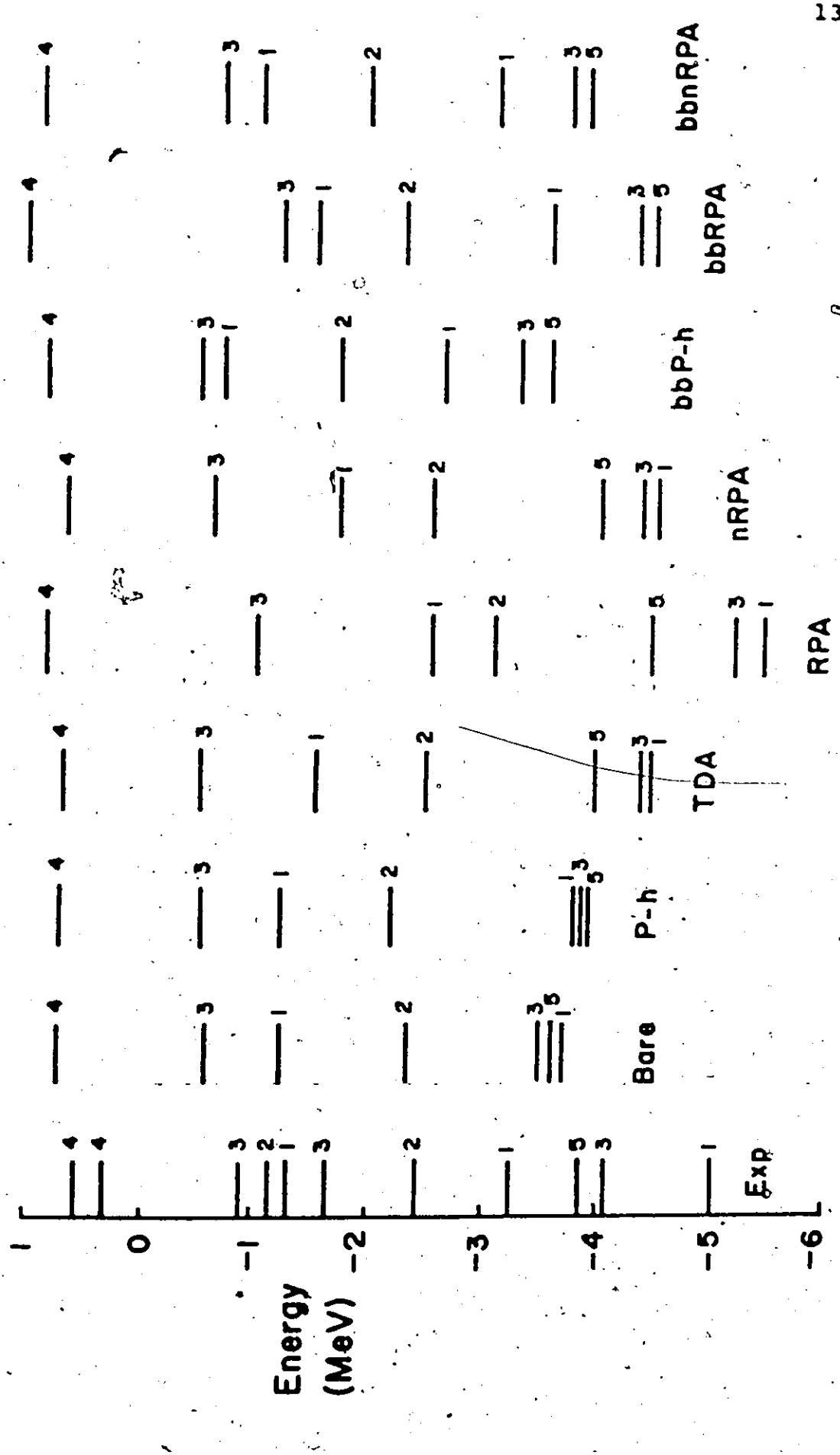
Energy (MeV)
1
0
-1
-2
-3
-4
-5
-6
Exp
Bare
P-h
TDA
RPA
nRPA
bbP-h
bbRPA
bbnRPA

Fig 4.3

Fig 4.4

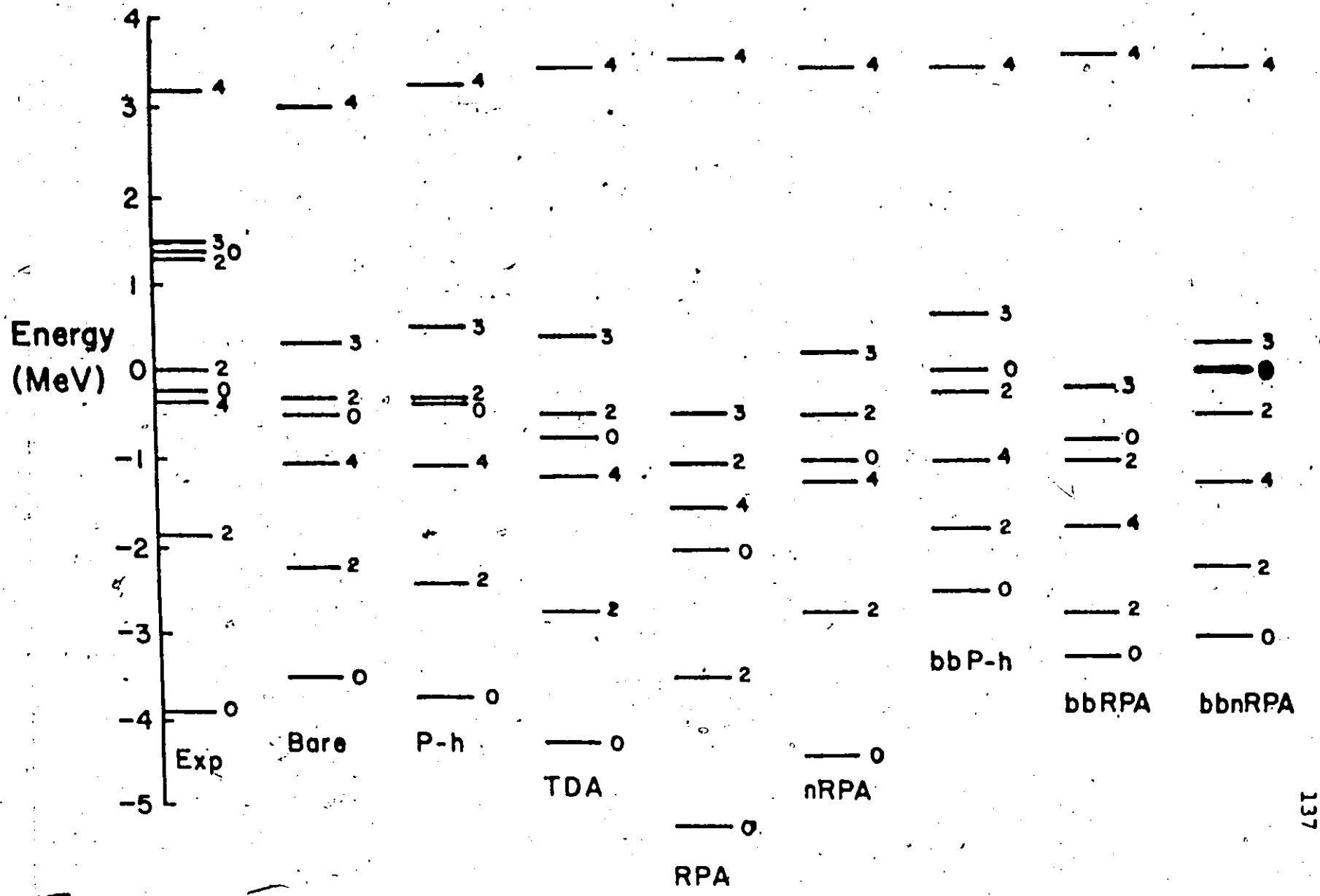
Energy (MeV)
4
3
2
1
0
-1
-2
-3
-4
-5
Exp
Bare
P-h
TDA
RPA
nRPA
bbP-h
bbRPA
bbnRPA

Fig 4.5

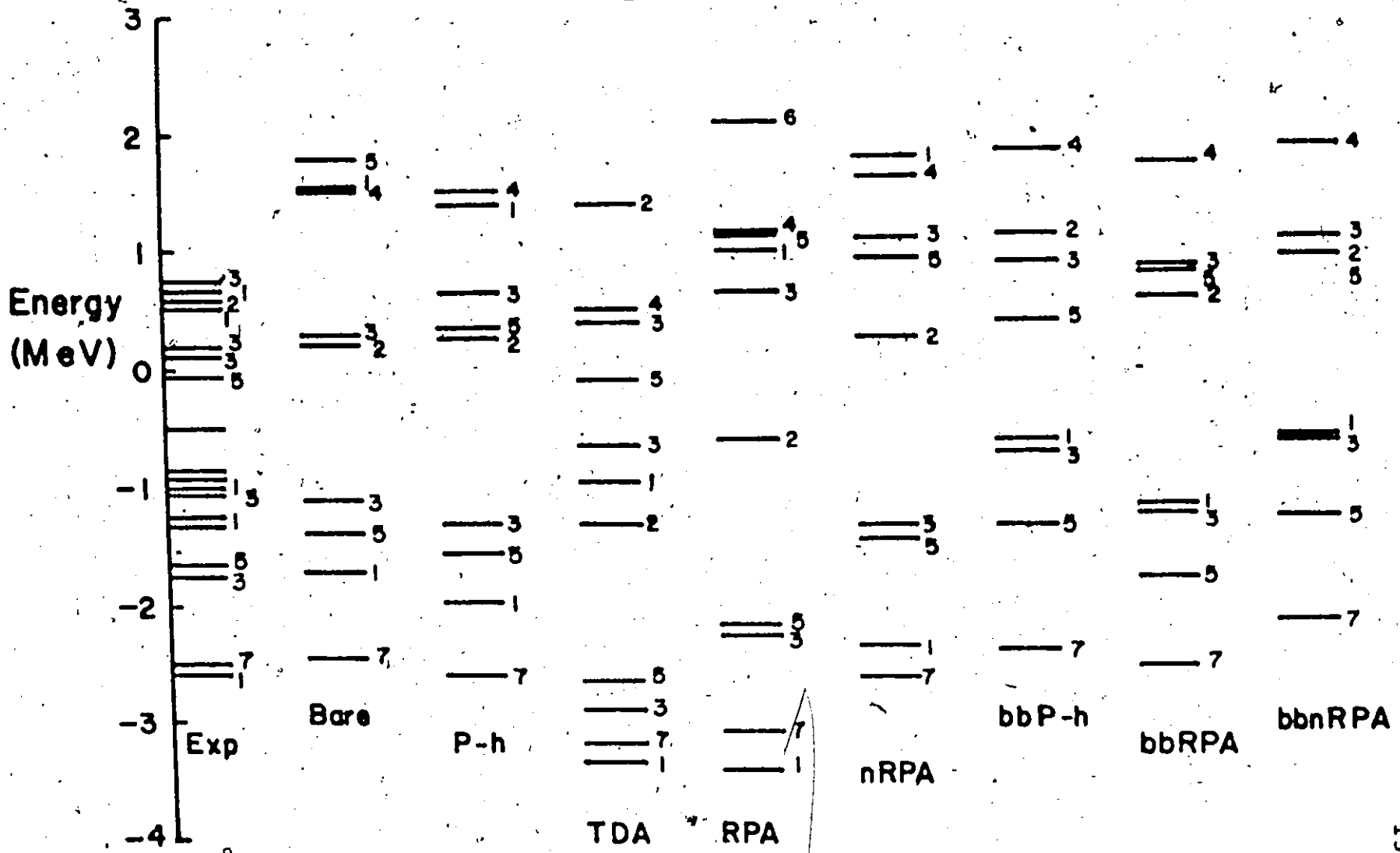
Energy (MeV)
3
2
1
0
−1
−2
−3
−4
Exp
Bare
P-h
TDA
RPA
nRPA
bbP-h
bbRPA
bbnRPA

Fig 4.6

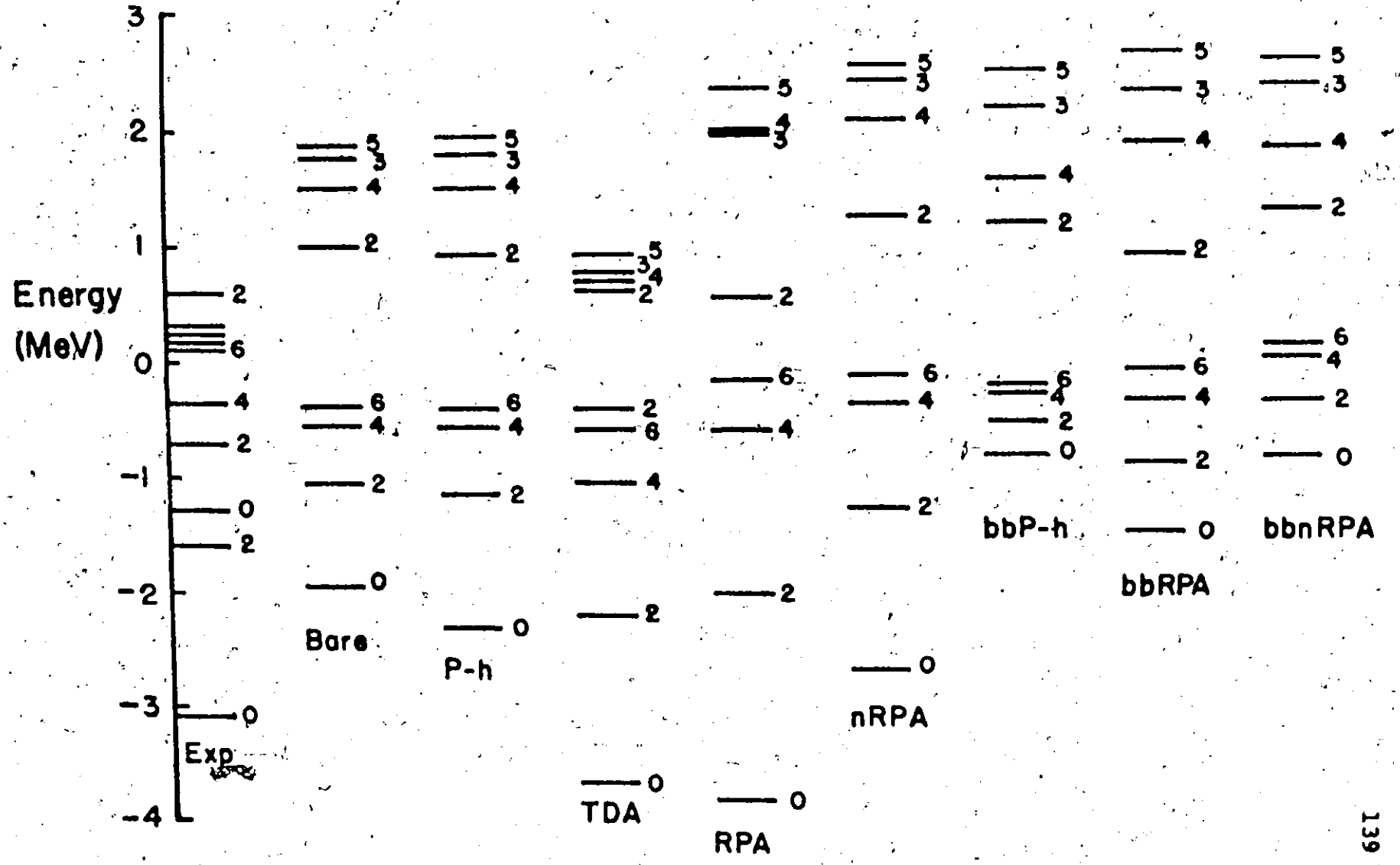
Energy (MeV)
3
2
1
0
-1
-2
-3
-4
Exp
Bare
P-h
TDA
RPA
nRPA
bbP-h
bbRPA
bbnRPA

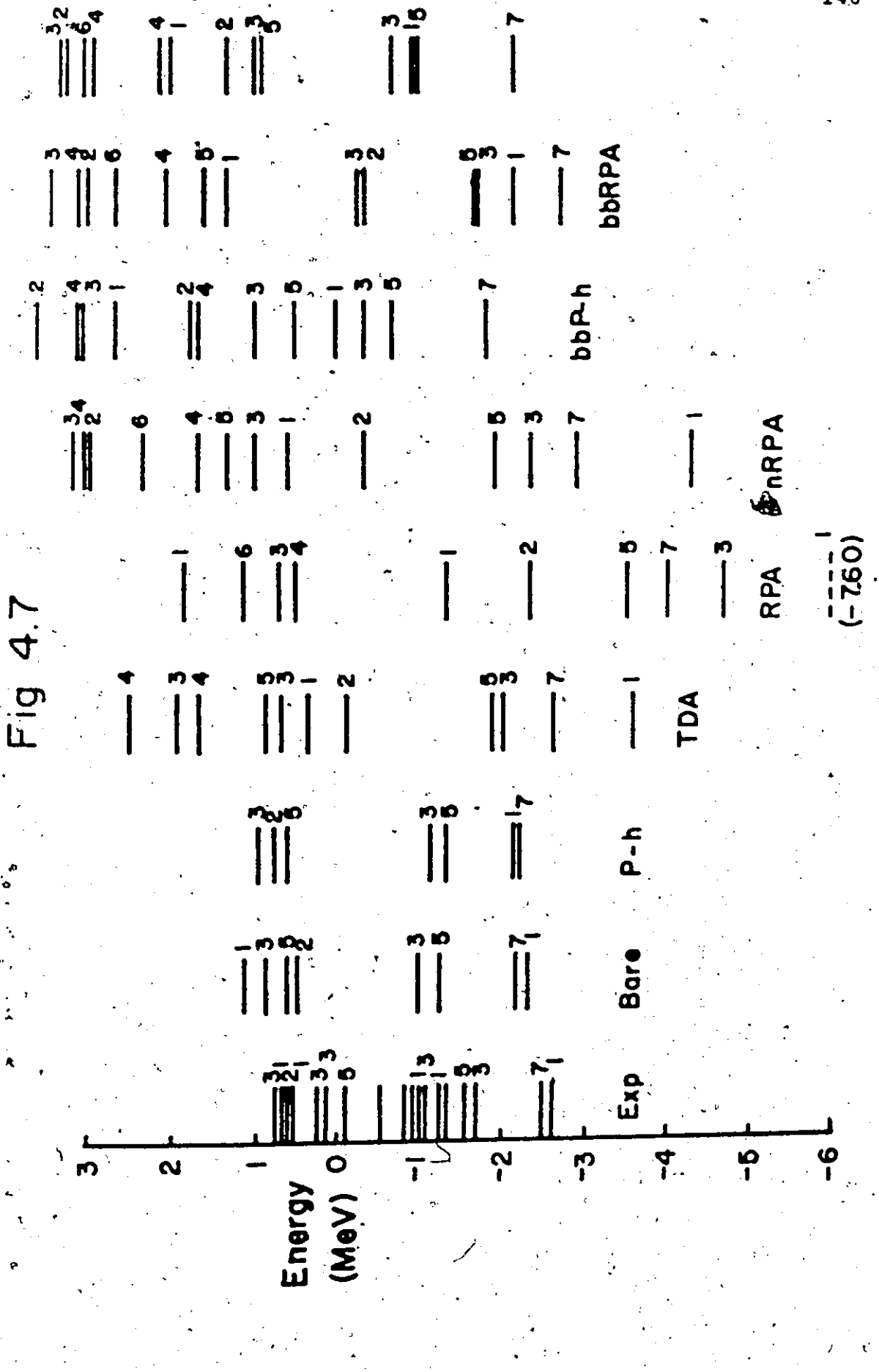
Energy (MeV)
3
2
1
0
-1
-2
-3
-4
-5
-6
Exp
Bare
P-h
TDA
RPA
nRPA
(-7.60)
bbP-h
bbRPA

Fig 4.7

Fig 4.8

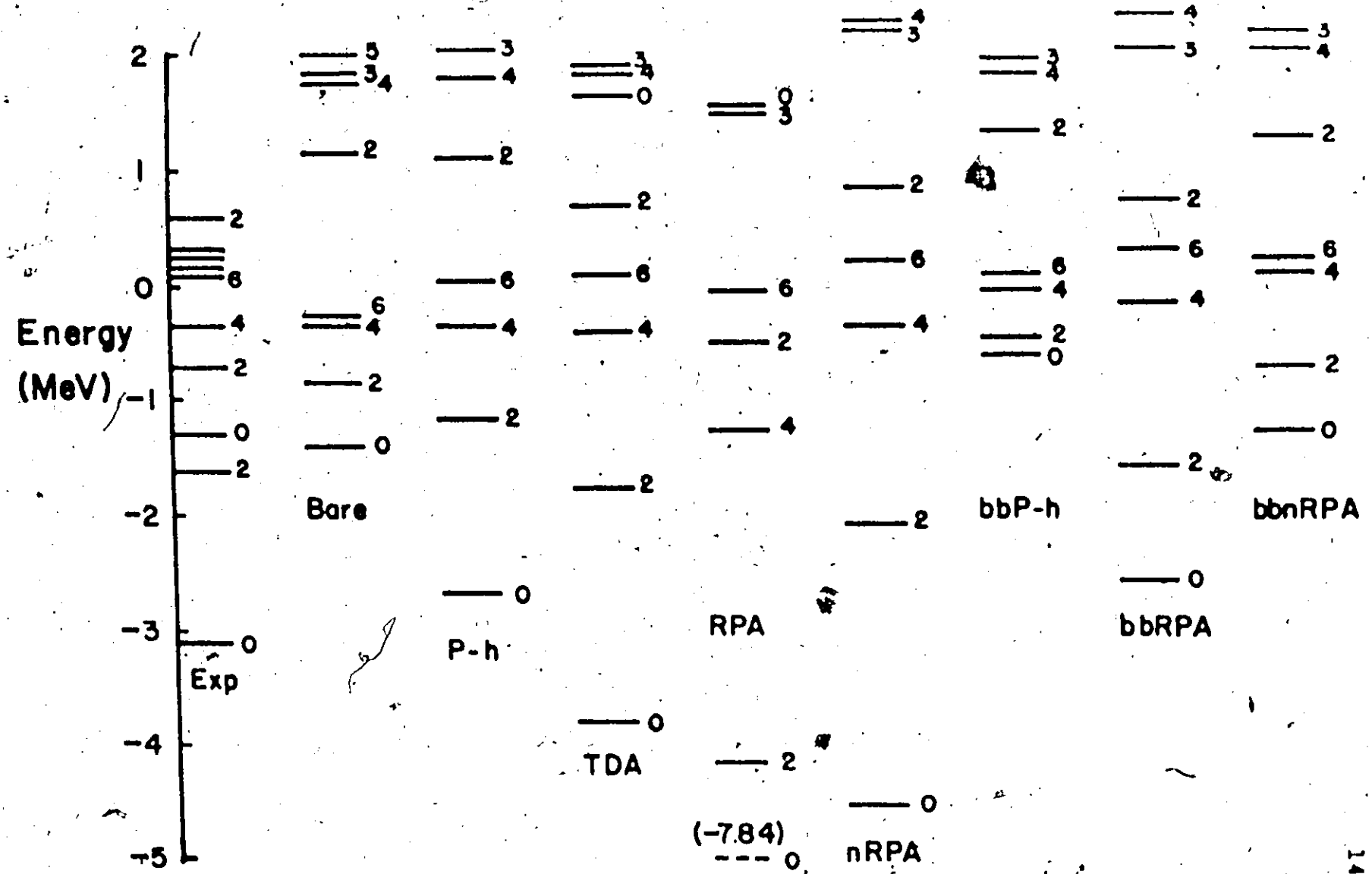
Energy
(MeV)
2
1
0
-1
-2
-3
-4
-5
Exp
Bare
P-h
TDA
RPA
(-7.84)
nRPA
bbP-h
bbRPA
bbnRPA

We now compare our 3p-1h core polarization corrections in calcium to an empirical fit of Federman and Pittel (1970) and to a similar core polarization calculation by Kuo. These matrix elements are given in Table 4.12. The matrix elements of Federman and Pittel (FT) were obtained by a least squares fit to 38 levels throughout the spectrum of calcium isotopes. Unfortunately only the $f_{7/2}$ and $p_{3/2}$ levels were active so that a complete comparison between their calculation and ours may not be meaningful. In our calculation we have used the full p-f shell for the shell model calculation. For these reasons, the poor agreement between FT and Kuo for the first ten matrix elements may not be taken too seriously. Furthermore, Federman and Pittel did not fit all matrix elements in the two levels. They take the last five matrix elements as fixed from the calculation of Kuo. The agreement is otherwise reasonable except for the diagonal $(f_{7/2}p_{3/2})^2$ matrix element. No explanation is available for this.

Comparing G^{Kuo} and G^{KLS} we find very similar matrix elements as we should. Both forces are derived from the Hamada-Johnston potential but differ in the treatment of the Pauli operator. The agreement between G^{KLS} and G^{PSA} is not as good but this may be explained in that the PSA matrix elements are not nuclear reaction matrices except as a first approximation. Again, the largest discrepancies occur for the diagonal $(f_{7/2}p_{3/2})^2$ matrix elements.

TABLE 4.12

COMPARISON OF FEDERMAN-PITTEL, KUO, AND THE AUTHOR'S RESULTS FOR VARIOUS MATRIX ELEMENTS OF GIVEN J IN THE p-f SHELL.

	J	G^{FT}	G^{Kuo}_{3p-1h}	G^{KLS}_{3p-1h}	G^{PSA}_{3p-1h}
<77|77>	0	-2.802	-1.81	-1.775	-1.586
	2	-1.294	- .79	- .793	- .897
	4	- .167	- .09	- .087	- .344
	6	.338	.23	.205	- .152
<78|78>	2	- .347	- .86	- .960	-1.053
	3	.775	- .03	- .030	- .233
	4	- .601	- .05	- .102	- .339
	5	.596	.15	.126	- .126
<88|88>	0	-1.347	-1.21	-1.199	-1.495
	2	- .278	- .38	- .572	- .657
<77|88>	0	- .783	- .78	- .799	- .772
	2	- .269	- .22	- .294	- .283
<77|78>	2	- .502	- .50	- .562	- .466
	4	- .307	- .31	- .388	- .337
<78|88>	2	- .325	- .32	- .375	- .384

CHAPTER V

DISCUSSION AND SUMMARY

In this final chapter we summarize the results achieved. To put the work in perspective, other approaches to the calculation of the effective interaction are described, and comparison is made to these results where possible.

5.1 Improvements on the Perturbative Approach

Because of the relatively small amount of success with the perturbative approach, attempts have been made to understand this failure. One weak point is the assumption that the harmonic oscillator single particle wave functions are adequate. It is well known that the nuclear density can be quite adequately described as a Woods-Saxon function. The short range character of the nuclear force then implies that the one body nuclear potential well should also be of Woods-Saxon shape, at least for the ground state. The wave functions in such a well will differ from oscillator functions. The major difference between the two types of single particle wave functions is the behaviour near and

outside the edge of the potential well. For the Woods-Saxon well, the wave function shows exponential decay but for the harmonic oscillator well, the wave function shows gaussian decay. The effect of this difference has been investigated by Pradhan and Shakin (1971) who calculated both the G-matrix elements and lowest order core polarization for the effective interaction in mass 18 nuclei using the Tabakin potential. In ^{18}O, they found that the low lying spectrum using the bare G-matrix from the Woods-Saxon wave function was roughly $\frac{1}{2}$ MeV higher than the spectrum using the G-matrix from H.O. wave functions. When the core polarization was included, the ground state was 1 MeV higher for the Woods-Saxon case. In ^{18}F, for both G_{Bare} and G_{3p-1h}, the low lying spectrum using the Woods-Saxon wave function was 1 MeV higher than the H.O. case. From these results, it appears that the good results of Kuo using the lowest order core polarization were more or less fortuitous. With the Woods-Saxon core polarization only depressing the ground state half as much as with H.O., it is likely that the results of TDA and RPA using Woods-Saxon may be in better agreement with experiment, since these will lower the ground state even more. The effect on the black box vertex corrections is not known but it is suspected that the black box interaction will be less repulsive.

Another reason for the poor results of the perturbative approach may be in the use of H.O. wave functions. The next level of improvement would be the use of self consistent single particle Hartree-Fock wave functions. It is well known that in the H-F basis, there are no matrix elements for exciting particle hole states. Of course, when one goes to the neighbouring nucleus with two valence particles, such matrix elements will reappear. It is easy to believe that the use of the self consistent well will have considerable influence on their value. This is indeed the case, as found by Rowe (1973).

The TDA and RPA series are formally derived in a H-F basis.. This has serious consequences. For example, when the core excitations are treated in the RPA, there is a tendency for the $J^{\pi} = T^{\pi} = 0$ phonon (breathing mode) to collapse as found by Blomquist and Kuo (1969), and Ellis and Siegel (1970). According to Thouless' theorem, if some solution of the RPA collapses, it is symptomatic of an unsatisfactory H-F ground state. Numerical calculations by Rowe confirm that collapse is prevented if a H-F wave function of the ground state is used. In the usual RPA, the collapse of the nucleus appears as an imaginary eigenvalue (so the time dependence is no longer periodic but the state would collapse exponentially). In the calculation of Kirson and the author, no diagonalization is performed in the RPA as such, but rather the RPA series

is summed geometrically. For this reason we have no direct evidence for the collapse of the breathing mode in the calculations other than observing if the renormalization by the 0^+0 phonon is unusually large. Such a case has not been observed for the effective interaction. Ellis (1972) has claimed that the large RPA results are due to the H.O. wave function not being self consistent.

Another possible improvement in the use of perturbation theory is to relax the restriction of considering only 2hω type p-h excitations. Such an improved calculation was performed by Vary et. al. (1973) for ^{18}O using the lowest order core polarization diagram and using a "realistic" nuclear force with a strong tensor force component. He found that convergence of these contributions did not occur until excitations up to 12 hω were included. The new ground state level was shifted upwards approximately halfway to the position of the bare G interaction. The neglect of this effect is, therefore, comparable to using H.O. wave functions instead of Woods-Saxon ones. What this would do to the TDA and RPA calculations is unknown.

Although the second order 3p-1h contribution is significant while 4p-2h contribution is not, it is of importance to enquire of the convergence of the perturbative series. Partial summations to all orders such as TDA and RPA seem to provide a large contribution to the effective

interaction even though tempered by previous remarks. A complete calculation of third order diagrams was done by Barrett and Kirson (1970) who found that the perturbative series does not converge rapidly, if at all. This casts serious doubt on the perturbative approach. It soon became apparent that other approaches may be necessary.

Such an improved approach was undertaken by Barrett (1974) following the suggestion of Brandow (1969) and Brown (1971). He calculated the effective interaction in a doubly partitioned Hilbert space to avoid the problem of double counting p-p ladders in the G-matrix and its application to the effective interaction. It was found that the convergence of the perturbation expansion to third order in G was improved but was not conclusive.

A different approach was taken by Lovas and Vegh (1974) who treated the two valence nucleons and the core as a three body problem where the heavy core contains excited states. Unfortunately the number of coupled equations increases with the number of core states. The application of this method to a realistic calculation has yet to be made.

In addition to the above refinements to the perturbative approach, one may attempt non-perturbative calculations for these nuclei. The first such calculation for ^{18}O which involved all 2p and 3p-1h basis states was completed by Lo Iudice et al. (1971). Only p-h excitations

with $2\hbar\omega$ energy were included so the usual core polarization diagrams as well as others were included. The size of matrices to be diagonalized was approximately 600 × 600.

The interesting result of the calculation was that the complete shell model calculation gave spectra which were very close to the spectra using the one bubble core polarization diagram in perturbation series. In the same spirit as the above calculation, Goode (1971) calculated the fully excited $2\hbar\omega$ excitation of the core via a shell model calculation. Included in this case are all 1p-1h and 2p-2h excitations of the core which are coupled to the valence nucleus. Although the calculation contains some p-p ladders (which may imply some overcounting since these are in the G-matrix), the results of the model are very similar to the lowest order core polarization contributions and the usual TDA and RPA enhancements of the effective interaction are eliminated.

A different approach has been taken by Rowe et al. (1968, 1969, 1970) to extend the RPA to open shell nuclei. Instead of coupling the two valence neutrons in ^{18}O to the RPA excitation of the ^{16}O core, the Equation-of-Motion formalism of Rowe treats these valence nucleons in the RPA as well. Such a calculation for A = 18 nuclei has not as yet been done. Perhaps the reason is that the formalism is more readily applicable to odd parity 1p-1h excitations

which would not occur at low energy in the mass-18 nucleus. Nevertheless, in calculations that have been done, the open shell RPA raises the low lying excitation levels when compared to nuclei where the standard RPA has been applied. It appears that a more complete treatment using this approach is desirable for a comparison to the results of perturbation theory.

5.2 Summary

In this thesis we have carried out the core polarization corrections considered by Kirson for mass 18 nuclei, using the RSA and KLS forces. We have not, however, computed the case SCCE because of the technical problem of large core storage and computing time requirements. The results of PSA parallel those for Kirson who used the Kuo-Brown G-matrix elements. In particular, the effective interaction became more attractive than the lowest order core polarization correction when TDA and RPA propagators were used. Screening of the p-h interaction weakened the attractive result of the RPA bringing it in closer agreement to TDA as found by other authors. When vertex renormalization is included, the effective interaction becomes extremely repulsive which is directly opposite to the (as shown in Fig. 5.1)

Fig 5.1

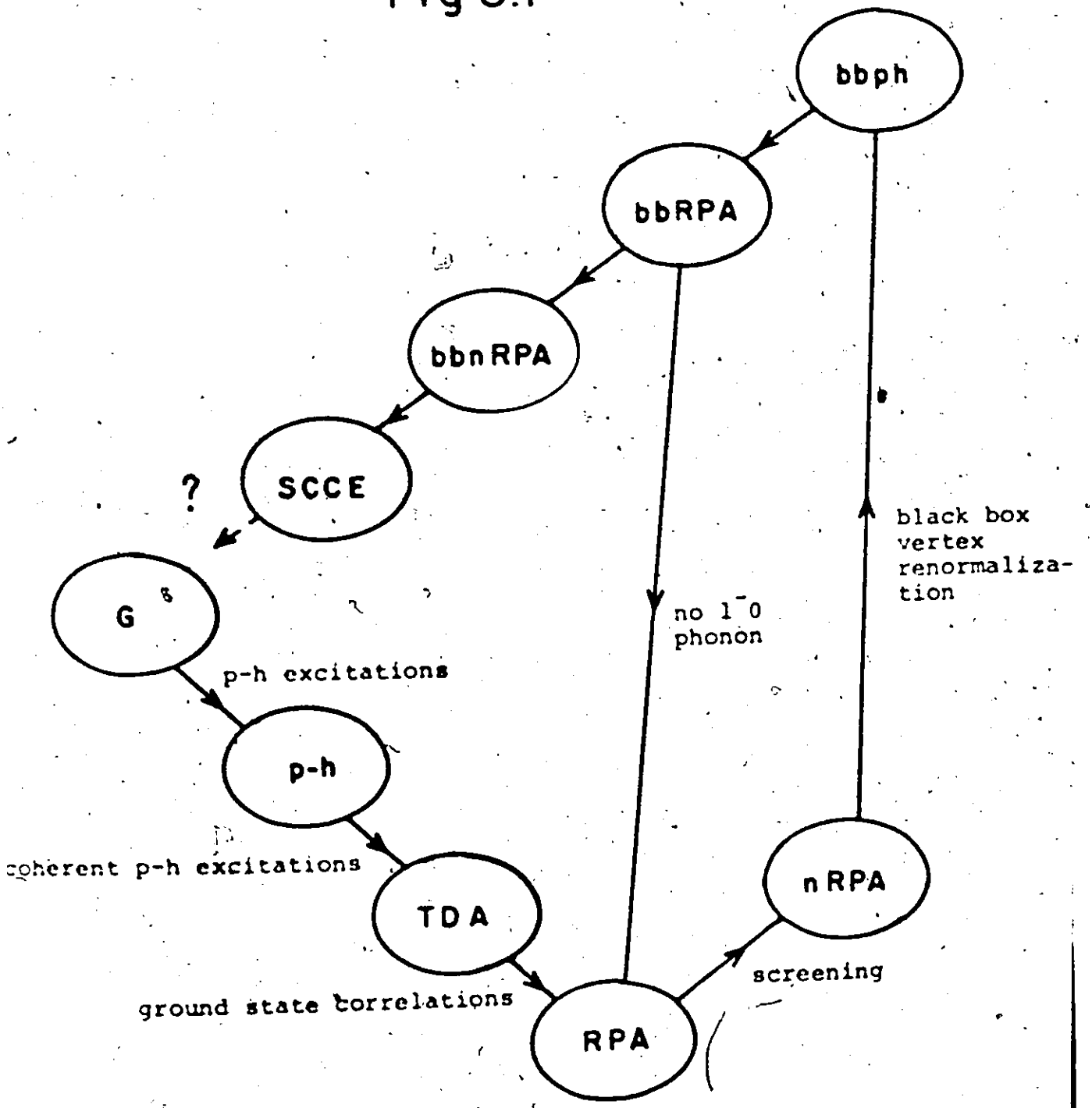

Illustrating the direction of core polarization calculations.

large attraction in RPA. When both of these effects are included simultaneously, the effective interaction is very similar to that of the bare G interaction.

The results for the KLS force in oxygen were not satisfactory, however. A thorough investigation of the computer programs reproduced the same results. For example, the 0^+1 ground state in the RPA occured at - 10.4 MeV compared to - 5.2 MeV for the PSA and - 6.2 MeV for the Kuo-Brown force in Kirson's calculation. A shell model calculation using the bare interaction produced a reasonable T=1 spectrum but the T=0 spectrum was rather different from other bare G interactions. For example, the 1^+0 ground state occurs 4 MeV below the ground state of the Kuo-Brown force. The first excited 3^+0 and 5^+0 for this force are 1 MeV below the corresponding states for Kuo-Brown interaction. Because of these differences in the T=0 force, it appears the results for both the T=0 and T=1 renormalizations are unsatisfactory.

The above calculations were repeated for the calcium region using both the PSA and KLS forces. Since our work was completed some similar calculations have been made, up to RPA renormalization. For example, Kuo and Osnes (1974) considered the screened RPA (to second order only) and their results are in qualitative agreement with ours.

There are no other known calculations including vertex renormalization for the effective interaction in the p-f shell.

Nevertheless, the trend for the vertex renormalization in calcium is very similar to that in oxygen. The results for PSA and KLS are very similar in calcium, contrary to the results for oxygen. In particular, the explanation of the large repulsive effect for bb vertices was found. When the bb vertices were computed omitting the 1^-0 phonon, the bb vertices became very similar to the bare vertices. This was true for both oxygen and calcium. Since the 1^-0 phonon contains some center-of-mass spuriosity, for ^{18}O (but not ^{16}O) the effect of the bb vertices on the spectrum of ^{18}O cannot be conclusively determined until the amount of spuriosity is known.

We have corrected the sequence of energy denominators used by Kirson in his calculation of the screened p-h interaction. The deviation in our results amounts to only a few percent. It is expected that a similar deviation will occur for the SCCE.

We have demonstrated a transformation between higher order diagrams which is identical to the transformation between the two body vertices. One needs to remember only that the energy denominators change between one higher order diagram and its transformation. This result is not considered new but the author has not seen a discussion of this point in the literature and several physicists that were questioned agreed that a clear exposition of this point was desirable.

As a means of understanding the results of the detailed calculation, we have applied the core polarization corrections to the schematic p-h interaction of Brown and Bolsterli. The results of the schematic model are obtained analytically except for screened RPA and SCCE. For these cases, iterations are required and these were computed on the CDC 6400. It is very satisfying that both the 0^+0 and 2^+0 phonons are well approximated by a separable interaction whose strength parameter does not change significantly for oxygen and calcium. These phonons were found to produce the largest renormalizations in most cases.

In particular, the same trends were observed for the schematic model and the detailed calculation. The TDA correction was more than the p-h correction but less than the RPA. In fact, the RPA correction would diverge for a slightly more attractive p-h interaction. Screening in the schematic model reduces the RPA to nRPA over a large range of strength parameters. The final result for SCCE was very little renormalization in agreement with our detailed results.

In addition the schematic model favours our result for a difference in the screened RPA correction obtained by Kuo for the 8888 and 9999 matrix element. Both Kuo and ourselves find that for these two matrix elements the RPA correction is smaller than the TDA in contrast to other matrix elements where the opposite occurs. This implies that the p-h interaction for these states is repulsive.

However, Kuo finds that the screened RPA for even these two cases is very similar to TDA. We find, however, that the screened RPA is roughly equal in magnitude but opposite in sign to the TDA. The prediction of the schematic model for a repulsive p-h interaction is that the TDA result is most attractive, the RPA is more repulsive and the screened RPA is more repulsive still. This is in agreement with our result.

APPENDIX A

In this appendix, a derivation of Eq. (2.33) will be given to demonstrate the application of Wick's Theorem and angular momentum algebra. This equation corresponds to one bubble core polarization shown in Fig. 2.7(a).

In the following we will omit isospin but will generalize to include it at the end. The second order diagram of Fig. 2.7(a) may be written as

$$\sum_{\substack{phJ'' \\ Y}} \langle (p_2p_4)J|V|\overbrace{p_2\overbrace{p_3(ph)J''}^{Y}}^{J}\rangle \frac{1}{-\varepsilon} \langle \overbrace{p_2\overbrace{p_3(ph)J''}^{Y}}^{J}|V|(p_1p_3)J\rangle \ . \tag{A.1}$$

In the first interaction, the matrix element is independent of p_2, so we recouple so as to remove reference to p_2 as follows

$$|(p_2p_4)Jm\rangle = \sum_{m_{p_2}m_{p_4}} \langle p_2m_{p_2}p_4m_{p_4}|Jm\rangle|p_2p_4\rangle \tag{A.2}$$

$$|(p_2Y)Jm\rangle = \sum_{m'_{p_2}m_Y} \langle p_2m'_{p_2}Ym_Y|Jm\rangle|p_2Y\rangle \ .$$

Therefore,

$$\langle (p_2p_4)Jm|V|(p_2Y)Jm\rangle = \sum_{\substack{m_{p_2}m_{p_4} \\ m'_{p_2}m_Y}} \langle p_2m_{p_2}p_4m_{p_4}|Jm\rangle\langle p_2m'_{p_2}Ym_Y|Jm\rangle \times \langle p_2m_{p_2}p_4m_{p_4}|V|p_2m'_{p_2}Ym_Y\rangle \tag{A.3}$$

but the matrix element on the right is equal to

$$\delta_{m_{p_2},m_{p'_2}} \times \delta_{m_{p_4},m_\gamma} \times \delta_{p_4,\gamma} \langle p_4 m_{p_4} | V | p_4 m_{p_4} \rangle \ .$$

The second matrix element in Eq. (A.1) is independent of p_3 but cannot easily be removed since it is deeply coupled. However, using the 6-j transformation (from De Shalit (1963), for example), we have

$$\overbrace{p_2 \overbrace{p_3 (ph) J''}^{p_4}}^{Jm} = (-)^{p_3+J''-p_4} \overbrace{p_2 (ph) \overbrace{J'' p_3}^{p_4}}^{Jm}$$

$$= \sum_\gamma (-)^{p_3+J''-p_4} (-)^{p_2+J''+p_3+J} \sqrt{\hat{p}_4 \hat{\gamma}} \begin{Bmatrix} p_2 & J'' & \gamma \\ p_3 & J & p_4 \end{Bmatrix}$$

$$\times \overbrace{p_2 (ph) \overbrace{J'' p_3}^{\gamma}}^{Jm} \ . \qquad \text{(A.4)}$$

We now have

$$\langle \overbrace{p_2 \overbrace{(ph)}^{\gamma} J''}^{Jm} | V | (p_1 p_3) Jm \rangle = \sum_\gamma (-)^{p_3+J''-p_4+p_2+J''+p_3+J} \sqrt{\hat{p}_4 \hat{\gamma}} \begin{Bmatrix} p_2 & \gamma & J'' \\ p_3 & p_4 & J \end{Bmatrix}$$

$$\times \langle \overbrace{p_2 (ph) \overbrace{J'' p_3}^{\gamma}}^{Jm} | V | (p_1 p_3) Jm \rangle \ . \qquad \text{(A.5)}$$

But from the previous information, we have

$$\langle \overbrace{p_2 (ph) \overbrace{J'' p_3}^{\gamma}}^{Jm} | V | (p_1 p_3) Jm \rangle = \langle \overbrace{p_2 (ph) J''}^{} | V | p_1 \rangle \delta_{\gamma p_1} \ . \qquad \text{(A.6)}$$

After some rearrangement, the second order contribution is, including isospin.

$$\sum_{phJ''T''} (-)^{p_3+J''-p_4+p_2+J''+p_3+J+\frac{1}{2}+T''-\frac{1}{2}+\frac{1}{2}+T''+\frac{1}{2}+T} \times \sqrt{\hat{p}_4\hat{p}_1\hat{\tfrac{1}{2}}\hat{\tfrac{1}{2}}} \begin{Bmatrix} p_1 & p_3 & J \\ p_2 & p_4 & J'' \end{Bmatrix} \begin{Bmatrix} \frac{1}{2} & \frac{1}{2} & T \\ \frac{1}{2} & \frac{1}{2} & T'' \end{Bmatrix} \times \langle p_4\ \tfrac{1}{2}|V|\overbrace{p_3(ph)J''T''}^{p_4\ \frac{1}{2}}\rangle \frac{1}{-\epsilon} \langle \overbrace{p_2(ph)J''T''}^{p_1\ \frac{1}{2}}|V|p_1\ \tfrac{1}{2}\rangle \quad . \tag{A.7}$$

Now we consider the overall sign of the diagram. Writing V in second quantized form

$$V = \frac{1}{2} \sum_{\alpha\beta\gamma\delta} \langle\alpha\beta|V|\gamma\delta\rangle_{N.A.}\ a_\alpha^\dagger a_\beta^\dagger a_\delta a_\gamma \quad . \tag{A.8}$$

Then

$$\langle p_2p_4|VV|p_1p_3\rangle = \sum_{\substack{\alpha\beta\delta\gamma \\ ijk\ell}} \frac{1}{4} \langle\alpha\beta|V|\gamma\delta\rangle_{N.A.} \langle ij|V|k\ell\rangle_{N.A.} \times \langle a_{p_4} a_{p_2} a_\alpha^\dagger a_\beta^\dagger a_\delta a_\gamma a_i^\dagger a_j^\dagger a_\ell a_k a_{p_1}^\dagger a_{p_3}\rangle \quad . \tag{A.9}$$

Using Wick's Theorem, the possible contractions are

a) $\langle a_{p_4} a_{p_2} a_\alpha^\dagger a_\beta^\dagger a_\delta a_\gamma a_i^\dagger a_j^\dagger a_\ell a_k a_{p_1}^\dagger a_{p_3}^\dagger\rangle$

$$= + \langle p_4h|V|pp_3\rangle_{N.A.} \langle p_1h|V|pp_2\rangle_{N.A.}$$

b) 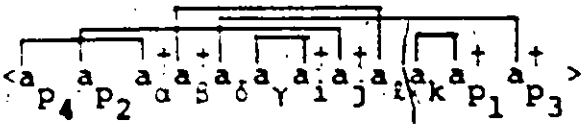

$$= + \langle p_4 h|V|pp_3\rangle_{N.A.} \langle p_1 h|V|pp_2\rangle_{N.A.} \tag{A.10}$$

c) 

$$= - \langle hp_4|V|pp_3\rangle_{N.A.} \langle hp_1|V|pp_2\rangle_{N.A.}$$

d) 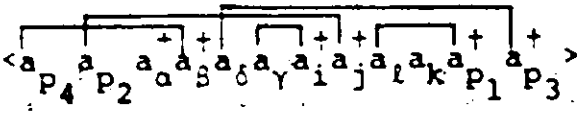

$$= - \langle hp_4|V|pp_3\rangle_{N.A.} \langle hp_1|V|pp_2\rangle_{N.A.}$$

Adding up the four contributions, we finally have for the matrix elements

$$\frac{1}{2} \langle p_4 h|V|pp_3\rangle_{A.S.} \langle p_1 h|V|pp_2\rangle_{A.S.} \tag{A.11}$$

However, Eq. (2.33) is expressed in terms of p-h matrix elements and by using contractions, these are opposite in sign to the p-p matrix elements as follows

$$\frac{1}{2} (-) \langle p_4 \bar{p_3}|V|p\bar{h}\rangle_{A.S.} (-) \langle p_1 p_2|V|p\bar{h}\rangle_{A.S.} \tag{A.12}$$

Since these two p-h matrix elements correspond to those in Eq. (A.11), the sign of this diagram is positive. By making

the substitution of the ν vertices, one easily obtains the expression in Eq. (2.33).

APPENDIX B

All the angular momentum algebra in Section 2.2 may be done graphically according to Brink and Satchler (1968). The application here will be to transform the coupling in Fig. B.1(a) to Fig. B.1(b). From Fig. B.1(a), we have

Coupling	Graphical Representation
$(ab)^{Jm_J}$	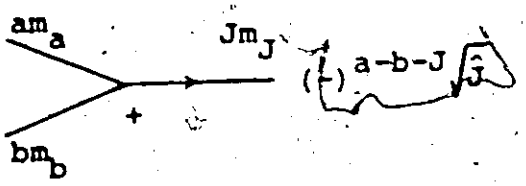 $(-)^{a-b-J}\sqrt{\hat{J}}$
$(cd)^{Jm_J}$	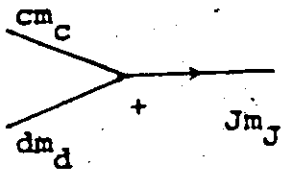 $(-)^{c-d-J}\sqrt{\hat{J}}$

(B.1)

From Fig. B.1(b), we have

$(ab)^{Jm_J}$ 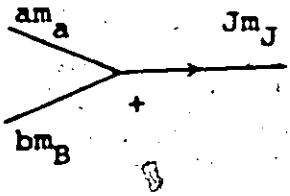 $(-)^{a-b-J}\sqrt{\hat{J}}$.

Fig BI

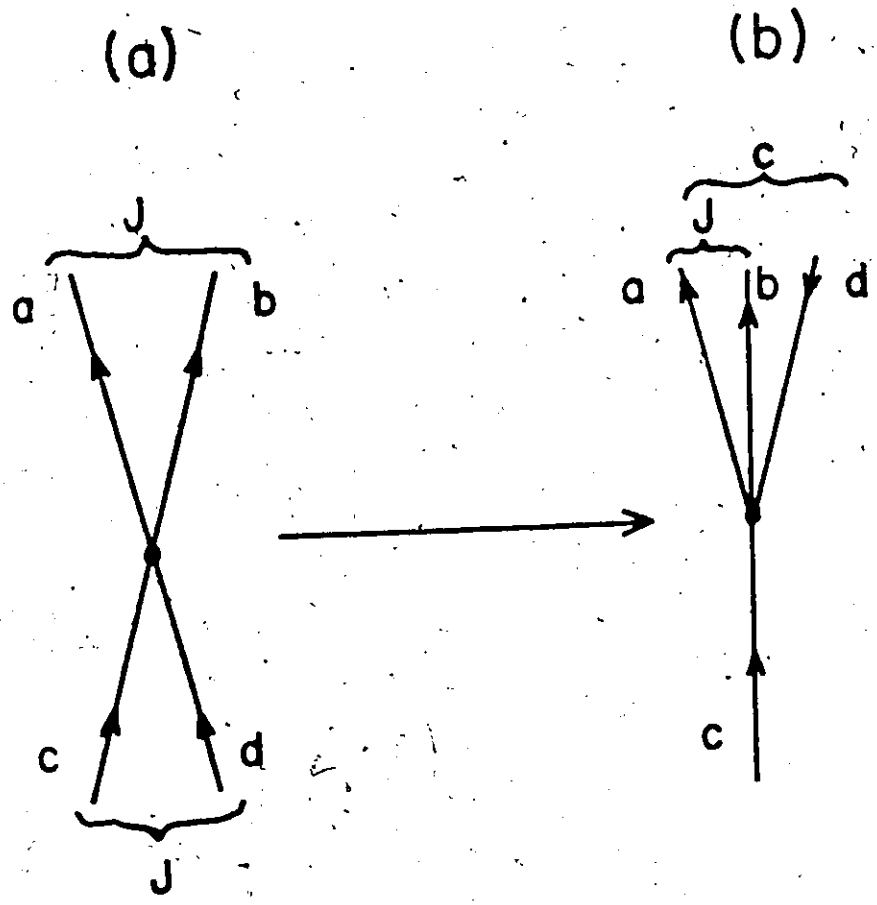

Example of Angular Momentum Recoupling.

For the hole state, we have

$$(Jd^{-})^{cm_c} \qquad \text{(Jm}_J\text{, cm}_c\text{, d-m}_d\text{ vertex)} \qquad (-)^{J-d-c}(-)^{d-m_d}\sqrt{\hat{c}}\ .$$

The only changes are the sign of the z component of the hole state angular momentum and the additional phase factor. We also use the fact that

$$a\alpha \longrightarrow a\text{-}\alpha = (-)^{a-\alpha}\ a\alpha \longrightarrow a\alpha\ . \qquad \text{(B.2)}$$

The final result is obtained by joining the four vertices so as to reduce and simplify the diagrams. Only lines with the same angular momentum may be joined. One must keep in mind when manipulating these diagrams, that they must only slide along the paper and not be lifted from the paper and turned over. Combining the first and third vertices, we have after changing the sign of one vertex by interchanging two legs

$$\text{(am}_a\text{, Jm}_J\text{, Jm}_J\text{, bm}'_b\text{ vertex)} \qquad (-)^{a-b-J+a-b-J}\ \hat{J}\ . \qquad \text{(B.3)}$$

To change this to the form below

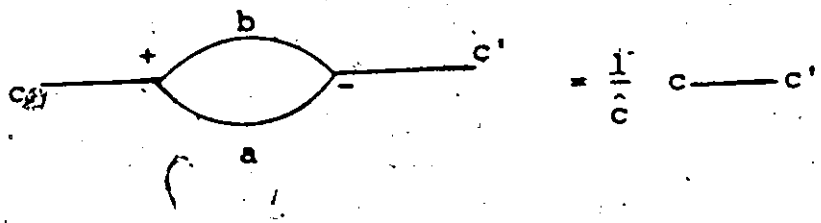

(B.4)

we add arrows to obtain

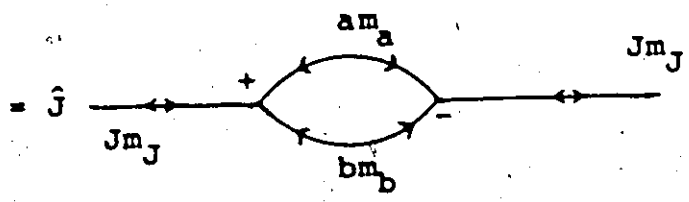

(B.5)

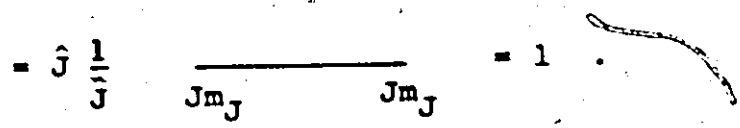

This is interpreted as saying that when the angular momentum coupling is unchanged under a transformation, we do not need to consider it. In the above example, a and b were coupled to Jm_J before and after the transformation.

Combining the second and fourth term, we have

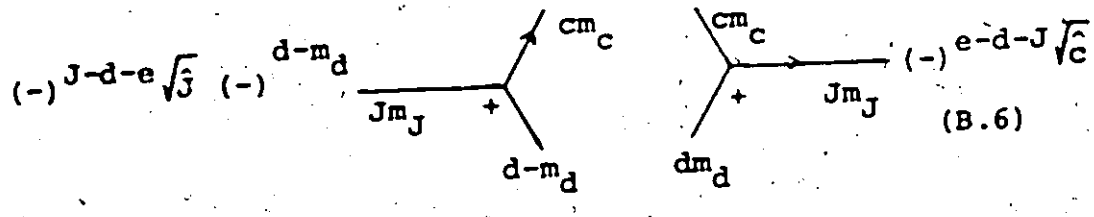

(B.6)

When we join the lines dm_d, we sum over m_d but when we join cm_c, we cannot sum because m_c is fixed. Since the interaction

is scalar, the value cannot depend on m_c, therefore, when we join cm_c, we sum over m_c but divide by $\hat{c} = (2m_c + 1)$.

The new result is, summing over m_J

$$(-)^{J-d-c+e-d-J+d-m_d+c+d+J+d-m_d} \sqrt{\frac{\hat{J}}{\hat{c}}}$$

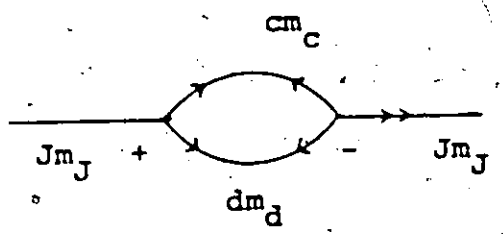

$$= - (-)^{c+d+J} \sqrt{\frac{\hat{J}}{\hat{c}}}$$

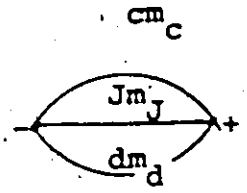

$$= - (-)^{c+d+J} \sqrt{\frac{\hat{J}}{\hat{c}}} \quad . \tag{B.7}$$

When generalized to isospin, the factor is

$$(-)^{c+d+J+T+1} \sqrt{\frac{\hat{J}\ \hat{T}}{\hat{c}\ \hat{\frac{1}{2}}}} \quad . \tag{B.8}$$

As in the algebraic method, in addition to the angular momentum coupling, the sign of the new vertex must be determined from Wick's Theorem. In this case the sign remains positive.

APPENDIX C

As shown in Appendix B, one may use graphical analysis of angular momentum recoupling. The other method is to use the algebraic approach which will be illustrated below for the recoupling from p-p to p-h matrix elements. The derivation will not include isospin, but generalization is straightforward. We want the following matrix element:

$$\langle (ph^{-})^{JM} | V | (p'h'^{-})^{JM} \rangle$$

$$= \frac{1}{2} \sum_{\substack{mpmh \\ mp'mh' \\ \alpha\beta\gamma\delta}} \langle p'm_p, h'm_h, | JM \rangle \langle pm_p hm_h | JM \rangle \langle \alpha\beta | V | \gamma\delta \rangle$$

$$\times \langle 0 | \xi_{h m_h} \xi_{p m_p} a_\alpha^\dagger a_\beta^\dagger a_\gamma a_\delta \xi_{p' m_p'}^\dagger \xi_{h' m_h'}^\dagger | 0 \rangle \qquad \text{(C.1)}$$

Making the substitution of Eq. (2.21), the operator part of Eq. (C.1) becomes

$$(-)^{h+m_h+h'+m_{h'}} \langle 0 | a_{h-m_h} a_{pm_p} a_\alpha^\dagger a_\beta^\dagger a_\delta a_\gamma a_{p'm_p'}^\dagger a_{h'-m_{h'}}^\dagger | 0 \rangle \quad . \qquad \text{(C.2)}$$

Since m_h and $m_{h'}$ are dummy indices, we will make them negative everywhere in Eqs. (C.1) and (C.2). Applying Wick's theorem, we can easily show that the expectation value can be written

$$- 2\,\delta_{\alpha p}\delta_{\beta h'}\delta_{\gamma p'}\delta_{\delta h} \qquad (C.3)$$

The simplified form of Eq. (C.1) becomes,

$$- \sum_{\substack{m_p m_h \\ m_{p'} m_{h'}}} \langle p' m_{p'}, h'-m_{h'} | JM \rangle \langle p m_p h - m_h | JM \rangle (-)^{h-m_h+h'-m_{h'}}$$

$$\times \langle p m_p h' m_{h'} | V | p' m_{p'}, h m_h \rangle \qquad (C.4)$$

The p-p matrix elements in Eq. (C.1) are not coupled to total angular momentum as yet and this is accomplished by further coupling. The coupled form of Eq. (C.1) becomes

$$- \sum_{\substack{m_p m_h \\ m_{p'} m_{h'} \\ J' m_{J'} J'' m_{J''}}} (-)^{h-m_h+h'-m_{h'}} \langle p' m_{p'}, h'-m_{h'} | JM \rangle \langle p m_p h - m_h | JM \rangle$$

$$\times \langle p m_p h' m_{h'} | J' m_{J'} \rangle \langle p' m_{p'}, h m_h | J'' m_{J''} \rangle$$

$$\times \langle (ph')^{J'}_{m_{J'}} | V | (p'h)^{J''}_{m_{J''}} \rangle \delta_{J' J''} \delta_{m_{J'}, m_{J''}} \qquad (C.5)$$

The four Clebsch-Gordon coefficients can be replaced by a 6-j symbol in the following way. Write each C-G coefficient as a 3-j and rearranging one obtains

$$(-)^{h-m_h+h'-m_{h'}}\hat{J}\hat{J}'(-)^{p'-h'+m_J+p-h+m_J+p-h'+m_{J'}+p'-h+m_{J'}+p+h+J+p'+h'+J}$$

$$\times \begin{pmatrix} p & n & J \\ m_p & -m_h & -m_J \end{pmatrix} \begin{pmatrix} p & h' & J \\ -m_p & -m_{h'} & +m_J \end{pmatrix} \begin{pmatrix} p' & h & J' \\ m_{p'} & +m_h & -m_{J'} \end{pmatrix} \begin{pmatrix} p' & h' & J \\ -m_{p'} & +m_{h'} & +m_J \end{pmatrix} \tag{C.6}$$

Comparing this to Eq. (15.12) in de Shalit and Talmi (1963) and inserting $\frac{1}{\hat{J}} \sum_{m_J}$, one finally obtains

$$\langle (ph)^{JM}|V|(p'h')^{JM}\rangle = -\sum_{J'} \hat{J}' \begin{Bmatrix} p & h & J \\ p' & h' & J \end{Bmatrix} \langle (ph')^{J'm_{J'}}|V|(p'h)^{J'm_{J'}}\rangle . \tag{C.7}$$

Generalizing to isospin (but remembering that the minus sign in front of the summation index must not be generalized since it comes from Wick's Theorem), we finally obtain

$$\langle (ph)^{JT}|V|(p'h')^{JT}\rangle = -\sum_{J'T'} \hat{J}'\hat{T}' \begin{Bmatrix} p & h & J \\ p' & h' & J' \end{Bmatrix} \begin{Bmatrix} \frac{1}{2} & \frac{1}{2} & T \\ \frac{1}{2} & \frac{1}{2} & T' \end{Bmatrix} \times \langle (ph')^{J'T'}|V|(p'h)^{J'T'}\rangle \tag{C.8}$$

which is given in Eq. (2.28) of Chapter II.

APPENDIX D

The RPA approximation in the schematic model is described. From p. 46 of Brown's textbook (Brown (1967)), we have the RPA equations of motion.

$$[E - (\epsilon_m - \epsilon_i)]x_{mi} = \sum_{nj} [f_{mi,nj}x_{nj} + B_{mi,nj}y_{nj}]$$

$$[E + (\epsilon_m - \epsilon_i)]y_{mi} = \sum_{nj} [-B_{mi,nj}x_{nj} - f_{mi,nj}y_{nj}] \quad (D.1)$$

The f and B matrices provide forward and backward going p-h vertices as in Fig. D.1. In the schematic model they are taken to have a separable form:

$$f_{mi,nj} = \lambda D_{mi}D_{nj} \quad , \quad B_{mi,nj} = \lambda C_{mi}C_{nj} \quad . \quad (D.2)$$

In the above ϵ_m are the energies of unoccupied orbitals and the ϵ_i of occupied orbitals in the nucleus; (mi) runs over the set of p-h states considered, and x_{mi}, y_{mi} are amplitudes of the wave function of a coherent p-h state of energy E. It is more convenient to enumerate the p-h states (mi) in some order and use a single index r to label them. In this case $\epsilon_m - \epsilon_i \rightarrow \epsilon_r$. In all discussions we have seen it has been supposed that the C_r are proportional to the D_r, so the f and B matrices differ by at most a constant factor,

but here we will avoid that assumption. We rewrite Eq. (D.1) as

$$x_r = \frac{-\lambda}{\epsilon_r - E} D_r \sum_s D_s x_s + C_r \sum_s C_s y_s \quad , \tag{D.3}$$

$$y_r = \frac{-\lambda}{\epsilon_r + E} C_r \sum_s C_s x_s + D_r \sum_s D_s y_s \quad .$$

If we define $N_{dx} = \sum_s D_s x_s$ and three similar quantities and then multiply Eq. (D.3) by D_r or C_r and sum over r, we obtain four linear homogeneous equations for the unknowns N_{dx}, N_{dy}, N_{cx}, and N_{cy}. The condition for solubility is that the determinant of the coefficients be zero; this determines the eigenvalues E. The first of these equations is

$$N_{dx} = -\lambda \sum_r \frac{D_r^2}{\epsilon_r - E} N_{dx} - \lambda \sum_r \frac{D_r C_r}{\epsilon_r - E} N_{dy} \quad . \tag{D.4}$$

A further simplification occurs when we go to the degenerate schematic model, in which we suppose that initially all the p-h states have a common energy ϵ. The sums occurring in Eq. (D.4) then consist of

$$\sum_r D_r^2 = F \quad , \quad \sum_r C_r D_r = G \quad , \quad \sum_r C_r^2 = H \quad . \tag{D.5}$$

The eigenvalue condition is

$$\det \begin{vmatrix} 1+\lambda F/(\varepsilon-E) & 0 & 0 & \lambda G/(\varepsilon-E) \\ \lambda G/(\varepsilon-E) & 1 & 0 & \lambda H/(\varepsilon-E) \\ 0 & \lambda G/(\varepsilon+E) & 1+\lambda F/(\varepsilon+E) & 0 \\ 0 & \lambda H/(\varepsilon+E) & \lambda G/(\varepsilon+E) & 1 \end{vmatrix} = 0 \quad (D.6)$$

This turns out to be a quadratic equation in the unknown $X = E^2 - \varepsilon^2$:

$$X^2 - \{2\lambda\varepsilon F + \lambda^2(F^2-H^2)\}X + \{2\varepsilon\lambda^3 H(G^2-FH) - \lambda^4(G^2-FH)^2\} = 0 \quad (D.7)$$

whose solution is of course obvious. Some insight into the meaning of the result is obtained if we go back to the usual assumption that the C_r are proportional to D_r: C is then a vector parallel to D. This makes $G^2 = FH$; the last term of Eq. (D.7) vanishes and the solutions are either $X = 0$ (when $E = \varepsilon$: no energy shift) or

$$E^2 = \varepsilon^2 + 2\lambda\varepsilon F + \lambda^2(F^2-H^2) \quad (D.8)$$

If we assumed that C were zero, there would be no B-matrix. This would be the TDA. Then

$$E = \varepsilon + \lambda F = \varepsilon + \lambda \sum_r D_r^2 \quad (D.9)$$

a well known result. The shift in the energy is equal to the trace of the p-h interaction matrix, showing the highly

coherent nature of this state.

On the other hand, we could suppose that C is actually equal to D, as assumed by Brown (1967). Then F = H, so the solution is

$$E^2 = \epsilon^2 + 2\lambda\epsilon F \quad . \tag{D.10}$$

Equation (D.8) contains the result for other values of H between the limits of TDA and this extreme RPA case. These intermediate cases are of some relevance in understanding the results of actual calculations with more complicated forces.

For example, in Table D.1, we give the f and B matrices for the Kuo-Brown and Kallio-Kolltveit (Kallio and Kolltveit (1964)) forces appropriate to the $J^\pi = 0^+$, T = 0 phonon. Also given are the form factors D and C which provide a reasonable fit to these matrices. In both cases the condition that $G^2 - FH$ be small is satisfied. Also, H is a third to a half of F. It is convenient to think of C and D as vectors of length squared H and F respectively. Then Schwartz's inequality guarantees

$$G^2 - FH = - FH \sin^2\theta \leq 0 \quad . \tag{D.11}$$

For the Kallio-Kolltveit force from Table D.1, we have $\cos\theta = 0.9947$; for Kuo-Brown, $\cos\theta = 0.906$. The condition

TABLE D.1

THE f AND B MATRIX ELEMENTS FOR THE $J^{\pi} = 0^{+}$, $T = 0$ PHONON AND THE SEPARABLE APPROXIMATION TO THEM. THE SEPARABLE FORCE WAS JUST CHOSEN TO REPRODUCE THE DIAGONAL MATRIX ELEMENTS.

Matrix Element	Kallio-Kolltveit Force		Kuo-Brown Force	
	Calc.	Approx.	Calc.	Approx.
$(-f_{11})^{1/2}$	2.09	2.09	0.78	0.78
$(-f_{22})^{1/2}$	3.03	3.03	2.62	2.62
$(-f_{33})^{1/2}$	3.44	3.44	3.03	3.03
$-f_{12}$	6.72	6.33	7.37	2.05
$-f_{13}$	5.40	7.20	2.19	2.37
$-f_{23}$	7.64	10.46	6.87	7.94
$(-B_{11})^{1/2}$	1.62	1.62	0.42	0.42
$(-B_{22})^{1/2}$	2.34	2.34	1.91	1.91
$(-B_{33})^{1/2}$	2.87	2.87	2.22	2.22
$-B_{12}$	4.04	3.78	3.59	0.81
$-B_{13}$	3.20	4.64	0.18	0.94
$-B_{23}$	4.52	6.72	3.84	4.24

that C and D be nearly parallel is thus well satisfied for this phonon. The fact that $H \ll F$ helps to minimize the importance of nonparallelism, making Eq. (D.8) a good approximation. In any case, one can always go back to Eq. (D.7) if necessary.

When the interaction is too strongly attractive, the energy E can become negative indicating an instability of the system. In the TDA, this occurs when $\epsilon \leq |\lambda F|$ ($\lambda < 0$ for attraction). In the extreme RPA it requires $\epsilon \leq 2|\lambda F|$: for given ϵ, only half the force strength is required to promote instability. For the Kallio-Kolltveit force in Table D.1, rounding off the values to F = 25, H = 16, and G = 20 we find using Eq. (D.8) that instability would occur for ϵ = 41 MeV, rather less than 50 MeV = $2|\lambda F|$. For the Kuo-Brown force, F = 16, H = 8, and G = 12 similarly give instability for ϵ = 24 MeV. For calculations in the oxygen region one generally uses $\epsilon = 2\hbar\omega \approx 28$ MeV. One indeed finds that the Kallio-Kolltveit force gives instability while the Kuo-Brown force does not. Equation (D.8) accurately reflects the results of detailed calculations.

D.1 Kirson's Formulation of RPA

In this section we will discuss the diagrams summed by Kirson. In his paper a slightly different version of the RPA was given, and shown to be equivalent to the usual RPA although different wave functions and different energy eigenvalues are found in his formulation. We will call this modified formalism the RKA. The RKA equation of motion is

$$[\varepsilon + f - B \frac{1}{\varepsilon+f} B]|X\rangle = E|X\rangle \qquad (D.12)$$

Here f and B are the same matrices as before; ε is a diagonal matrix containing the p-h energies, and the wave function $|X\rangle$ can be related indirectly to the (X,Y) occurring in the usual formulation.

From the discussion it appears to be a good approximation to assume C parallel to D, so we adopt this simplification. We can write

$$f = \lambda|D\rangle\langle D| \qquad (D.13)$$

$$B = \mu|D\rangle\langle D| \qquad (D.14)$$

with $\mu^2 \approx (1/3)\lambda^2$ for the interactions in Table D.1. The solubility of the schematic model rests on the fact that we can explicitly invert the matrix $(\varepsilon+f)$:

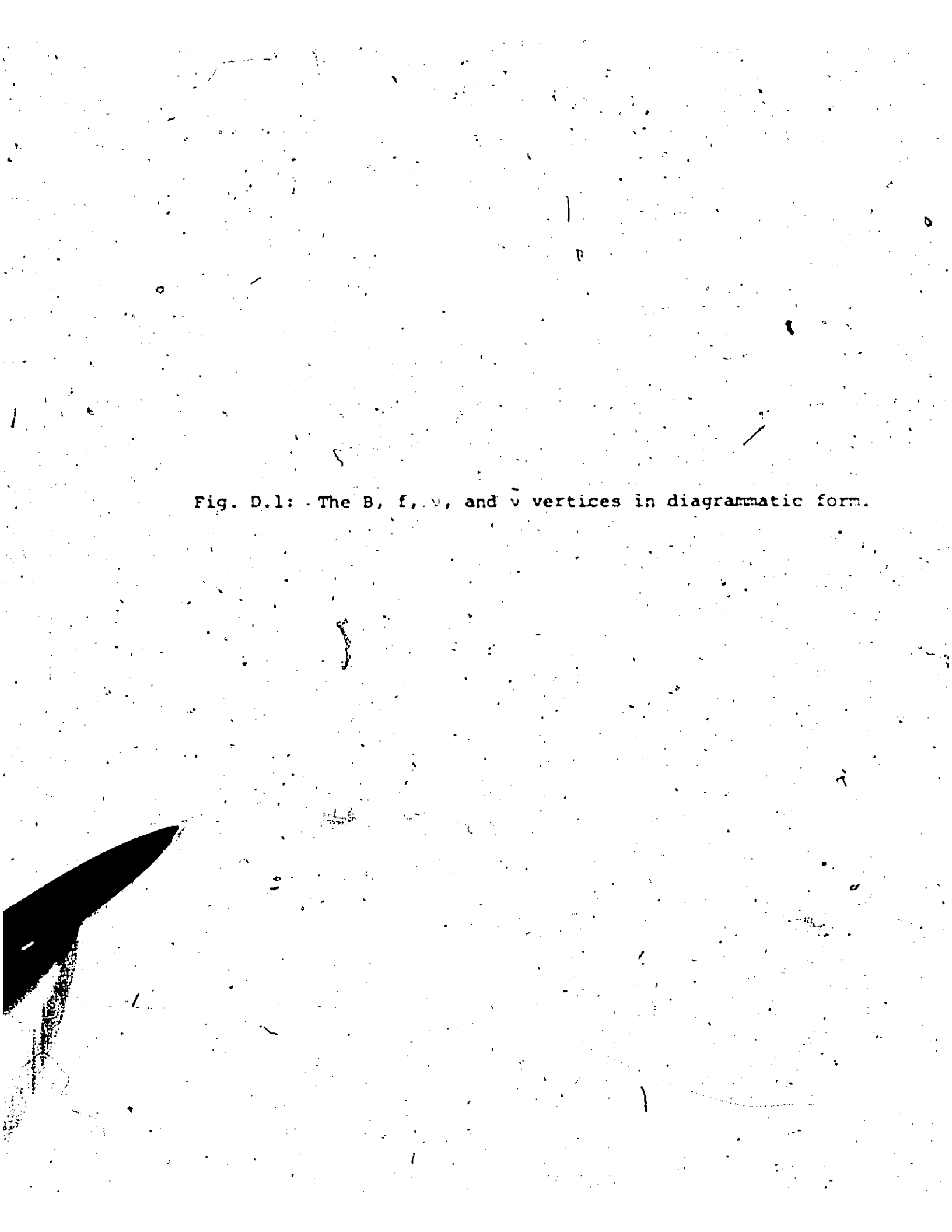

Fig. D.1: The B, f, ν, and $\tilde{\nu}$ vertices in diagrammatic form.

Fig DI

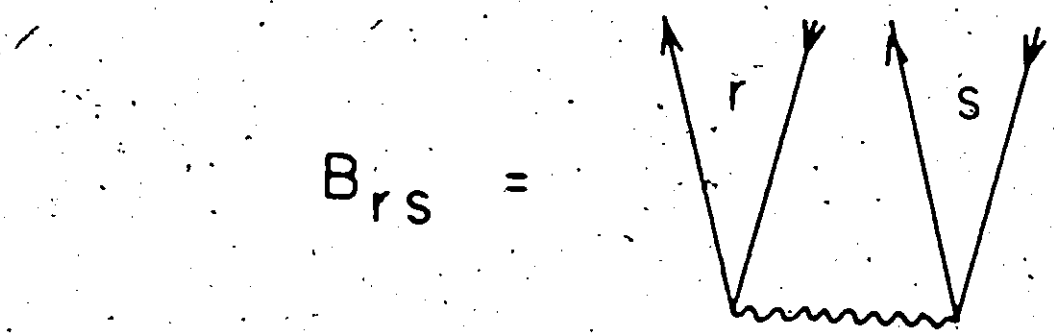

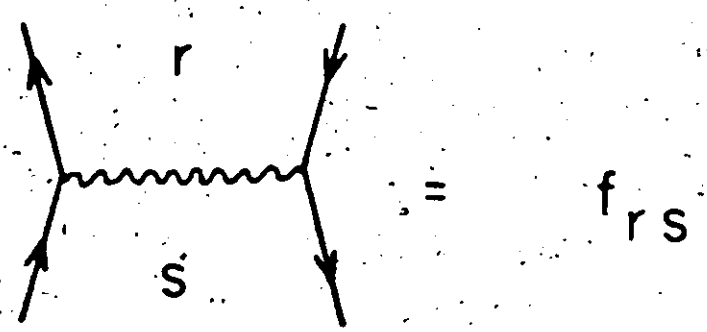

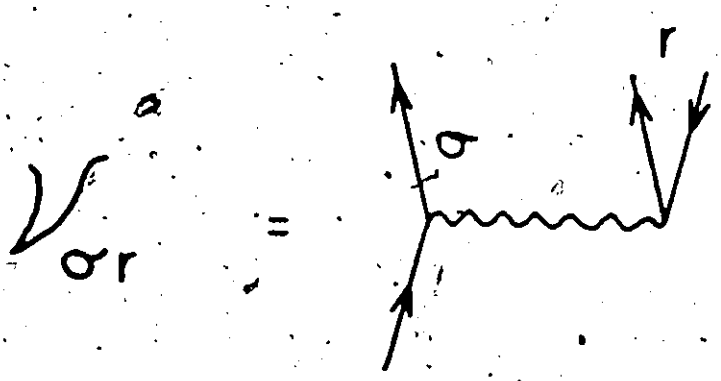

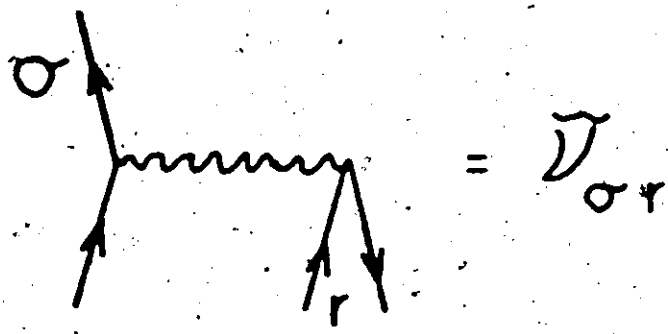

$$(\varepsilon+f)^{-1} = R \begin{pmatrix} \frac{1}{\varepsilon_1}(1 + \sum_i{}' \lambda D_i^2/\varepsilon_i) & -\lambda D_1 D_2/\varepsilon_1\varepsilon_2 & \cdots \\ -\lambda D_1 D_2/\varepsilon_1\varepsilon_2 & \frac{1}{\varepsilon_2}(1 + \sum_i{}' \lambda D_i^2/\varepsilon_i) & \cdots \\ \vdots & \vdots & \end{pmatrix} \tag{D.15}$$

with

$$R^{-1} = 1 + \sum_i \lambda D_i^2/\varepsilon_i \tag{D.16}$$

and the primed summation omits the obvious term. We find

$$B \frac{1}{\varepsilon+f} B = \frac{\mu^2}{\lambda} |D><D| \{ \sum_i \lambda D_i^2/\varepsilon_i / [1 + \sum_i \lambda D_i^2/\varepsilon_i] \} \tag{D.17}$$

Following Kirson we may define a strength parameter c by

$$\sum_i \lambda D_i^2/\varepsilon_i \equiv \lambda/c \tag{D.18}$$

We let the constant λ carry the dimensions energy, so c is also an energy, and λ/c is large when the force is strong relative to the single p-h excitation energies. From Eq. (D.12) we find a dispersion relation

$$\sum_i \frac{\lambda D_i^2}{E-\varepsilon_i} \{1 - \frac{\mu^2}{\lambda^2} (\frac{\lambda}{\lambda+c}) \} N = N \tag{D.19}$$

with $N = \langle D|X\rangle$. The roots may be found from a diagram such as Fig. D.2.

In the degenerate schematic model, all but one of the eigenvalues E are caught at $E = \epsilon$; for these solutions $|X\rangle$ is orthogonal to $|D\rangle$. For the other root $|X\rangle$ is parallel to $|D\rangle$ and

$$E_{RKA} = \frac{\epsilon}{c} \frac{(\lambda+c)^2 - \mu^2}{\lambda+c} \tag{D.20}$$

as found by Kirson. When $\mu = 0$ we recover the TDA result, Eq. (D.9).

To calculate the core polarization contribution to the effective interaction we use a formula from Kirson's paper

$$V_{RKA} = \nu[\mathcal{A} - B\mathcal{A}^{-1}B]^{-1}[\nu - B\mathcal{A}^{-1}\tilde{\nu}] \tag{D.21}$$

The vertices ν and $\tilde{\nu}$ shown in Fig. D.2 represent interactions between valence orbitals and p-h excitations. Kirson writes $\mathcal{A} = c + f$. These we will also take to be separable

$$\nu_{\sigma r} = \lambda D_\sigma D_r \quad , \quad \tilde{\nu}_{\sigma r} = \mu D_\sigma D_r \quad . \tag{D.22}$$

The point is to recognize that $\tilde{\nu}$ has the character of a B matrix. Noting that the first square bracket in Eq. (D.21) is the quantity already calculated, we find in the

Fig. D.2: Graphical solution of the dispersion formula for the energies of coherent p-h excitations in the RKA formalism. The dotted horizontal line is low when the interaction is strong, shifting one of the eigenvalues far from the unperturbed energies. The example shown is for a repulsive force.

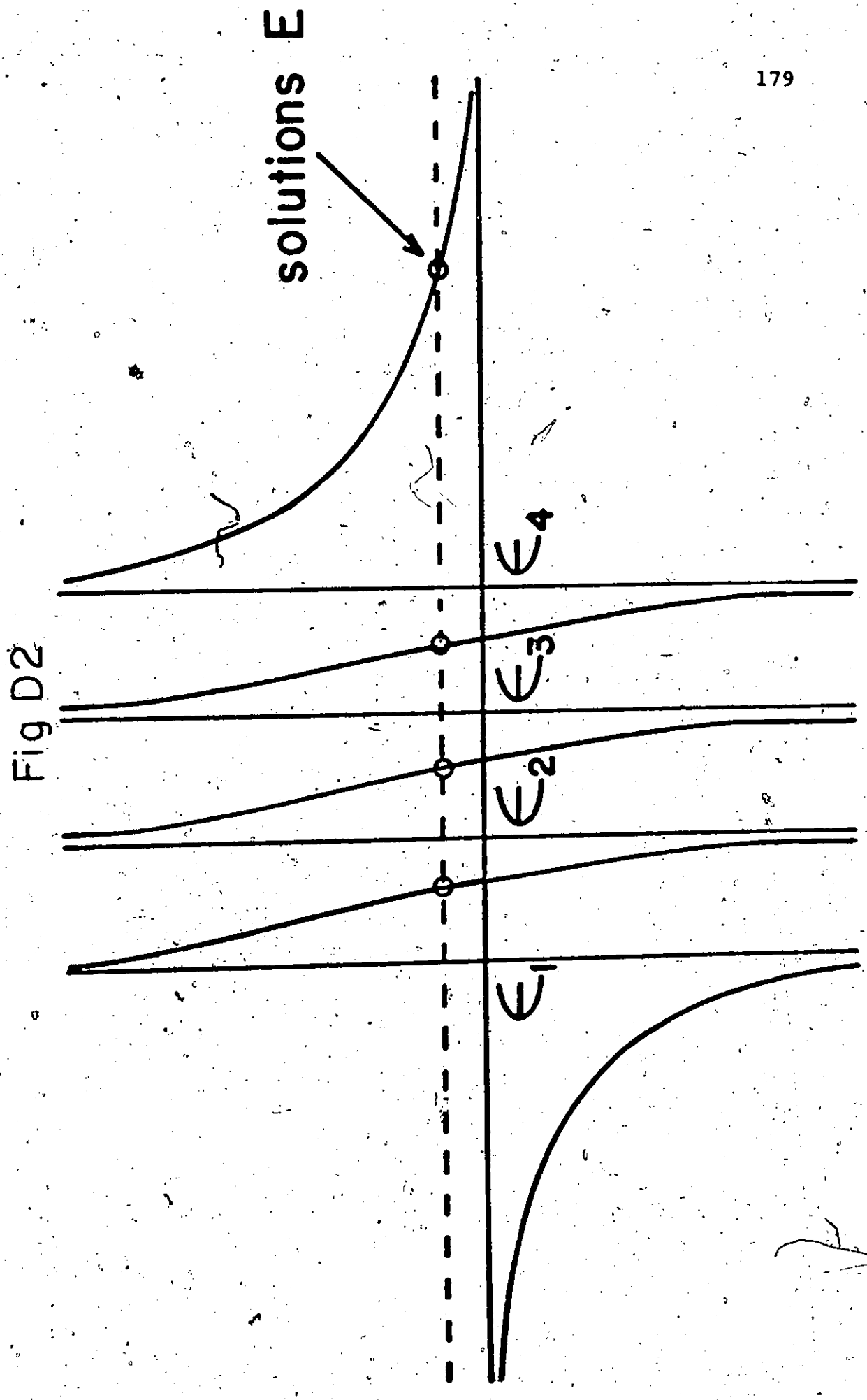

Fig D2

degenerate case where $|C\rangle$ is the vector of particle-hole amplitudes

$$V_{RKA} = |C\rangle\lambda\langle C|\left\{\frac{\lambda \sum_r D_r^2}{E}\left(1 - \frac{\mu^2}{\lambda^2}\frac{\lambda \sum_r D_r^2}{\epsilon + \lambda \sum_r D_r^2}\right)\right\} = |C\rangle\lambda\langle C|\left(\frac{E-\epsilon}{E}\right) \quad (D.23)$$

The renormalized interaction, original plus core polarization, becomes

$$V_{TOT} = |C\rangle\lambda\langle C|\left\{\frac{1 + 3\lambda/c + 2(\lambda^2-\mu^2)/c^2}{1 + 2\lambda/c + (\lambda^2-\mu^2)/c^2}\right\} \quad (D.24)$$

The factor in curly brackets represents an amplification factor of the original coupling constant λ. If we had considered only the single p-h bubble process, we would have had

$$V_{p-h} = v + v\frac{1}{\epsilon}v = |C\rangle\lambda\langle C|(1 + \lambda/c) \quad (D.25)$$

We now compare the amplification factors for the three cases

$$S^{ph} = 1 + \frac{\lambda}{c}$$

$$S^{TDA} = \frac{1 + 2\frac{\lambda}{c}}{1 + \frac{\lambda}{c}} \quad (D.26)$$

$$S^{RPA}_{\mu=\lambda} = \frac{1 + 3\frac{\lambda}{c}}{1 + 2\frac{\lambda}{c}}$$

For a weak force ($\frac{\lambda}{c} \to 0$) these all agree as they should. For a strong force, they differ considerably. For an attractive force, the effect is a reduced coupling strength followed by divergence at the point where instability occurs. Since instability occurs more easily in RPA than in TDA, the effects are correspondingly larger. For repulsive forces, the renormalization is always less dramatic. The RPA showing less effect than the TDA or p-h.

REFERENCES

1. Barrett, B. R. and Kirson, M. W. Nucl. Phys. A148 (1970) 145
2. Barrett, B. R., Hewitt, R. G. L. and McCarthy, R. J. Phys. Rev. C 3 (1971) 1137
3. Barrett, B. R. and Kirson, M. W. in Advances in Nuclear Physics 6 (1972) Plenum Press, New York
4. Barrett, B. R. Nucl. Phys. A221 (1974) 299
5. Barrett, B. R. Invited paper given at Gull Lake Symposium on the Two Body Force in Finite Nuclei (September 1971)
6. Bertsch, G. F. Nucl. Phys. 74 (1965) 234
7. Bloch, C. and Horowitz, J. Nucl. Phys. 8 (1958) 91
8. Blomquist, J. and Kuo, T. T. S. Phys. Lett. 29B (1969) 544
9. Bohr, A. and Mottelson, B. Nuclear Structure (1969). Benjamin, New York.
10. Bohr, N. and Wheeler, J. A. Phys. Rev. 56 (1939) 426
11. Brandow, B. H. Phys. Rev. 152 (1966) 863
12. Brandow, B. H. Rev. Mod. Phys. 39 (1967) 771
13. Brandow, B. H. Ann. Phys. (N.Y.) 57 (1970) 214
14. Brink, D. M. and Peierls, R. E. Comments Nucl. Particle Phys. 1 (1967) 146

15. Brink, D. M. and Satchler, G. R. Angular Momentum (1968) Clarendon Press, Oxford

16. Brody, T. A. and Moshinsky, M. Tables of Transformation Brackets (1960) Gordon and Breach, New York

17. Brown, G. E. and Bolsterli, M. Phys. Rev. Lett. 3 (1959) 472

18. Brown, G. E. Unified Theory of Nuclear Models (1967) Wiley and Sons, New York

19. Brown, G. E. and Kuo, T. T. S. Nucl. Phys. A92 (1967) 481

20. Brown, G. E. Rev. Mod. Phys. 43 (1971) 1

21. Brueckner, K. A., Levinson, C. A. and Mahmoud, H. M. Phys. Rev. 95 (1954) 217

22. Brueckner, K. A. and Levinson, C. A. Phys. Rev. 97 (1955) 344

23. Brueckner, K. A. and Gammel, J. L. Phys. Rev. 109 (1958) 1023

24. Clement, D. M. and Baranger, E. U. Nucl. Phys. A108 (1968) 27

25. Condon, E. U. and Shortley, G. H. The Theory of Atomic Spectra (1959) Cambridge University Press, New York

26. Dawson, J. F., Talmi, I. and Walecka, J. D. Ann. Phys. (N.Y.) 18 (1962) 339

27. Dieperink, A. E. L., Leenhouts, H. P. and Brussard, P. J. Nucl. Phys. A116 (1968) 556

28. Dworzecka, M. and McManus, H. Phys. Lett. 37B (1971) 331

29. Ellis, P. J. and Siegel, S. Nucl. Phys. A152 (1970) 547

30. Ellis, P. J. and Osnes, E. Phys. Lett. 42B (1972) 335

31. Elliott, J. P. and Flowers, B. H. Proc. Roy. Soc. A229 (1955) 536

32. Elliott, J. P. and Flowers, B. H. Proc. Roy. Soc. A242 (1957) 57

33. Elliott, J. P., Mavromatis, H. A. and Sanderson, E. A. Phys. Lett. 24B (1967) 358

34. Pederman, P. and Pittel, S. Nucl. Phys. A155 (1970) 161

35. Feynman, R. P. Phys. Rev. 76 (I949) 749

36. Gerace, W. J. and Green, A. M. Nucl. Phys. A93 (1967) 110

37. Gillet, V. Nucl. Phys. 54 (1964a) 472

38. Gillet, V. Nucl. Phys. 57 (1964b) 698

39. Gillet, V. and Vinh Mau, N. Nucl. Phys. 54 (1964c) 321

40. Gillet, V. Nucl. Phys. 88 (1966a) 321

41. Gillet, V. Proceedings of the International School of Physics Enrico Fermi Course 36 (1966b) Academic Press, New York

42. Goldstone, J. Proc. Roy. Soc. A239 (1957) 267

43. Goode, P. Nucl. Phys. A172 (1971) 66

44. Hamada, T. and Johnston, I. D. Nucl. Phys. 34 (1962) 383

45. Hugenholtz, N. M. Physica 23 (1957) 481

46. Johnson, M. and Baranger, M. Ann. Phys. (N.Y.) 62 (1971) 172

47. Jopko, A. M. and Sprung, D. W. L. Can. J. Phys. 51 (1973) 2275

48. Kahana, S., Lee, H. C. and Scott, C. K. Phys. Rev. 185 (1969) 1378

49. Kallio, A. and Kolltveit, K. Nucl. Phys. 53 (1964) 87

50. Kirson, M. W. and Zamick, L. Ann. Phys. (N.Y.) 60 (1970) 188

51. Kirson, M. W. Ann. Phys. (N.Y.) 66 (1971) 624

52. Kuo, T. T. S. and Brown, G. E. Nucl. Phys. 85 (1966) 40

53. Kuo, T. T. S. Nucl. Phys. A90 (1967) 199

54. Kuo, T. T. S. and Brown, G. E. Nucl. Phys. A114 (1968) 241

55. Kuo, T. T. S. and Osnes, E. Nucl. Phys. A226 (1974) 204

56. Kurath, D. Phys. Rev. 101 (1956) 216

57. Goldhaber, M. and Teller, E. Phys. Rev. 74, (1948) 1046

58. LoIudice, N., Rowe, D. J. and Wong, S. S. M. Phys. Lett. 37B (1971) 44

59. Lovas, I. and Vegh, L. Nucl. Phys. A220 (1974) 335

60. Mavromatis, H. A., Markiewicz, W. and Green, A. M. Nucl. Phys. A90 (1967) 101

61. Mayer, M. G. and Jensen, J. H. D. Elementary Theory of Nuclear Shell Structure (1955) Wiley and Sons, New York

62. Osnes, E. and Warke, C. S. Phys. Lett. 30B (1969) 306

63. Osnes, E., Kuo, T. T. S. and Warke, C. S. Nucl. Phys. A168 (1971a) 190

64. Osnes, E., Kuo, T. T. S. and Warke, C. S. Phys. Lett. 34B (1971b) 113

65. Parikh, J. C. and Rowe, D. J. Phys. Rev. 175 (1968) 1293

66. Pradhan, H. C. and Shakin, C. M. Phys. Lett. 37B (1971) 151

67. Rainville, E. D. Special Functions (1960) MacMillan & Co., London

68. Redlich, M. G. Phys. Rev. 99 (1955) 1427

69. Reid, R. V. Ann. Phys. (N.Y.) 50 (1968) 411

70. Rowe, D. J. Nucl. Phys. 80 (1966) 209

71. Rowe, D. J. Rev. Mod. Phys. 40 (1968) 153

72. Rowe, D. J. and Wong, S. S. M. Phys. Lett. 30B (1969) 147

73. Rowe, D. J. and Wong, S. S. M. Nucl. Phys. A153 (1970) 561

74. Rowe, D. J. Phys. Lett. 44B (1973) 155

75. Seamon, R. E., Friedman, K. A., Breit, G., Haracz, R. D., Holt, J. M. and Prakash, A. Phys. Rev. 165 (1968) 1579

76. Shakin, C. M., Waghmare, Y. R., Tomaselli, M. and Hull, M. H., Jr. Phys. Rev. 161 (1967) 1015

77. deShalit, A. and Talmi, I. Nuclear Shell Theory (1963) Academic Press, New York

78. Slater, L. J. Confluent Hypergeometric Functions (1960) Cambridge University Press, London

79. Sprung, D. W. L. and Jopko, A. M. Can. J. Phys. 50 (1972) 2768

80. Srivastava, M. K., Jopko, A. M. and Sprung, D. W. L. Can. J. Phys. 47 (1969) 2459

81. Stapp, A. P., Ypsilantis, T. J. and Metropolis, N. Phys. Rev. 105 (1957) 302

82. Tabakin, F. Ann. Phys. (N.Y.) 30 (1964) 51

83. deTakacsy, N. Nucl. Phys. A95 (1967) 505

84. Talmi, I. Helv. Phys. Acta. 25 (1952) 185

85. Thouless, D. J. The Quantum Mechanics of Many Body Systems (1961) Academic Press, New York

86. deTourreil, R. and Sprung, D. W. L. Nucl. Phys. A201 (1973) 193

87. deTourreil, R., Sprung, D. W. L. and Rouben, B. Preprint (1974)

88. Vary, J. P., Sauer, P. U. and Wong, C. W. Phys. Rev. C 7 (1973) 1776